FINITE ELEMENT ANALYSIS OF UNBRACED STRUCTURAL WOOD I-JOISTS UNDER CONSTRUCTION LOADS

Paul Timko

Thesis submitted to the faculty of the

Virginia Polytechnic Institute and State University

in partial fulfillment of the requirements for the degree of

MASTER OF SCIENCE

in

CIVIL ENGINEERING

Daniel P. Hindman, Co-Chair

Elisa D. Sotelino, Co-Chair

Maury A. Nussbaum

April 27th, 2009

Blacksburg, Virginia

Keywords: Lateral Torsional Buckling, Composite Wood I-joist, Finite Element, Construction Loads

FINITE ELEMENT ANALYSIS OF UNBRACED STRUCTURAL WOOD I-JOISTS UNDER CONSTRUCTION LOADS

Paul Timko

Abstract

The research summarized the experimental analysis and finite element modeling of the lateral and rotational response of unbraced wood composite I-joists to worker loads. All experimentation and modeling was conducted on simply supported I-joists varying from 11-7/8 inches to 14 inches in depth and 20 feet to 24 feet in length. I-joists were subjected to static and dynamic loads. The deflections of the top and bottom flanges, as well as the rotation, were measured or calculated at both one-half and one-quarter the span length. The overall goal of this project is to accurately model the lateral and rotational displacements caused by human load effects.

I-joists were first tested statically by subjecting each joist to a three point bending test, free from all lateral restraints. This test was necessary to prove that the performance of the joists was repeatable. Lateral and rotational stiffness of the joist were calculated at one-half and one-quarter of the span length. The static experimental tests results were statistically analyzed using an analysis of variance (ANOVA) test. The results from this analysis indicated no difference between repetitions of the same joist; however, the test did indicate that there was a significant difference between joists of the same manufacture and size. Dynamic testing was then conducted. Dynamic loads were induced by having test subjects traverse each I-joist. The resulting loads induced at the top and bottom flanges were recorded for use in the finite element model. The lateral deflections and induced loads were compared to the static weight of the test subject and analyzed with an ANOVA test. The results indicated an increase in both the induced load and resulting deflection with an increase in weight. The analysis also indicated an increase in load and deflection with a decrease in lateral and rotational joist stiffness.

The recorded load values from the dynamic test were used as inputs into a finite element model. The resulting lateral deflections of the midpoint and quarter point were generated. The rotation of the

beam was calculated from the difference between the top and bottom flange. Experimental results and finite element model results were compared by calculating a running average of the error between the acquired data and the finite element model. The model was said to be valid until the average model error reached 10 percent of the maximum acquired test value. All six deflection readings were analyzed in this manner. The percent of beam at which the model no long represented the test data was determined for each data set. This point was averaged across all deflection readings of similar joists and across all data sets of the same joist type. The model predicted the 20 foot long 11-7/8 and 14 inch deep joists until 54.5 percent and 51.2 percent, respectively, of the beam completed by the test subject. However, the 24 foot long 11-7/8 inch deep joist was only accurate to 31.2 percent of the beam completed by the test subject.

Differences in peak values, and the time at which the peak values occurred were also analyzed using an ANOVA test. There was a significant difference between the peak values of the acquired test data and the deflections generated with the finite element model. However, there was no significance within the time that the peak values occurred between the model and experimental results.

A simplified pseudo dynamic analysis was conducted using a constant percentage of the test subject's static weight applied to the top and bottom flange. This approximation proved adequate for the lateral displacement and rotation of the 11-7/8 inch and 14 inch deep and 20 foot long I-joists. However, the model became un-conservative for the 11-7/8 inch deep and 24 foot I-joists.

Acknowledgements

This research has been the result of a grant from the National Institute of Occupational Safety and Health (NIOSH) with materials furnished by the Brooks Forest Products Center at Virginia Tech.

I would like to express my deepest gratitude to advisor, Dr. Daniel Hindman, for his support and expert guidance over the past two years. I am very grateful for the opportunity he afforded me to participate in his line of research. Dr. Hindman's constant encouragement kept me focused and determined during my career as a graduate student. I would also like to thank Dr. Maury A. Nussbaum for his advice and guidance through the statistical portion of this project. Furthermore, I would like to thank Dr. Elisa D. Sotelino for her guidance in helping me construct and test the finite element model.

I would like to recognize the excellent staff at the Brooks Forest Product Center, who devoted their time and advice to my project. My deepest gratitude goes to Rick Caudill, Kenny Albert, David Jones, and Angela Riegel, without whose help I would have never finished.

Additionally, I would like to recognize the members of my research group for their input and feedback through my research: Ryan Bamberg, John Bouldin, Jose Villasenor, and Gi Young. I would like to thank all of my friends and colleagues in the Structural Engineering program and the Wood Science for making my experiences at Virginia Tech unforgettable.

Finally, I want to express a my deepest appreciation to my loving family, my parents Dave and Karen Timko and my brother Chris Timko, for their support and guidance throughout my life. Were it not for their encouragement, in the many aspects of my life, I would not be where I am today.

Table of Contents

List of Figures

Note: All figures in this paper were created by the author.

List of Tables

Chapter 1: Introduction

1.1 Background

Wood composite I-joists represent a sizeable portion of new residential construction floor systems. I-joists are created from solid sawn, or more commonly, structural composite lumber (SCL) flanges connected with an oriented strand board (OSB) web (Hindman et al. 2005c). As the complexity of residential housing increases, wood I-joists are being used in various configurations, including longer span distances and continuous and cantilevered beams (Hindman et al. 2005a). The OSB web element constitutes a thin walled structure. This leaves the joist vulnerable to buckling, more specifically lateral torsional buckling. Little research has been conducted with respect to the lateral torsional capacity of wood I-joists (Zhu et al. 2005). Furthermore, no research has been conducted pertaining to the lateral torsional buckling of unbraced I-joists under construction loads. This condition is commonly seen in residential construction before the sheathing is attached to the joists.

Falls are the leading source of injuries and fatalities in the construction industry, accounting for nearly one third of fatalities. Furthermore, fall accidents have been steadily rising over the past several years (Huang and Hinze 2003). Since 1997, approximately half of all fall accidents have occurred on commercial and single family or duplex construction sites. The average fall height is around 11 meters, meaning that most falls are occurring on structures three stories or less. Almost half of fall accidents occur on job sites with a total value of less than $250,000 (Huang and Hinze 2003). These facts indicate that the majority of fall accidents may be occurring on residential construction sites.

Since construction workers have a notably higher rate of fatal and nonfatal work related injuries than other occupations, there is a significant cost born by the building industry. Non-fatal falls rank third in construction trade injuries behind injuries from being struck and overexertion. Falls from the same level and falls from elevations have resulted at a rate of 1.8 and 2.3 per 200,000 hours worked, respectively. (Lipscomb et al. 2003). Other than the direct monetary loss associated with medical bills and the loss of the worker on the job site, there are indirect losses associated with a loss of productivity.

Hinze and Applegate (1994) attributed the loss of productivity not just to the injured individual, but the entire work crew, as they may slow down or even stop. When individuals are absent for an extended period of time, replacement crew members may be needed. These replacements may not be adjusted to the crew and specific methods of construction, resulting in further loss of productivity.

1.2 Justification

There is no design standard for wood composite I-joists subjected to lateral torsional buckling under dynamic loading, in spite of growing fall rates. Wood composite I-joist manufactures give general recommendations for temporary bracing of I-joists under construction loads; however, the guidelines are vague and not based on any calculations. A better understanding of the dynamic loads applied by construction workers while installing I-joists and decking and the effect of these loads on lateral torsional buckling will contribute to enhanced safety specifications and reducing construction accidents due to falls. Furthermore, this knowledge could lead to reduced direct and indirect costs associated with injuries and loss of productivity by defining criteria to limit lateral torsional buckling of unbraced wood I-joists.

1.3 Objectives

The previous sections have shown a need for understanding the effects of dynamic loads on the lateral torsional buckling of wood I-joists. Capturing the effects of dynamic loads would be helpful in determining when a construction worker might fall and could be used to develop design criteria relevant to human loads placed on unbraced wood composite I-joists. However, this research will focus on the induced loads and maximum deflections created by construction workers as they traverse the I-joist. The overall goal of this project is to be able to accurately model the lateral and rotational displacements caused by human load effects. The results from this experiment may be used to develop safety regulations pertaining to the lateral and torsional stiffness of wood I joists. Statistical comparisons were performed between the developed computer model and the loaded specimens. Furthermore, a statistical comparison between static and dynamic loading was performed. Objectives of this work include:

1. Measure the amount of variation in lateral stiffness and rotation within the tested sample size of I-Joists
2. Measure the dynamic loads caused by a typical construction worker and conduct physical test of wood composite I-joists of various geometries
3. Develop and test a finite element model of several wood composite I-joists to predict degree of rotation and lateral displacement of loaded joists
4. Compare physically tested beams to the FE models results

Chapter 2: Literature Review

This literature review provides a summary of the properties of wood I-joists, the loads induced by a worker traversing a beam, stability, lateral torsional buckling, the current design method for construction, and methods of nonlinear finite element analysis of wood and I-joists. The discussion will focus on the development of a test method for determining when a construction worker might fall. Research related to dynamic load effects on the elastic stability and lateral torsional buckling will be summarized.

2.1 Properties of Wood I-joists

While metals and plastics possess isotropic mechanical properties, wood contains different properties dependent on grain direction and as a result, is considered anisotropic. For simplification, wood is considered orthotropic since it displays different mechanical properties along three perpendicular axes corresponding to grain orientation: longitudinal, tangential, and radial. While it is not possible to predict the radial-tangential grain direction since both flat sawn and edge sawn lumber may be used, a single value is assigned to both axes and called the perpendicular to grain property. This assumption is justified in that the radial and tangential directions exhibit similar strength values compared to the equivalent longitudinal values (Bowyer et al. 2002). The orthotropic behavior of the material yields three moduli of elasticity, three shear moduli, and three independent Poisson's ratios. Each of the preceding values corresponds to one of the three primary directions of an orthotropic material. Taking into account all of the previous variables, the stress strain relationship, or Hooke's law, for an orthotropic material is shown in equation 2.1.1. The subscripts denote the corresponding planar relationship defined by Bodig and Jayne (1982). The orientation of the axes for solid sawn wood is shown in Figure 1.

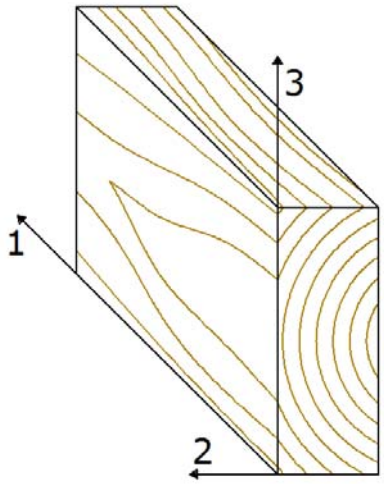

Figure 1. Three orthogonal directions for solid sawn wood.

$$\begin{bmatrix} \gamma_1 \\ \gamma_2 \\ \gamma_3 \\ \gamma_{23} \\ \gamma_{13} \\ \gamma_{12} \end{bmatrix} = \begin{bmatrix} \frac{1}{E_1} & -\frac{\nu_{12}}{E_2} & -\frac{\nu_{13}}{E_3} & 0 & 0 & 0 \\ -\frac{\nu_{21}}{E_1} & \frac{1}{E_2} & -\frac{\nu_{23}}{E_3} & 0 & 0 & 0 \\ -\frac{\nu_{31}}{E_1} & -\frac{\nu_{32}}{E_2} & \frac{1}{E_3} & 0 & 0 & 0 \\ 0 & 0 & 0 & \frac{1}{G_{23}} & 0 & 0 \\ 0 & 0 & 0 & 0 & \frac{1}{G_{13}} & 0 \\ 0 & 0 & 0 & 0 & 0 & \frac{1}{G_{12}} \end{bmatrix} \begin{bmatrix} \sigma_1 \\ \sigma_2 \\ \sigma_3 \\ \sigma_{23} \\ \sigma_{13} \\ \sigma_{12} \end{bmatrix} \quad (2.1.1)$$

where,

$\gamma = strain$

$E = Modulus\ of\ Elasticity$

$G = Shear\ Modulus$

$\sigma = Stress$

$\nu = Poisson's\ ratio$

The stress-strain relationship can further be simplified by assuming that the material is transverse isotropic. This means that the there is a single plane where the mechanical properties are identical. Under the assumption that the tangential and radial grain directions have identical properties equation 2.1.1 transforms to (Jones 1999):

$$\begin{bmatrix}\gamma_1\\ \gamma_2\\ \gamma_3\\ \gamma_{23}\\ \gamma_{13}\\ \gamma_{12}\end{bmatrix} = \begin{bmatrix} \frac{1}{E_1} & -\frac{\nu_{21}}{E_1} & -\frac{\nu_{31}}{E_3} & 0 & 0 & 0\\ -\frac{\nu_{21}}{E_1} & \frac{1}{E_1} & -\frac{\nu_{31}}{E_3} & 0 & 0 & 0\\ -\frac{\nu_{31}}{E_1} & -\frac{\nu_{31}}{E_1} & \frac{1}{E_3} & 0 & 0 & 0\\ 0 & 0 & 0 & \frac{1}{2G_{13}} & 0 & 0\\ 0 & 0 & 0 & 0 & \frac{1}{2G_{13}} & 0\\ 0 & 0 & 0 & 0 & 0 & \frac{1+\nu_{12}}{E_1} \end{bmatrix} \begin{bmatrix}\sigma_1\\ \sigma_2\\ \sigma_3\\ \sigma_{23}\\ \sigma_{13}\\ \sigma_{12}\end{bmatrix} \quad (2.1.2)$$

The web of an I-joist can be made from plywood, but is more commonly made from oriented strand board (OSB). OSB is created from layers of wood strands placed in an oriented manner and bonded by resin through elevated temperature and pressure. This material demonstrates orthotropic behavior with stronger strength characteristics along the direction of the strands on the face of the OSB (Guan and Zhu 2004). Panel products such as OSB tend to exhibit more transverse isotropic properties than solid wood since the reconstitution process uses cross-grain oriented layers within the panel. The process of creating panel products creates to more uniform strength characteristics but sacrifices maximum strength when compared to the parallel to grain direction of solid wood. The flanges of an I-joist, made from laminated veneered lumber (LVL), can possess stronger mechanical properties than those of solid sawn wood. The lamination process randomizes the placement of knots and other defects within the member, while solid sawn defects may extend all the way through the member. The laminations also serve to discourage the formation and propagation of cracks (Bowyer et al. 2002).

The OSB web and the LVL flanges of a wood composite I-joist can be modeled as transverse isotropic materials. For the remainder of this research the axes or orientation are defined by Figure 2. Since the web of the I-joist has identical properties in the 1-2 plane and the flanges have identical properties in the 2-3 plane, the mechanical properties of the web must be transformed into the global axes orientation.

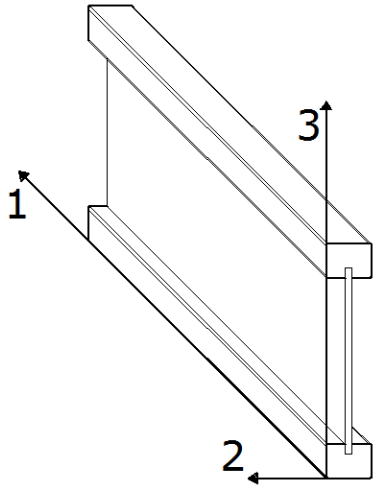

Figure 2. Coordinate Axes Orientation for Composite Wood I-Joist

2.2 Walking / Construction Loads

Dynamic load effects have been a concern among structural engineers since the early 1800's. According to Figueiredo et al. (2007), Tredgold was among the first to state that long girders should be made deep enough to avoid inconveniencing others on the floor. Conventional design criteria limit the amount of deflection to a fraction of the span length (L), L/360 for live load deflection of steel and wood floor elements. Other criteria demand a minimum stiffness for a floor element subjected to a concentrated load. Figueiredo et al. (2007) also noted that Tilden and Fuller were the first to study the dynamic load effects of individuals and groups of people.

The motion of walking can be characterized by an ascending and descending movement of the effective mass of the human body as well as a lateral propulsion. This motion, corresponding to the reactions, is periodic with respect to the step frequency. Harmonic loads develop due to the loading of one foot and the simultaneous unloading of the other foot. Furthermore, an increase in the dynamic load can be observed due to the impact of the heel. This dynamic load usually results in a vertical load higher than the static load, or weight, of an individual. (Figueiredo et al. 2007).

Research on pedestrian footbridges has led to the formation of force functions characterizing the dynamic effect of human movement; however, these force functions are assumed to be applied uniformly across the member. The forcing function caused by walking can be categorized into one of four types

depending on the step frequency: slow walk, normal walk, brisk walk, and fast walk. Each of the four categories contains a range of force frequencies. The functions describe the applied force with respect to the category the step frequency falls into and the actual frequency of the step. The force function of an individual step is given by equations 2.2.1 through 2.2.3 (Huang et al. 2006).

The dynamic load due to walking can be divided into three components: vertical dynamic force, lateral dynamic force, and vertical static force. Huang et al. (2006) developed a mathematical model that defines these forces normalized by static weight. The total vertical force of a single step, with respect to a normal walking frequency, is defined as $F_n[t]$ (Huang et al. 2006).

$$F_n[t] = \begin{cases} 0, & t < 0 \text{ or } t > T_{nc} \\ F_n[t], & 0 \le t \le T_{nc} \end{cases} \tag{2.2.1}$$

where,

$t = time$

$T_n = period\ of\ normal\ walk$

$T_{nc} = foot\ contact\ time$

Both the continuous vertical force function $F_{nv}(t)$ and the lateral force function $F_{nl}(t)$ are functions of $F_n[t]$. These functions are normalized by the normal walking function, and adjusted depending on the actual set frequency (Huang et al. 2006).

$$F_{nv}(t) = \sum_{k=0}^{\infty} F_n\left[\alpha\left(t - kT_p\right)\right] \tag{2.2.2}$$

$$F_{nl}(t) = \sum_{k=0}^{\infty} F_n\left[\alpha\left(t - 2kT_p\right)\right] - F_n\left[\alpha\left(t - (2k+1)T_p\right)\right] \tag{2.2.3}$$

where,

$F_{nv}(t) = continous\ vertical\ force\ function$

$F_{nl}(t) = continous\ lateral\ force\ function$

$\alpha = \frac{T_n}{T_p}\ or\ \frac{f_p}{f_n}$

$T_p = period\ of\ walking\ load\ \left(\frac{1}{f_p}\right)$

$f_p = pace\ frequency\ of\ walking\ load$

$f_n = pace\ frequency\ of\ normal\ walking$

$k = integer\ number$

Recently several different mathematical models, varying in complexity, have been developed to model the effects of human movement. These models are based on the type of activity engaged in as well as the location of the activity. These models represent the peak acceleration due to gravity that would be tolerable by the average person (Figueiredo et al. 2007).

2.3 Stability

The concept of stability is the underlying principle in almost any application of structural engineering. By the most basic definition of stability, an object is stable if a disturbance in displacement or velocity results in a force restoring the object to its original equilibrium state. With respect to beams and columns, buckling occurs when the equilibrium path becomes unstable. A loaded structure follows its primary load versus deflection path until buckling occurs. The structure then moves to a secondary path that is stable, but separate, from the primary path (Croll and Walker 1972). According to Simitses (1986), there is an explicit difference between the buckling load and the critical load of a structure. The buckling load refers to the load at which a structure begins to buckle, with respect to an physically loaded structure in a test, whereas the critical load results from computational analysis, based on theory (Simitses 1986).

There are several methods developed to ascertain the critical loads of an elastic system including the bifurcation, energy, and dynamic methods. The bifurcation or eigenvalue method is the oldest method for determining these values. Bifurcation occurs when the structure deflects an infinitesimally small amount to an adjacent equilibrium position. The load at which this occurs is known as the bifurcation load (Simitses 1986). To solve these problems, a stiffness matrix is developed based on the number of degrees of freedom of the system. The determinant of the structure's tangent stiffness matrix is set to zero to determine the system's critical loads represented as eigenvalues. One drawback to this method

arises from the presence of imperfections. It is not always practical to assume that a structure is ideal or perfect. When imperfections are present in the structure, buckling may occur as soon as a load is applied. This produces a load-deflection problem rather than bifurcation, and the eigenvalue approach cannot be used (Chen and Lui 1987).

An alternative to the eigenvalue approach is the energy method. This method only applies to elastic systems subjected to conservative forces. Conservative forces are those for which the potential energy is only dependent on the final displacement value and not the path to reach the final value. This method generalizes displacement and applied forces into an equation. The equilibrium point is reached when the equation of total potential energy is stationary. This can be accomplished by setting the derivative of the potential energy equation, with respect to each generalized displacement, to zero. The critical load can then be calculated from the equilibrium equation. The drawback to this method is that only the value of the critical load is determined; higher order derivatives of the potential energy equation must be evaluated in order to determine whether or not the equilibrium condition is stable (Chen and Lui 1987).

Finally, the critical load of an elastic member can be determined by the dynamic method. In this method, a system of equations is derived in which the motion of the structure is captured. The equations are functions of the externally applied loads and the generalized displacements. The critical load is defined by the amount of load that will cause the motion of the member to no longer be bound (Chen and Lui 1987). The primary advantage of the dynamic method is that it is able to analyze a system that is subjected to a dynamic load. Although the concept of this method is relatively simple the derivation of the solution can be quite complex (Simitses 1986).

Adding to the complexity of any problem is the presence of a dynamic load caused by walking. According to Bolotin (1964), the effects of dynamic loads have been studied since the 1920's when N. M. Beliaev first studied members with variable longitudinal forces. Bolotin (1964) and other researchers investigated the effects of dynamic stability on plane bending stating that while the static portion of a load may be below the critical load for a member, the beam may experience longitudinal vibrations. Under

certain conditions relating to the natural frequency of the beam and the forcing frequency of the load, the beam may become dynamically unstable and the longitudinal vibrations may become large (Bolotin 1964).

2.4 Lateral Torsional Buckling

2.4.1 Basic Concepts

As structural elements have become increasingly slender through the demand for efficiency, lateral torsional buckling has become a major controlling factor in structural design. Lateral torsional buckling is a critical failure mode that can occur when the flexural rigidity with respect to the bending plane is large when compared to the lateral or out-of-plane bending rigidity. The torsional rigidity of a member influences the lateral torsional buckling capacity through the shear modulus and torsional constant. A beam that meets this criteria will carry load until a slight rotation and lateral deflection occur, causing an instability (Timoshenko and Gere 1961). This failure method is illustrated in Figure 3.

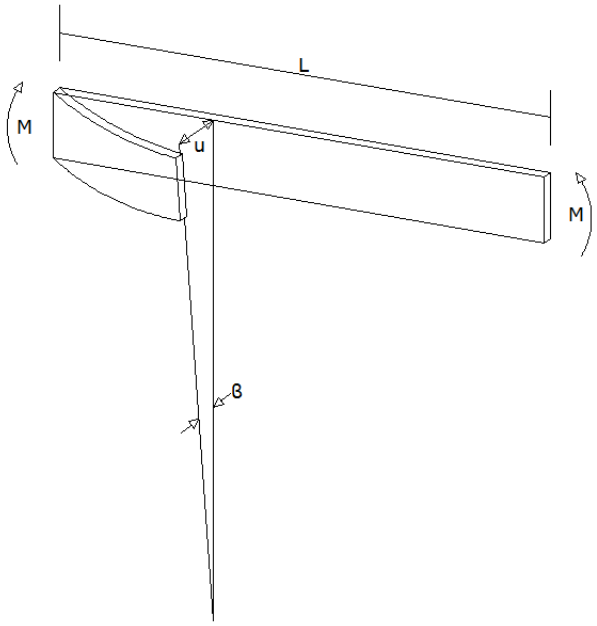

Figure 3. Lateral torsional buckling of rectangular beam

There are many factors that influence the lateral torsional buckling of a member including the cross sectional geometry, unbraced length, and end restraint conditions. While it is apparent that the type and placement of the load along the member will affect the buckling load, the location of the load with respect to the centroidal axis of the cross section also has a significant affect (Chen and Lui 1987).

The lateral buckling of an element can be derived from equations of equilibrium. Neglecting shear deformations and shortening of an element, the basic moment curvature relationship for any element is defined by Timoshenko and Gere (1961).

$$EI_{\xi}\frac{d^2v}{dz} = M_{\xi} \tag{2.4.1}$$

$$EI_{\eta}\frac{d^2u}{dz} = M_{\eta} \tag{2.4.2}$$

The *EI* terms in the preceding equations represent the flexural rigidity of the beam with respect to the local x and y axis, ξ and η respectively. The derivative terms in the equations represent the curvature of the beam in the direction of the deflected axis. This approximation is valid only for small deflections. When a member undergoes pure torsion, the only stresses that develop are shear stresses and the rotation, θ, which can be calculated by equation 2.4.3, where M_t is the applied torque and *C* is the torsional rigidity of the element. Torsional rigidity is a product of the shear modulus, G, and the torsional constant, J (Timoshenko and Gere 1961). For isotropic elements, the shear modulus and torsional constant are independent; however, for orthotropic elements the two terms cannot be separated. The torsional rigidity is a factor of the shear modulus of the various material planes in wood composites.

$$\theta = \frac{M_t}{C} \tag{2.4.3}$$

Figure 4 shows the different material axes with respect to the grain direction and torsion and the following equation defines the torsional constant for an orthotropic rectangular section (Hindman et al. 2005b) .

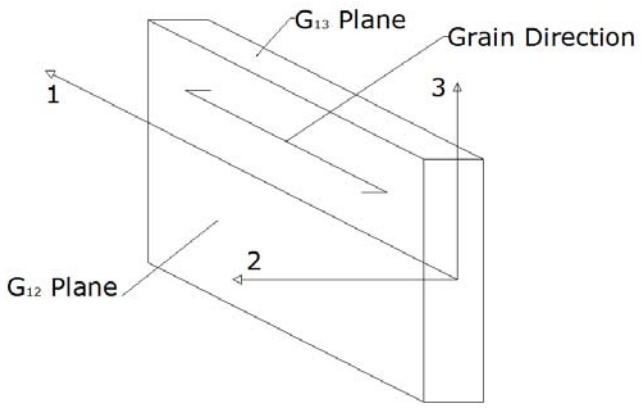

Figure 4. Definition of axes with respect to torsional loading

$$GJ = G_{12}\left[\frac{b^3 h}{3}\left(1 - \frac{192b}{\pi^5 h}\sqrt{\frac{G_{12}}{G_{13}}}\right)\right] \tag{2.4.4}$$

where,

$G_{12}, G_{13} = Planar\ shear\ moduli\ from\ Figure\ 6$

$b = width\ of\ rectangular\ section$

$h = height\ of\ rectangular\ section$

Since most structures do not undergo pure torsion, it is necessary to account for the warping of the cross section. The applied torque is resisted by pure torsion, denoted as M_{t1}, and the bending resistance of the flanges, M_{t2}. The pure torsion equation, Equation 2.4.3, is rewritten to define the applied torque M_{t1} with respect to the longitudinal axis of the element:

$$M_{t1} = C\frac{d\theta}{dz} \tag{2.4.5}$$

The cross section is assumed to be symmetric; therefore, rotation will occur with respect to the longitudinal axis. Based on this assumption, the second part of the torque, M_{t2}, can be quantified:

$$M_{t2} = -EC_w\frac{d^3\varphi}{dz^3} \tag{2.4.6}$$

The term C_w represents the warping constant of the cross section. By combining these equations, the complete differential equation for non-uniform torsion is:

$$M_\zeta = C\frac{d\theta}{dz} - EC_w\frac{d^3\varphi}{dz^3} \tag{2.4.7}$$

where M_ζ represents the twisting moment about the longitudinal axis of the member. This differential equation along with Equation 2.4.1 and 2.4.2 represent the equilibrium equations for lateral torsional buckling of an element under static loading. From these equations the critical load can be determined (Timoshenko and Gere 1961). For a simply supported beam subjected to a uniformly applied load, the elastic buckling moment can be simplified to:

$$P = \frac{\pi}{L}\sqrt{EI_y GJ}\sqrt{1 + \frac{\pi^2 EC_w}{L^2 GJ}} \tag{2.4.8}$$

The definition of stability becomes slightly more complex when considering dynamic loads. A beam is considered to be dynamically stable if small changes in the lateral forces are damped out over time. However, if these forces produce large lateral-torsional vibrations, the beam is dynamically unstable. The previous equilibrium equations must be modified to account for the inertial force of the beam. Considering a beam subjected to only dynamic end-moments, *M(t)* the equilibrium equations are:

$$EI_\xi \frac{\partial^4 v}{\partial z^4} + m\frac{\partial^2 v}{\partial t^2} = 0 \tag{2.4.9}$$

$$EI_\eta \frac{\partial^4 u}{\partial z^4} + M(t)\frac{\partial^2 \varphi}{\partial z^2} + m\frac{\partial^2 u}{\partial t^2} = 0 \tag{2.4.10}$$

$$M(t)\frac{\partial^2 u}{\partial z^2} - GJ\frac{\partial^2 \varphi}{\partial z^2} + m\rho\frac{\partial^2 \varphi}{dt^2} = 0 \tag{2.4.11}$$

where,

$m = mass\ per\ unit\ length$

$\rho = polar\ radius\ of\ inertia$

The equilibrium equations must satisfy the boundary conditions. The equations satisfying the boundary conditions can be substituted into the equilibrium equations and rewritten in terms of the natural frequencies of bending and torsional vibrations:

$$\omega_{n\xi} = \frac{n^2\pi^2}{l^2}\sqrt{\frac{EI_\eta}{m}} \tag{2.4.12}$$

$$\omega_{n\varphi} = \frac{n\pi}{\rho l}\sqrt{\frac{GJ}{m}} \tag{2.4.13}$$

The final matrix differential equation can be written in terms of the natural frequencies of the beam, the displacement matrix, the applied force, and the bending and torsional rigidities of the beam (Bolotin 1964).

2.4.2 Effect of Load Position

Research conducted by Ziemian et al. (2004) defined an out-of-plane midpoint displacement of L/120 for steel open web joists. The limit was based on tests that related the comfort of a worker traversing a joist to the measured lateral deflection. Dynamic tests were conducted by having a worker travel along the joist to a location two feet past the mid-span and measuring the amount of lateral deflection. Zieman recognized that every joist would contain some degree of initial imperfections. To account for these imperfections, all geometries were measured and multiple tests of each configuration were performed (Ziemian et al. 2004).

The placement of the load in the cross section can drastically affect the critical load of a member. Chen and Lui (1987) give a set of equations for predicting the critical load of such elements:

$$M_{cr} = C_b M_{ocr} \tag{2.4.14}$$

where M_{cr} is the maximum moment for the loading condition. $M_{cr} = \frac{P_{cr}L}{4}$ for a single concentrated load in the center. The C_b factor, defined by equation 2.4.15, accounts for the effect of the loading position within the cross section.

$$C_b = \begin{cases} AB, & \text{for bottom flange loading} \\ A, & \text{for shear center loading} \\ A/B, & \text{for upper flange loading} \end{cases} \tag{2.4.15}$$

where,

$$A = 1.35$$

$$B = 1 + 0.649W - 0.180W^2$$

$$W = {}^{\pi}/_{L}\sqrt{{}^{EC_w}/_{GJ}}$$

The variables above are defined for a simply supported beam with a single concentrated load applied at mid-span. Several other loading conditions have been researched and many of the C_b factors have been tabulated (Chen and Lui 1987)

2.4.3 Loading Conditions and Restraints

When the moment applied to a beam is not constant, the equilibrium equations will have variable coefficients, making any closed-formed solution derivation impossible. Alternative techniques such as numerical solutions or approximate methods must be used. Chen and Lui (1987) describe an approximate method based on the equivalent moment concept and introduce an equivalent moment factor C_b. This factor is used to adjust the critical moment for a beam under uniform moment. Typical loading cases have been thoroughly researched and the equivalent moment factors are tabulated. For loading combinations that are not tabulated, the factor has been calculated by:

$$C_b = \frac{12}{3\left(M_1/M_{max}\right)+4\left(M_2/M_{max}\right)+3\left(M_3/M_{max}\right)+2} \tag{2.4.16}$$

where, M_1, M_2, and M_3 are the moments at the quarter point, midpoint, and three-quarter point respectively. M_{max} is the maximum moment that occurs at any point along the length of the beam (Chen and Lui 1987).

Any change in the support conditions of a beam will have a significant impact upon the critical lateral buckling load. For beams subjected to uniform moments, the original equilibrium equations are still valid, but the support or boundary conditions must be applied. An effective length factor, K, is used for determining the critical load of a beam subjected to different end restraint conditions. For beams, this factor will vary between 0.5 for fixed end restraints and 1.0 for pinned end restraints. The length factor in the elastic buckling moment equation is replaced by the length multiplied by the effective length factor. For a uniformly loaded beam the elastic moment equation becomes (Chen and Lui 1987):

$$M_{cr} = \frac{\pi}{KL}\sqrt{EI_y GJ}\sqrt{1+\frac{\pi^2 EC_w}{(KL)^2 GJ}} \tag{2.4.17}$$

Many support conditions have been studied as well as the location of the restraint in the cross-section of the member. The effective length values are tabulated and readily available (Chen and Lui 1987).

Most connections do not provide full restraint against lateral buckling or rotation. These connections usually provide some varying degree of restraint against these translations. Studies have been conducted that model the restraining actions by linear springs. The main difficulty in quantifying the effect is the need to model the connection; the flexibility of a connection can be implemented by introducing the stiffness of the connection. This can be measured by the slope of the various force-deflection properties for a particular connection (Wang et al. 1987).

2.4.4 Lateral Torsional Buckling of Wood composite I-joists

In recent years there have been several studies that have examined the lateral torsional buckling capacity of wood composite I-joists. A study by Hindman et al. (2005b) focused on measuring the torsional rigidity of wood composite I-joists for the purpose of estimating the lateral torsional buckling capacity. The study compared two different flange materials, laminated veneer lumber and laminated strand lumber and concluded that there was no significant difference of the torsional rigidity. A finite element model was implemented to predict the torsional rigidity of I-joists and test isotropic and orthotropic assumptions. The model predicted the torsional rigidity more accurately using mixed isotropic values representing the separate components: the web and the flanges (Hindman et al. 2005c).

As a follow up to the previous research, Hindman et al. (2005a) examined the effect of the flange material on the lateral torsional capacity of the beam as well as studying the accuracy of the current LRFD design methodology. This study showed that the LRFD equation drastically underestimated the buckling loads for wood I-joists. These equations failed to consider the effects of torsional stiffness and torsional warping. The study concluded that elastic buckling theory was much more accurate at predicting the buckling load, but further studies should be conducted including a larger variety of I-joist geometries and loading conditions (Hindman et al. 2005a). More recent research by Burow et al. (2006) tested a larger variety of I-joists with varying unbraced length and beam slenderness ratios. This research

yielded similar results as the previous study, except the LRFD equations under estimated the buckling loads over a vast range of beam slenderness ratios. The objective of the research was to compare the results of several different elastic stability models to determine which accurately predicted the buckling behavior. Burow concluded that an equivalent moment factor model was the best predictor of buckling behavior (Burow et al. 2006).

A study conducted by Zhu et al. (2005) examined the buckling capacity of the OSB web. The tests conducted showed that both local buckling of the web and lateral buckling were failure modes depending on the geometric configuration of the I-joist. Zhu et al. (2005) noted that the lateral buckling was closely associated with the span length, flange size, and degree of lateral restraint on the compression flange. The research also concluded that web openings do not affect the lateral buckling of the I-joist if there are few lateral restraints across the member. An increase in the number of lateral restraints shifts the failure mode from lateral buckling to a material strength failure (Zhu et al. 2005).

2.5 History of Lateral Torsional Buckling in Wood Design

The earliest provisions in the National Design Specification (NDS) address the issue of lateral torsional buckling through member bracing requirements. In 1977, the NDS introduced the effective length approach discussed earlier (AF&PA 2003). Basic support conditions such as simply-supported and cantilevered members were addressed as well as basic loading conditions. Conservative approximations were given for other load cases. These equations were largely based on the work of Hooley and Madsen (1964), who recommended that the unbraced length be increased by 15% to account for imperfect torsional restraint at the supports. In 1991 research done by Hooley and Devall (1972) led to new provisions for more diverse loading and support conditions (AF&PA 2003).

The NDS adjustments are applied to the allowable bending stress by a beam stability factor, C_L. This factor accounts for the ratio of the buckling stress to the bending stress (AF&PA 2003). The provisions for the beam stability factor in the 2005 version of the NDS are the same as the column stability factor, C_P, utilizing only the properties of the compression flange for I-joists. These calculations

are valid under the assumption that the compression flange is fully braced in the direction of the web (AF&PA 2005).

$$C_L = C_P = \frac{1+(F_{cE}/F_c^*)}{2c} - \sqrt{\left[\frac{1+(F_{cE}/F_c^*)}{2c}\right]^2 - \frac{F_{cE}/F_c^*}{c}} \quad (2.5.1)$$

where,

$$F_{cE} = \frac{0.822\ E'_{min}}{(l_e/d)^2}$$

$F_c^* = reference\ compression\ design\ value\ parallel\ to\ grain$

$mulitplied\ by\ all\ applicable\ adjustment\ factors\ except\ C_P$

$c = 0.9\ for\ structural\ glued\ laminated\ timber\ or\ structural\ composite\ lumber$

$E'_{min} = adjusted\ modulus\ of\ elasticity\ for\ stability\ calculations$

$l_e/d = slenderness\ ratio$

Adjustments for support conditions, various loading conditions, and load eccentricities are accounted for in the buckling stress through the use of tabulated effective lengths. While provisions for lateral torsional buckling are presented in the NDS, a more comprehensive method is described in the American Wood Council's *Technical Report 14: Designing for Lateral-Torsional Stability in Wood Members* (AF&PA 2003). This new method utilizes the ASCE 16 method of applying a beams stability factor for strong axis bending. Equivalent moment factors and load eccentricity factors are employed to account for the effects of loading, support, and eccentricities (AF&PA 2003).

2.6 Finite Element Analysis

Finite element analysis is a numerical technique used to find the approximate solution to a series of differential equations. In this particular case the equations represent a solid object; however, this technique is also used to analyze heat transfer, magnetic fields, and many other applications. The finite element process breaks a larger structure into a number of finite elements, separating it from the infinitesimal elements used in calculus. These elements are comprised of connected nodes and, as a whole, define a mesh. A finite element mesh represents a series of algebraic equations that are used to

solve for deflection, stress, or other unknowns. It is important to note that the finite element method is not an exact solution; the results are based on a spatial distribution between the elements and the dependent variables used to solve the model (Cook et al. 2002).

Wood is an anisotropic material which exhibits a wide range of variability with time, loading, temperature, and moisture content. For small deformations, wood is often assumed to be linearly elastic; however, this is not a valid assumption for wood subjected to compression parallel to grain. In compression, the cell walls begin to buckle, producing a nonlinear behavior. Wood is often modeled as an orthotropic material since it possesses independent properties in three different directions: longitudinal, tangential, and radial. The linear elastic behavior in wood can be associated with the longitudinal and transverse tension, while the portions of compression and shear in the member yield ductility and nonlinear behavior (Tabiei and Wu 2000).

Preliminary finite element models utilized linearly elastic behavior of the OSB web. These models did not capture the orthotropic properties that belong to OSB. More recent research has shown that OSB behaves elastically until failure when under tension; however, the material is perfectly elasto-plastic under compression (Guan and Zhu 2004).

The finite element method for analyzing structural components has been well established for years. In a paper presented by Nethercot and Rockey (1970), the accuracy of lateral buckling finite element models was examined. Increasing the number of elements across the beams depth will increase accuracy for rectangular sections; however, the correct depiction of stress in the flanges of I shaped beams is of such importance that increasing the number of elements within the web has little effect on the overall accuracy. Additionally, changes in the aspect ratio of the elements have little effect on the accuracy of the model (Nethercot and Rockey 1971).

As stated before, imperfections can have a profound impact on the buckling load of a member. There are two primary ways to model geometric imperfections in a finite element model. The first method involves applying the first buckling mode or a series of buckling modes to the member. The second method is to apply the initial geometries in a predefined or random form. Zhu et al. (2005)

conducted inspections of joist crookedness as part of their research. The amplitude of the initial imperfections was less than 5% of the flange width. While there is no specific rule that governs the amplitude of the induced imperfections, the I-joists modeled by Zhu et al. (2005) contained a 2.5% variation in the flange and 10% variation to the web (Zhu et al. 2005).

Chapter 3: Materials and Methods

This research focused on the lateral torsional buckling effects of wood composite I-joists subjected to dynamic loading. The dynamic loading was characterized by construction workers traversing the joists longitudinally. The extent of research and experimentation required to fully describe the lateral torsional buckling characteristics of wood composite I-joists is beyond the time frame of this project. Therefore, this research focused on materials and loading conditions that are commonly seen in typical residential and commercial construction. Experimentation in this research focused on construction workers walking on unbraced I-joists. This section outlines the materials tested, experimental testing methods, and statistical analyses that are necessary to fulfill the objectives:

5. Measure the amount of variation in lateral stiffness and rotation within the tested sample size of I-Joists
6. Measure the dynamic loads caused by a typical construction worker and conduct physical test of wood composite I-joists of various geometries
7. Develop and test a finite element model of several wood composite I-joists to predict degree of rotation and lateral displacement of loaded joists
8. Compare physically tested beams to the FE models results

3.1 Materials

Test specimens consisted of several different sizes and lengths of wood composite I-joists from different manufacturers. This research focused on 11 7/8 inch and 14 inch deep I-joists ranging in length from twelve to twenty-four feet. The joists came from two different manufacturers; Georgia Pacific and iLevel, a division of Weyerhauser (TJI). From the manufactures' specifications the two Georgia Pacific 65 series I-joist had a total height of 11 7/8" and 14", and are hereafter referred to as GP12 and GP14 respectively. The TJI joist manufactured by iLevel had a total height of 11 7/8" and is referred to as TJI12. Table 1 depicts the manufacture's specifications for typical dimensions of the I-joists as well as the quantity of joists used for the static and dynamic tests. The ICC Evaluation Service report numbers

are also given in Table 1. While the specimens were not conditioned to any specific moisture content, the I-joists were allowed to acclimate to the testing environment of approximately 10% equilibrium moisture content (EMC) in the Wood Engineering Laboratory at the Brooks Forest Products Center.

Table 1. Wood composite I-Joist Dimensions

Name	Overall Depth	Length	Flange Width	Web Thickness	Static Samples	Dynamic Samples*	ICCES Report
GP12	11 7/8”	20’	2 7/16”	3/8”	5	3	ESR-1325
TJI12	11 7/8"	24’	2 5/16”	3/8”	4	3	ESR-1153
GP14	14”	20’	2 7/16”	3/8”	5	3	ESR-1325

*Dynamic samples were a subset of the static samples

3.1.1 Sample Size

A sample size of five joists of each size and span was used for the Static Test Procedure described below. Of the five joists tested according to the Static Test Procedure, three were selected to undergo the Dynamic Test Procedure. Preliminary testing has shown little to no damage or change in stiffness due to human walking loads. Each joist was loaded by a subject walking across the beam and subjected to ten different people with similar physical characteristics to that of a typical construction worker.

3.2 Test and Modeling Procedures

All testing for this project was conducted at the Wood Engineering Laboratory at the Thomas M. Brooks Research Center at the Virginia Polytechnic Institute and State University. Testing consisted of physical testing of I-joists subjected to static loads and human loads as well as virtual loading of I-joists through the use of finite element analysis.

3.2.1 Objective 1 - Static Test Procedure

The first objective of this research was to determine the amount of variability within the different sizes and types of I-joist. The variability within each joist type was determined by subjecting each joist to a three point bending test. The test was repeated six times. These tests were conducted on a servo-hydraulic Material Testing System (MTS) utilizing a MTS 661.20E-01 5000 lb load cell with an error of

less than 1 percent. Data was collected through the use of National Instruments LabVIEW 7.0. An overall view of the static test is seen in Figure 5.

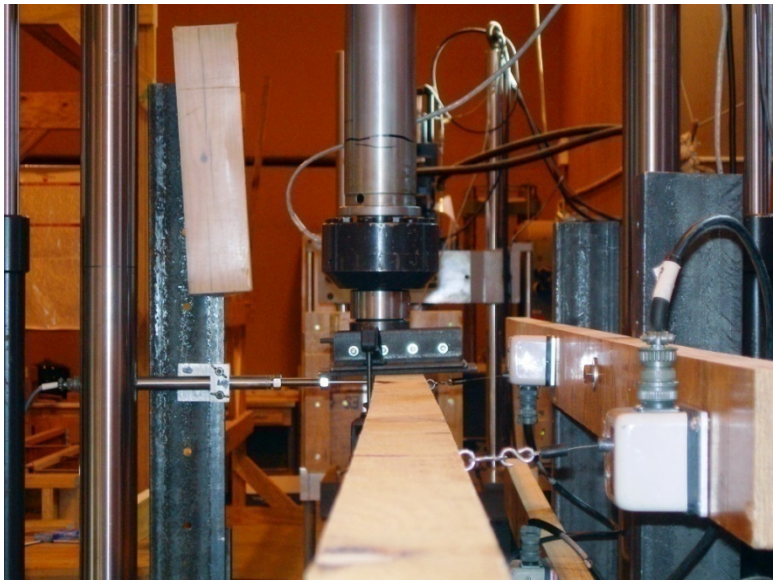

Figure 5. Picture of Static Test Along Length of I-Joist

The lateral displacements of the top and bottom flanges as well as the rotation of the beam were recorded at the midpoint and quarter point. UniMeasure PA-5-L3M and PA-2-L3M string potentiometers, with an error of less than 1 percent of the measured values, were attached to the beam at the midspan and quarter point of the top and bottom flange, as illustrated in Figure 6, to measure the lateral deflection. The 5 inch potentiometers were placed at the midspan of the joist to allow for the possibility of exceeding the 1 inch lateral movement of a 2 inch potentiometer. The other potentiometers were placed at the quarter point. The rotation was recorded through the use of AccuStar 11/DAS 20 clinometers, with an error of less than 1 percent, clamped at the midpoint and quarter point of the bottom flange.

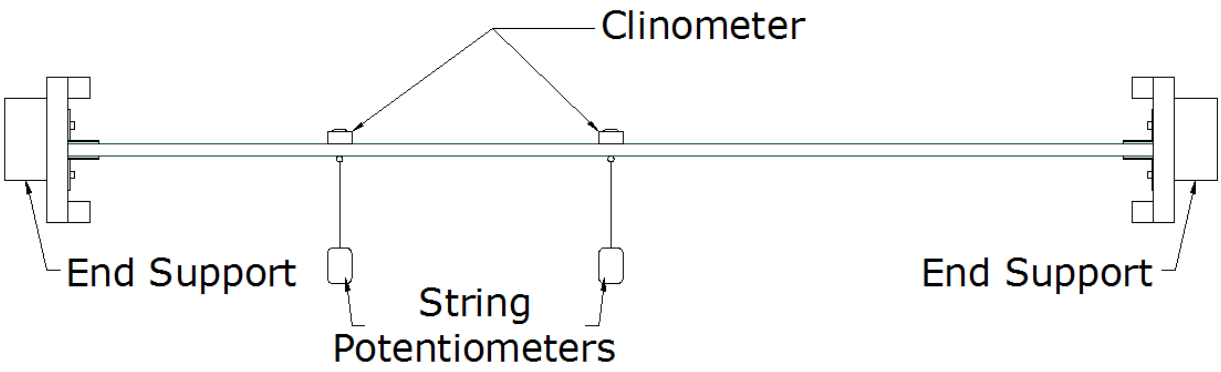

Figure 6. Plan View of Location of Measurement Devices Used in Static Bending Test

The string pots were attached to the testing machine and not allowed to move with the beam. Since the downward deflection of the hydraulic ram of the MTS testing machine was not measured, the lateral displacements included some effect from the vertical displacement. The potentiometers were mounted approximately 8 inches from the joist to minimize the angle occurring at the maximum vertical deflection. To ensure that the downward deflection was not a significant influence on the lateral displacement, initial test conducted using linear variable differential transformer (LVDT) placed at the midpoint of the top flange of the I-joist to measure lateral displacement. Any difference between the readings of the string potentiometer and the LVDT was attributed to the vertical deflection. These tests indicated that the string potentiometers were sufficiently distanced from the test specimen so that the downward deflection was not significant and found to be less than 0.015 inches.

A special end support was constructed using an appropriately sized joist hanger to replicate field conditions. The end supports, seen in Figure 7, were constructed from LVL and placed atop a steel post, to elevate the I-joist above the bed of the testing machine. Each joist was placed within the joist hangers and shimmed tight at the top and bottom flange. This prevented any global displacement, lateral or rotational, from occurring.

Figure 7. End Support with Joist Hanger

The use of a standard load head acts as a lateral and rotational bracing point inducing a higher order buckling mode. To account for this, a specialized roller bearing plate was placed under the load cell of the MTS machine. The roller bearing plate, shown in Figure 8, consisted of four rows of five linear bearings underneath a metal plate. This assembly allowed the joist to move laterally and rotate slightly in either direction allowing only vertical forces to load the joist. The specialized bearing plate, in combination with the swivel head, allowed the joist to move freely within the 500 lb test range.

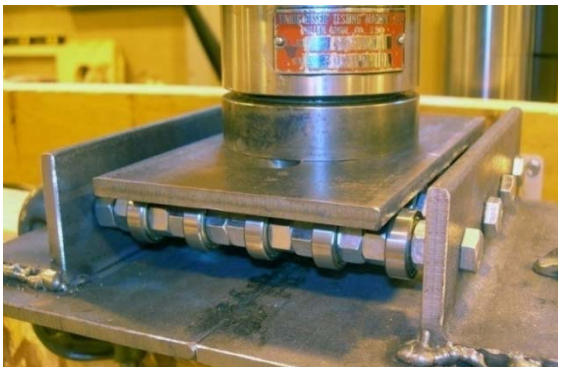

Figure 8. Bearing Support and Swivel Head

To begin each test, each joist was placed into the joist hanger on the end supports. Care was taken to make sure the joist was then directly centered underneath the load cell. Shims were installed between the top and bottom flanges of the joist and the joist hanger. Sufficient force was applied to the shims to prevent the joist from moving from side to side within the joist hanger. Metal eye hooks were

installed in the center of the top and bottom flanges at the midpoint and quarter point to receive the string potentiometers. The potentiometers were connected to the I-joist using brass wire with the length of wire adjusted so that each potentiometer was centered with respect to its sensor range. The roller bearing plate was then clamped to the center of the joist on the top flange and leveled by adjusting the tension of the clamps.

The MTS machine applied a constant deflection rate depending on the type of joist being tested. Table 2 shows the loading rates used for the static test; the loading rates were calculated to reach a 500 lb load in 5 min. The GP12 and GP14 joists were loaded to 500 lb. Due to the increased length, the TJI12 joists were loaded to 400 lb.

Table 2. Loading Rates for Static Test

Joist Size	Load Rate (in/min.)
GP12	0.10
TJI12	0.16
GP14	0.07

The data collected consisted of four deflection readings and two rotation measurements. The raw data was processed through the use of MATLAB R2008b. MATLAB was used to automate the process of reducing the data to a series of load-deflection and load-rotation graphs. The starting point of the test was adjusted to the time at which load was starting to be applied and the end point was taken at 500lb. The data was then stored into an Excel file for further manipulation. The statistical analysis focused solely on linear regressions of the load-deflection and load-rotation plots. The slopes of each regression were compiled and analyzed with JMP 7.0.1. The data was first analyzed using a two factor ANOVA test, with a significance level of $p < 0.05$. The independent variables, joist and replication, were modeled as random effects. After confirming that there was no significant difference between the replications, the data was reanalyzed without the replication factor.

3.2.2 Objective 2 - Dynamic Test Procedures

The second objective of this research was to record the induced loads and deflections of a construction worker traversing the joists. Figure 9 shows the safety platform used for all dynamic testing. The safety platform consisted of two portal frames connected with a truss-like safety rail on either side. A steel beam, to which test subjects would be tethered, was install spanning between the two portal frames.

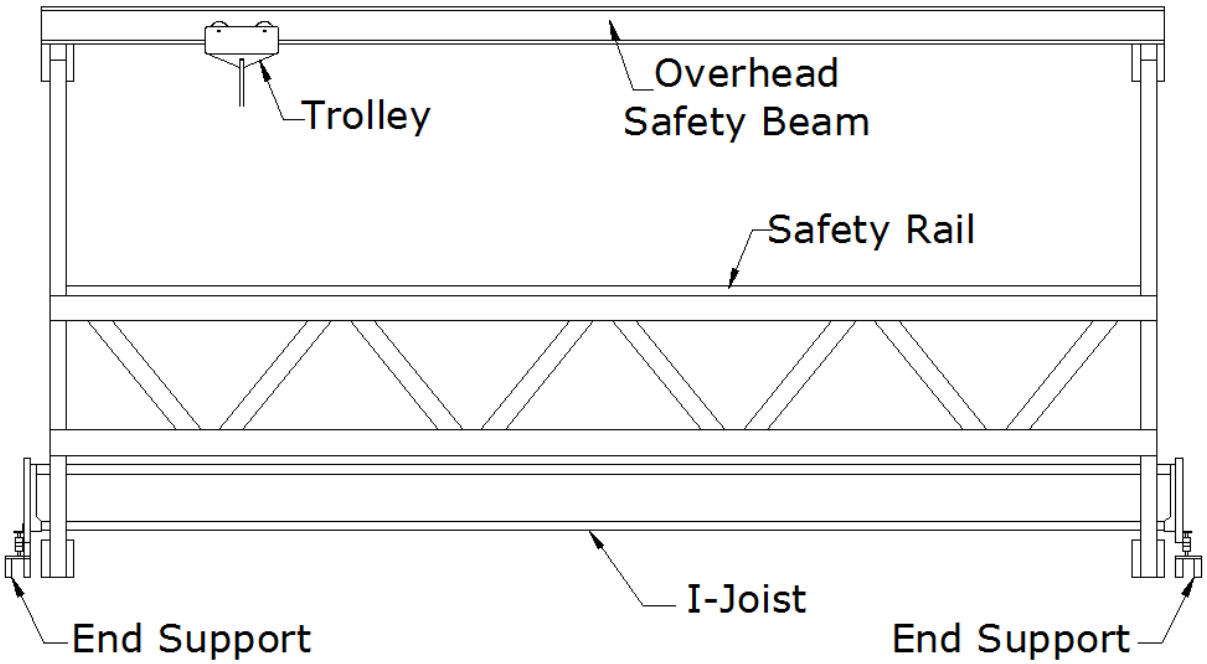

Figure 9. Side View of Safety Platform

Two different end supports were constructed to hold either end of the I-joist and the four load cells necessary to capture the induced loads. Vishay BHL U3SB-A "S" type load cells with a 5000 lb capacity and an error of less than 1 percent were be placed at both ends of the beam to record the end reactions and allow for calculating the test subject's position on the beam. Load cells were also attached in the vertical direction at both ends and also on the top and bottom flanges on one support. On the other support, a load cell was mounted only in the vertical direction while lateral forces were restrained. All load cells on the supports were attached to an LVL section to which a joist hanger was mounted. Figure

10 shows the two end supports used. The vertical load cells were only used to calculate the test subjects' position along the beam. The values from the flange load cells were corrected based on the position of the test subject on the beam. The end reactions combined with the I-joist flange reactions were then compiled resulting in a combination of loads the subject applied to the I-joist.

(a) **(b)**

Figure 10. (a) End Support with 3 Load Cells (b) End Support with 1 Load Cell

A pair of 20 inch string potentiometers, UniMeasure model PA-20-L3M, was placed at the mid-span and quarter-span, as seen in Figure 11. At each location, a potentiometer was attached to the top flange and another was attached to the bottom flange. Unlike the static test, the use of clinometers to measure the rotation of the beam was not possible. The clinometers were significantly affected by the rapid movement of the I-joist yielding inaccurate and muted results. Instead, the rotation was calculated through the difference in the string potentiometers connected to the top and bottom flanges. This calculation is based on the assumption that the web of the joist did not deform and remained perpendicular to the flanges. The data was collected using Vishay Micro-Measurements StrainSmart 4.31.

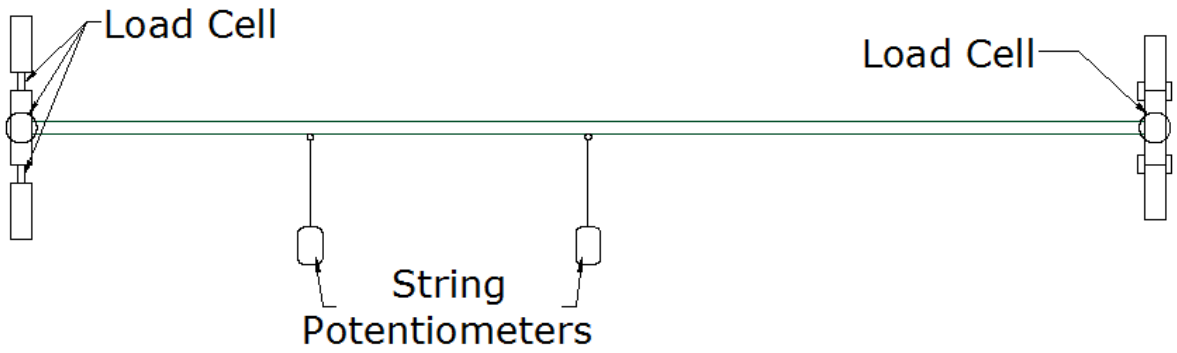

Figure 11. Plan View of Measuring Devices along I-Joist for Dynamic Testing

Test subjects consisted of males who were construction workers or graduate students. The test subjects were Caucasian, Hispanic, or Indian. The weight of the test subjects ranged from 133 lbs. to 283 lbs. All data collected from test subjects conformed to the Virginia Tech Internal Review Board. To begin each test, the subject's weight was recorded on an Arlyn Scale model 320m. An I-joist was then placed between the end supports. The flanges of the I-joist were shimmed against the joist hanger to prevent lateral movement. A test subject, wearing a construction safety harness, was tethered to the trolley that rides along the overhead safety beam. Each subject traversed the beam two times at a comfortable walking speed to the test subject. The test subject were allowed to walk at their own pace, but were instructed to maintain a constant speed. The test subjects were further instructed to use the safety rails only when necessary and to use them and continue traversing the beam. Figure 12, shows a test subject traversing one of the I-joists.

Figure 12. Test Subject Traversing I-joist

Two difference analytical procedures were created, one for the input into the full pseudo-dynamic analysis and the other for a simulated pseudo-dynamic analysis. For both procedures, data was condensed using MatLAB and Excel. The data was first condensed based on the starting and stopping point of the tests. The starting point of each test was defined when the test subject transferred a significant amount of their body weight, approximately 75 lbs, onto the joist while the stopping point was determined when the amount of load remaining on the joist was 75 lb. The lateral load data from the top and bottom flange was adjusted based on the position of the test subject assuming a linear relationship between time and walking speed. This data was then used as a direct input into the full pseudo-dynamic ANSYS model and the simplified ANSYS model discussed in section 3.2.2.

3.2.2 Objective 3

3.2.2.1Model Construction

A finite element analysis of each type of I-joist was conducted with ANSYS version 11. Three different models were developed utilizing the available properties of LVL and OSB, summarized in Table 3, to accurately depict the behavior of each wood composite I-joist. LVL and OSB materials were modeled as orthotropic materials with axis alignment described in Figure 2.

Table 3. Mechanical Properties of OSB and LVL

LVL			OSB	
E_X	8.94E+04		E_X	2.09E+05
E_Y	8.94E+04		E_Y	1.14E+06
E_Z	2.38E+06		E_Z	2.09E+05
ν_{XY}	0.382		ν_{XY}	0.054
ν_{YZ}	0.011		ν_{YZ}	0.328
ν_{XZ}	0.012		ν_{XZ}	0.362
G_{XY}	9.64E+03		G_{XY}	9.22E+04
G_{YZ}	5.14E+04		G_{YZ}	9.33E+04
G_{XZ}	6.57E+04		G_{XZ}	1.48E+04

The mechanical properties used in the finite element (FE) model were derived from previous research by Janowiak et al. (2001), the Wood Handbook (USDA 1999), as well as manufacturer specifications (Weyerhaeuser 2004). The modulus of elasticity, E, in the X and Y directions as well as the three shear moduli were determined according to the average southern yellow pine values reported by Janowiak et al. (2001). The LVL Poisson's ratio was the same value as loblolly pine from the Wood Handbook (USDA 1999). The E in the X and Y directions for the OSB web were determined from the manufacturer's specification (Weyerhaeuser 2004). Poisson's ratios and shear moduli for the OSB were considered equal to loblolly pine from the Wood Handbook (USDA 1999). Although from different manufacturers, all three joist types were assumed to have identical mechanical properties. The physical dimensions of the I-joists subjected to the Dynamic Test Procedure were averaged according to the joist type to determine the input dimensions of the models.

The 3D FE models were comprised of 10 node solid brick elements and were similar to the model in Figure 13(a). End conditions and loading points can be seen in Figure 13(b), while a cross sectional view of the FE mesh is illustrated in Figure 13(c).

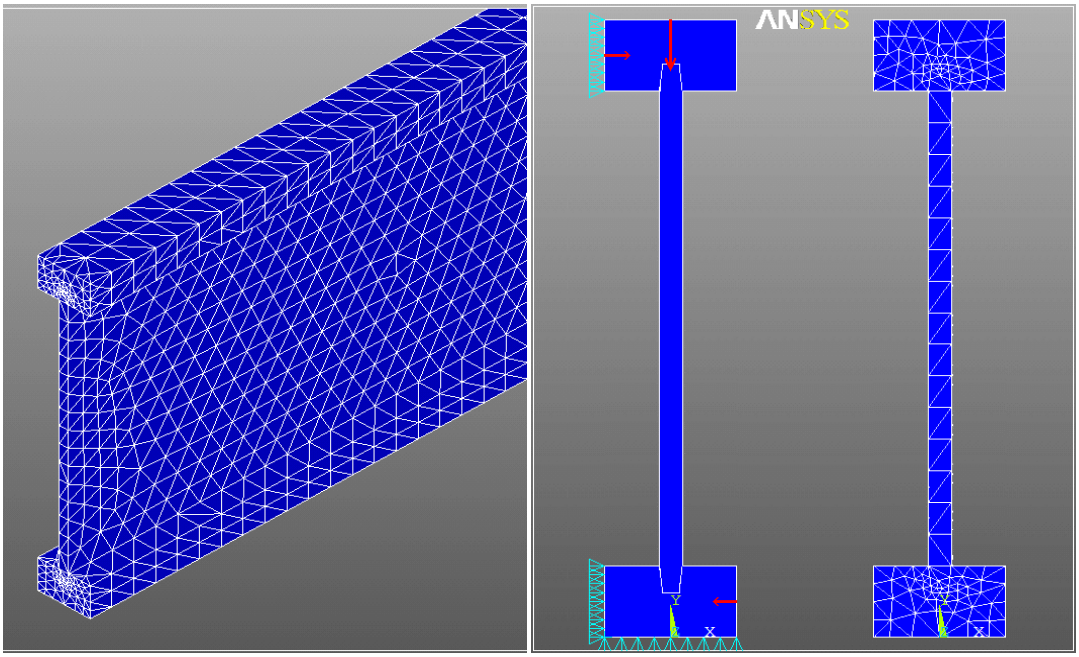

(a) **(b)** **(c)**

Figure 13. (a) 3D Model (b) Boundary/Loading Conditions and (c) FE Mesh

Three rows of hardpoints were created along the top and bottom flange. Hardpoints are used to map a known number to a corresponding node number generated by the meshing process. The hardpoints were part of the FE mesh and were located on the outer surface. For this model the hardpoints were used to control the application of load and interpret the displacement results. A single row of hardoints, spaced one inch apart along the center of the top flange, allowed for the placement of the test subject's static weight. Hardpoints spaced one inch apart along the side of the top and bottom flanges allowed for placement of the lateral loads.

The FE mesh was applied to each solid model through a free mapping process using tetrahedral shaped elements. The spacing of the elements in the FE mesh was controlled by the placement of the hardpoints. The amount of refinement required to avoid an abundance of mesh incongruities in the FE mesh was well beyond that which would have been required by a detailed convergence study. A convergence study of two iterations was performed on a single model by decreasing the distance between hardpoints by a factor of two. The model was loaded statically at the midpoint. The convergence study found a less than three percent difference at midpoint, indicating that the level of refinement was appropriate. No refinement between hardpoints was necessary. Additionally, only displacements were monitored in this research, requiring less refinement than models calculating stresses and strains.

The end boundary conditions of the FE model closely reflected conditions found in the field during joist installation. The bottom flanges of the joist were fully supported along the outer surface against deflections in the plane of the web. The top and bottom flanges were restrained against lateral deflections one side. Since the joist hangers used to install these beams lack sufficient rotational stiffness, only one side was braced against lateral deflections allowing the ends of the joist to rotate slightly. Only one node was restrained against deflections along the longitudinal axis of the joist to avoid instability problems when solving the model.

3.2.2.2 Model Analysis

The models were subjected to two analyses with different loading conditions. Both analyses were conducted as transient dynamic analyses without consideration for vibration, dampening, or any harmonic effects. Each analysis was treated as a series of load steps, with each load step capable of analyzing a given set of loading conditions at different points. This analysis also imposes the previous load step's deformations on the current load step before solving the analysis.

First a full pseudo-dynamic analysis was conducted using a point-by-point basis on the FE model. Lateral loads were applied to the model at the respective hardpoint, according to the top and bottom flange load cell readings recorded in Objective 2, adjusted for the placement of the load along the length of the joist. Simultaneously, the corresponding static weight of the test subject was applied as a vertical force to the corresponding hardpoint at the center of the top flange. The time index of this analysis was controlled by the time index of the lateral loads taken from Objective 2. Due to the complexity and length of time required to solve a full analysis, only three of the test subjects were modeled per joist type. For statistical purposes, both of the tests subject's attempts to traverse the three joists of each joist type were modeled.

A second FE analysis was conducted to generalize the results of Objective 2. This analysis utilized the maximum applied lateral load on the top flange and the average applied load on the bottom flange from Objective 2. The average value applied to the bottom flange compensated for the fact that the peak load for both flanges may not occur at the same time. The values were obtained from each test conducted and normalized to a percentage of the test subject’s static weight. This percentage was determined by minimizing the difference between the acquired values and the approximated loads. The two lateral loads were applied in opposite directions to simulate torsion in the I-joist, while the static weight of the test subject was also applied to the FE model. All three forces were applied at 24 evenly spaced points along the length of the member to produce the outer displacement bounds of the I-joist. This analysis was performed for each combination of test subject and I-joist type.

ANSYS model outputs consisted of only nodal displacements. As in the physical testing of the beams, the angular rotation was extracted from the lateral displacements generated by ANSYS. The rotation was computed from the difference in the top and bottom flanges at the hardpoints corresponding to the midpoint and quarter point of the joist. Since the hardpoints were located on opposite sides of the beam, it was assumed that the cross section remained planar, indicating both top and bottom flanges moved the same amount. The lateral displacements and angular rotations at the mid-span and quarter-points were analyzed and compared to the physical tests as described by Objective 4.

3.2.2 Objective 4

Statistical comparisons analyzed the similarity between the applied static and dynamic loads. The amount of lateral deflection and angular rotations of the dynamic tests were compared to deflections generated by the finite element model.

The recorded lateral deflection and rotation data from Objective 2 was compiled along with the data generated by the ANSYS model. Since it was difficult to statistically compare the two outputs in their raw form, this research focused on only the outer bounds of each test and simulation. This allowed for the model and actual test data to vary slightly with time, without being a significant detriment to the model's validity. To capture the outer bounds of both the ANSYS generated data and the acquired test data, the absolute value of each deflection and rotation was taken, forming the absolute value curve.

The maximum value of each test was then determined. The maximum value was used as a dividing point for the graph. Only increasing values were used from the start of the test until the maximum value. This process was reversed for a downward slope. For the remainder of this thesis, this curve will be referred to as the maximum value curve (MVC). Figure 14 illustrates the development of the MVC. The raw data in Figure 14(a) shows the lateral deflection in either direction with respect to time. The absolute value of all of the data points yielded the absolute value curve seen in Figure 14(b). Taking only increasing data points from both the start and the end of the absolute value curve creates the

maximum value curve seen in Figure 14(b). This curve represents the outer bounds that the joist traveled during the test.

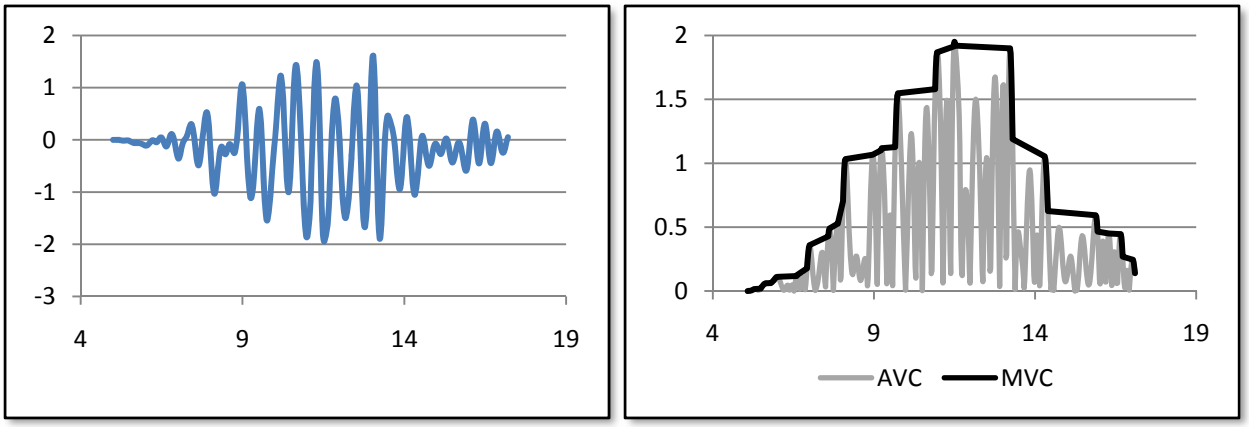

(a) **(b)**

Figure 14. (a) Acquired Test Data (b) Absolute Value Curve and Maximum Value Curve

The MVC for each deflection and rotation generated from the acquired data was matched to the corresponding MVC from the ANSYS model. The difference between the MVCs was calculated and considered to be the amount of error in the model. A running average of the model error was calculated and used to determine when the model no longer represented the acquired data. Using a running average allowed for some minor discrepancies between the model and experimental MVC's. When the error exceeded 10 percent of the maximum value acquired from the experimental MVC, the model was said to no longer be effective. Since the effects of vibration and dampening were not accounted for in the model, the model under 10% maximum value was considered acceptable.

Chapter 4: Results and Discussion

4.1 General

This section contains the results from the methods described in Chapter 3 along with related discussion. The results from the static test are discussed in Section 4.2, while the dynamic test results are discussed in Section 4.3. The results from the finite element models and comparisons to the dynamic test results are discussed in Section 4.4.

Throughout this chapter the specimens were referred to in accordance with Table 1 in Chapter 3. The static test and dynamic test joist designations differ slightly. The static tests designation contains the manufacture designation followed by two numbers representing the joist being tested and the replication number. For example, TJI12-3-5 indicates that the joist was the third TJI 11 7/8" high joist tested and the 5th replicate test. The dynamic test designation contains the manufacture designation followed by the joist reference number and test reference code. For example, GP12-5-S2b, indicates that the joist was the 5th Georgia Pacific 11 7/8 inch deep joist. The 'S2' corresponded to the second test subject, while the 'b' represented the second attempt by the worker to traverse the joist.

4.2 Static Test

This section compared the lateral displacement of the top and bottom flanges, as well as the rotation, at both the midpoint and quarter point to examine any significant differences between test replications and different joists of the same size. For dependent variable comparison, lateral displacements and rotations were analyzed separately to test for any significant differences. Five joists of each of the three sizes were tested six times, for a total ninety bending tests.

As described in Chapter 3, the slopes of the load deflection curves were used for the statistical analysis. Data was collected up to 500 lbs for the GP14 joists, 350 lbs for the GP12 joists, and 250 lbs for the TJI12 joists. This load range was based on the amount of slip that occurred during each test and the lateral/rotational stiffness of the joist size. As the load increased, the frictional force between the

bearings and the metal plate became greater. This created larger 'slips' in lateral deflections at higher loads; the slips in deflection are relative to the amount of load applied to the beam. A typical load-deflection curve is seen in Figure 15. Note the larger 'slips' in deflection occured at higher loads. In an idealized test, there would be no deflection slips. When the deflection slips occur in the actual test, the built up frictional force is released and the joist slips past where it would be in an ideal test. The force then has to build up above the idealized force-deflection curve before it would slip again. In this case the regression line indicates a linearized ideal force-deflection curve.

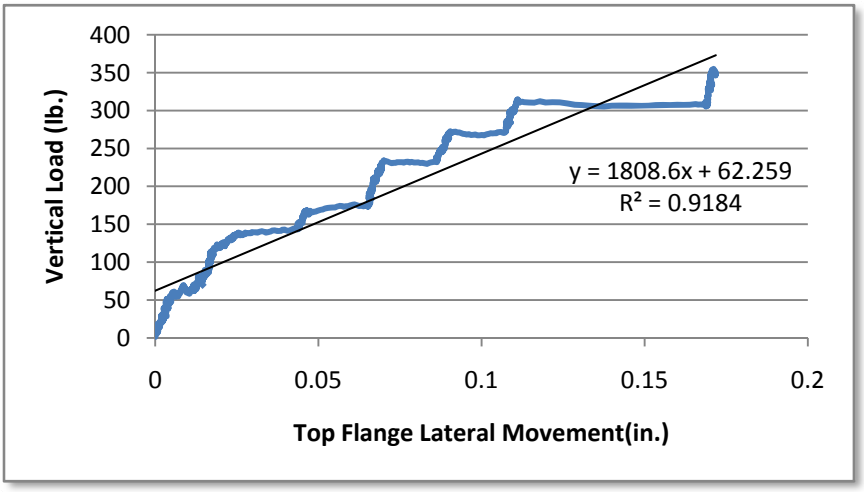

Figure 15. Typical Load-Deflection Curve

Table 4 shows the mean stiffness values and the coefficients of variation (COV) for each joist. Linear regressions of the load-deflection and load-rotation graphs were calculated for each test. The slopes from the load-deflection and load-rotation curves were compiled and averaged for each joist. From analyzing the mean stiffness values, the GP14 joists were the stiffest joist type followed by the GP12 and TJI12 joists. Some joists such as the GP14-3 and TJI12-2 have a noticeably greater average value; however, the COV for these joists was also greater. Stiffer joists exhibited a wider range of stiffness values. There is a considerable amount of variation in the COV within each joist type. More joists should be tested in order to generalize the results within an entire joist type. There was also a noticeable trend with respect to the deflection. The rotation of the joist exhibited lower COV when compared to the top and bottom flange lateral displacement. The top flange of the beam had a lower COV than the bottom

flange, indicating a more consistent performance. These deflection trends were apparent in both the midpoint and the quarter point measurements. There was a slight variation of the COV with respect to the measurement location. In general, all quarter point measurements exhibited lower variation than the midpoint measurements.

Table 4. Lateral/Rotational Stiffness of Joists

Lateral / Rotational Joist Stiffness (lb/in)												
Joist	Midpoint						Quarter Point					
	Top Flange		Bottom Flange		Rotation (lb/deg.)		Top Flange		Bottom Flange		Rotation (lb/deg.)	
	Mean	COV	Mean	COV	Mean	COV	Mean	COV	Mean	COV	Mean	COV
GP14-1	1232	8.0%	1712	11.1%	485	3.3%	1605	7.6%	2730	11.5%	2454	1.2%
GP14-2	2872	8.3%	3581	10.2%	1541	5.9%	3854	7.4%	5658	10.2%	2011	1.6%
GP14-3	2315	12.6%	5281	19.4%	472	3.1%	2872	10.6%	8833	18.0%	2380	2.1%
GP14-4	2000	3.7%	2944	4.7%	915	4.4%	2890	3.4%	4850	4.7%	2233	2.3%
GP14-5	1297	4.7%	1735	4.1%	659	4.8%	1818	5.6%	2859	5.0%	2200	1.4%
GP12-1	943	5.0%	800	5.4%	545	3.8%	1327	4.5%	1627	4.9%	1424	1.5%
GP12-2	1129	12.6%	918	13.1%	791	19.8%	1655	11.9%	1959	13.4%	1334	2.2%
GP12-3	1434	5.5%	1488	7.5%	457	3.3%	2182	5.5%	3553	8.6%	1518	1.8%
GP12-4	936	9.1%	816	11.6%	506	4.9%	1394	8.8%	1819	10.4%	1480	1.6%
GP12-5	1355	2.6%	1207	2.5%	541	1.8%	1915	2.4%	2620	3.1%	1524	1.3%
TJI12-1	541	18.2%	510	8.1%	217	16.6%	723	17.3%	1078	18.0%	1082	3.8%
TJI12-2	1017	33.5%	996	41.5%	279	7.3%	1396	28.8%	2573	55.5%	1136	3.2%
TJI12-3	804	10.0%	685	12.5%	353	5.5%	1111	9.7%	1578	14.0%	1088	0.4%
TJI12-4	412	10.7%	368	11.9%	195	6.6%	585	11.0%	833	12.4%	1135	0.9%

The stiffness data was then examined using a random-effects analysis of variance (ANOVA), to assess whether there were significant differences between joists of the same type and replications within a given joist. As illustrated in Table 5, there were no significant differences between replicate tests on the same joist; however, significant differences did exist between joists of the same size. This supports the previously discussed trend that a larger sample is needed in order to characterize a given joist type.

Table 5. Static ANOVA Test Results: p-Values[1]

Joist Type	Factor	Midpoint			Quarter		
		Top Flange	Bottom Flange	Rotation	Top Flange	Bottom Flange	Rotation
GP14	Joist	0.0001	0.0001	0.0001	0.0001	0.0001	0.0001
	Replication	0.4953	0.4057	0.8916	0.6200	0.4412	0.5265
GP12	Joist	0.0001	0.0001	0.0001	0.0001	0.0001	0.0001
	Replication	0.2402	0.3822	0.3552	0.3070	0.4009	0.1957
TJI12	Joist	0.0001	0.0009	0.0001	0.0001	0.0045	0.0037
	Replication	0.3601	0.4739	0.2146	0.3767	0.4507	0.3394

[1] Highlighted cells indicate $p < 0.05$

Since the difference within the replications was not significant, the data was reanalyzed using a single factor, random-effects ANOVA to identify the components of variance related to differences between joists of a given type and within a given joist. The percent variance attributed to the joist and residual effects are shown in Table 6. The less rigid joists, such as the TJI12, had a higher proportion of the total variance related to within-joist variability. These higher residual values indicate larger amounts of variation within joist types. Since less rigid joists will be more susceptible to outside effects, slight misalignment of the joist underneath the load cell or friction forces generated in the bearing support beneath the load cell are critical to obtaining accurate measurements of the lateral displacements and rotations.

Table 6. Static ANOVA Test Results: % Variance

Joist Type	Variance Component	Midpoint			Quarter		
		Top Flange	Bottom Flange	Rotation	Top Flange	Bottom Flange	Rotation
GP14	Joist	93.698	89.697	98.868	95.214	90.993	94.810
	Residual	6.302	10.303	1.132	4.786	9.007	5.190
GP12	Joist	87.506	91.810	75.466	89.496	93.514	91.146
	Residual	12.494	8.190	24.534	10.504	6.486	8.854
TJI12	Joist	66.789	59.117	89.719	72.653	48.549	48.146
	Residual	33.211	40.883	10.281	27.347	51.451	51.854

The results of the static test indicated that the joists tested were repeatable in their performance. However, due to the variability within a joist type, more joists are needed to fully characterize and entire joist type. Due to time limitations of this project, only three joists from each type could be tested

dynamically. This will not undermine the validity of the ANSYS model, but more testing is required to validate the model for an entire joist type.

4.3 Dynamic Test

Figure 16 shows the relationship between the weight of the test subject and maximum induced load on the top flange. A linear regression was fit for each joist type. The GP12 and GP14 I-joists have similar values and regressions. There is a significantly greater amount of variance within the TJI12 joists than the other two joist types.

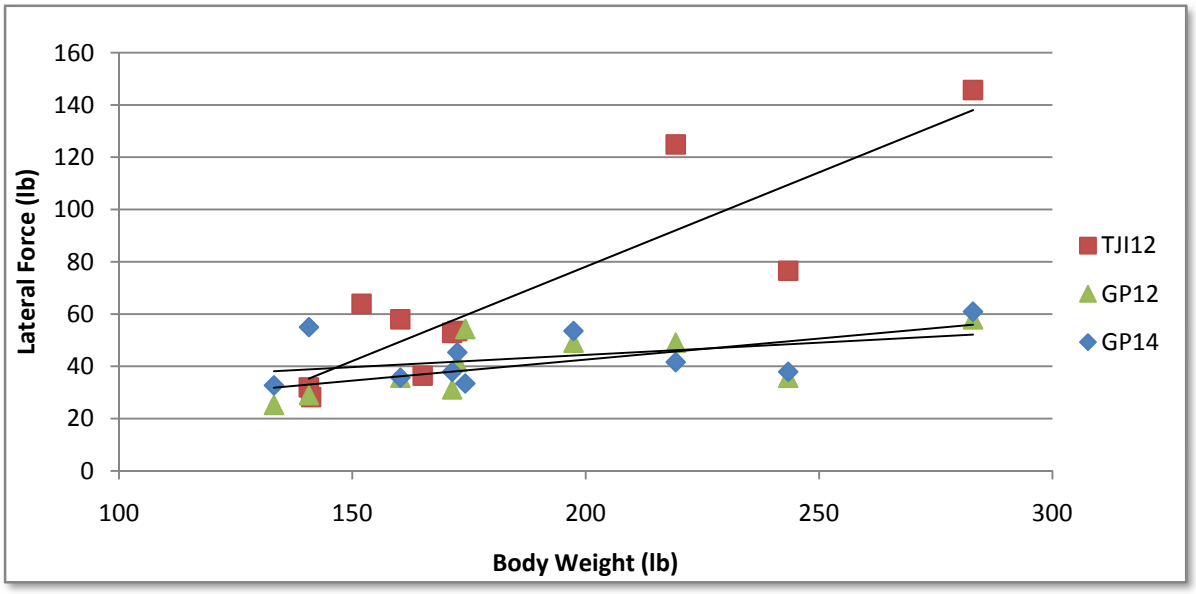

Figure 16. Body Weight versus Maximum Applied Lateral Load on Top Flange

Table 7 shows the slopes of these regression lines and corresponding coefficients of determination, r^2, as well as the lateral and polar moment of inertia, and the length of each joist type. The lateral and polar moments of inertia were calculated by assuming the material was isotropic. While this is not a precise method for determining the polar moment of inertia for an orthotropic material, it is provided for the comparison of rotational stiffness of each joist type. The GP14 joists were the stiffest joists with respect to lateral and rotational stability, while the TJI12 joists were the least stiff. Although the low r^2 values for the two GP joist types indicate that a linear regression may not be a suitable fit to the data points, there appears to be a trend among the weight of the test subject, the maximum applied lateral

force, and the joist type. In general, as the weight of the test subject increases, the maximum applied lateral force also increases. The higher r^2 for the TJI12 joists points toward this trend. Furthermore, as the lateral stiffness of the joist type is reduced, a higher load will be induced. This effect is illustrated by the increasing r^2 values with a decrease in joist stiffness.

Table 7. Trends in Body Weight and Applied Lateral Force

Joist Type	Slope	R-Squared	Lateral Moment of Inertia ($in.^4$)	Polar Moment of Inertia ($in.^4$)
GP14	0.093	0.20	3.19	243.8
GP12	0.161	0.45	3.18	208.9
TJI12	0.721	0.78	2.77	201.6

The top and bottom flange load cells did not measure similar load values as equilibrium would suggest. Figure 17 is a typical depiction of the lateral load caused by walking versus time graph. There are many possible explanations as to why the top and bottom flange load values are different. The load cells placed on the end supports attempted to capture the induced effects caused by the weight of the test subjects and divided the load into three components. In order to fully capture the induced loads, readings would have to be taken at the test subject's feet utilizing triaxial load cells. This method would prove technically difficult and time consuming. The load values are similar at the beginning and conclusion of the test, indicating that the load may disperse as it travels through the beam to the load cells. Second order effects are also present due to the loading of the I-joist away from the shear center, as well as a constantly changing center of mass of the test subject from walking. The graph also illustrates the vibration effects that occurred in the latter half of the beam represented by the closely spaced half-waves.

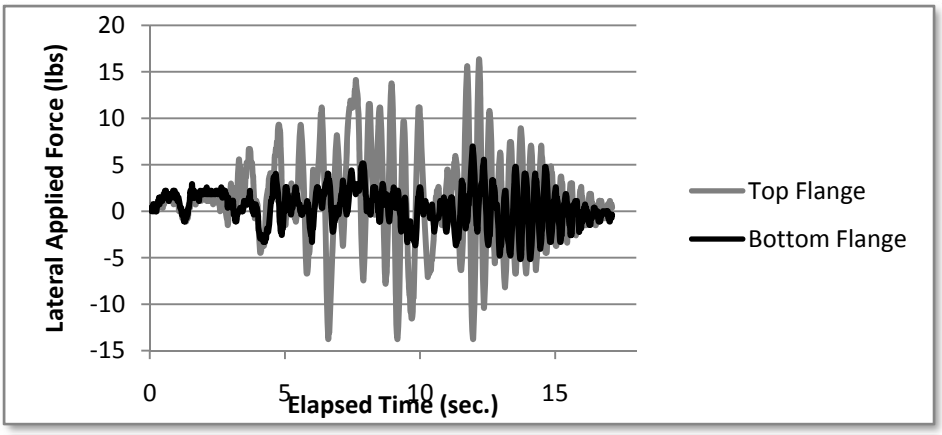

Figure 17. Variation of Top and Bottom Load Cell Readings

The relationship between body weight and maximum deflection was also of interest. Figure 18 depicts each test subject's average maximum lateral deflection over the six trials for each joist type and their corresponding weight. The maximum values were determined from the mid-span top flange data. For each joist type a regression was formulated. The slopes from the GP12 and GP14 were 0.008 and 0.007 respectively, while the slope for the TJI12 joists was considerable higher at 0.034. This suggests that the maximum applied deflection was more effected by the length of the I-joist rather than the geometric configuration. An ANOVA was also conducted with these results; no significant effect of the test subject's weight or joist type was found for the recorded deflection. For both tests the *p*-value was less than 0.001.

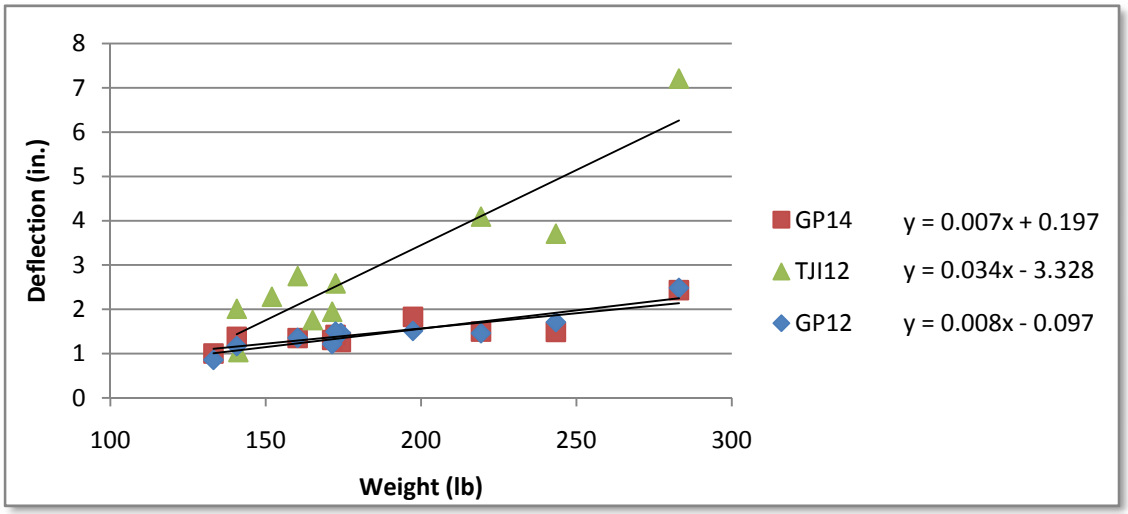

Figure 18. Average Maximum Deflection of Top Flange

The results of the dynamic test indicated that there is a strong relationship between the overall stiffness of the I-joist and the maximum load induced by the test subject. The results also indicated a strong relationship between the test subject's weight and the maximum applied load and maximum deflection of the joist.

4.4 Finite Element Modeling

This section compared the lateral displacement of the top and bottom flanges as well as the rotation at both the midpoint and quarter points to test the hypothesis that there was a significant difference between the data collected and the results from the finite element model. This section consisted of a quantitative analysis of the full pseudo-dynamic FE model and a qualitative analysis of the simulated FE model.

4.4.1 Full Pseudo-Dynamic Analysis

The full pseudo-dynamic analysis was compared to the acquired test data by the amount of error between the two maximum value curves (MVC). The MVC is generated from taking the magnitude of the largest values from a deflection curve; the full development is illustrated by Figure 19. The raw data is first normalized to an initial displacement of zero, Figure 19(a). The absolute value of this curve generates the absolute value curve seen in Figure 19(b). To create the MVC, Figure 19(c), only increasing data points were taken until the peak value; this process was applied from both ends of the graph. Details of the calculation of the MVC are provided in the Appendix.

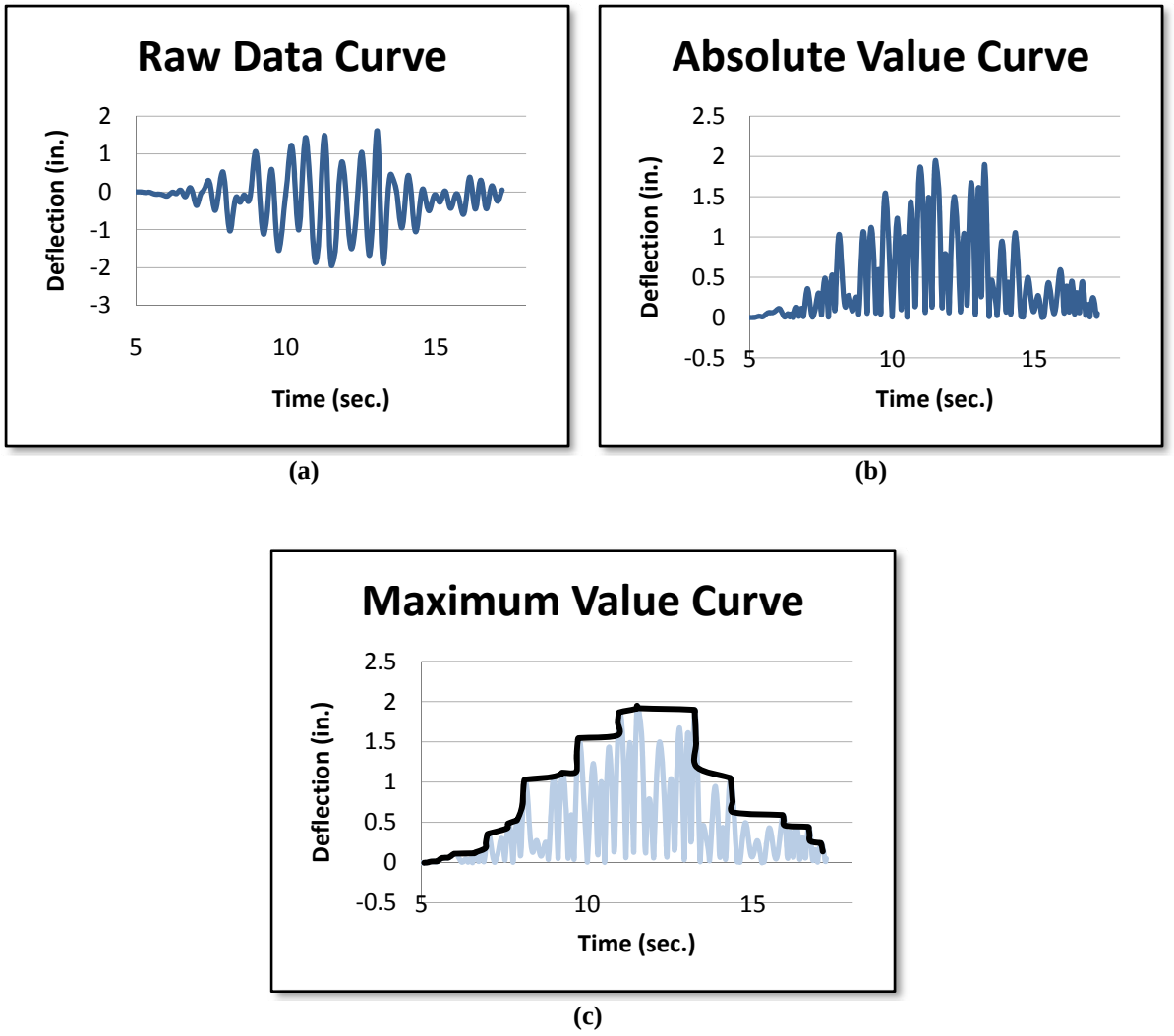

Figure 19. Development of the Maximum Value Curve

The data from the full pseudo-dynamic test was analyzed with two separate procedures. The first method compared the error between the two MVCs and compared the shapes of the curves. The second analysis focused on the peak values and the time at which they occurred.

4.4.1.1 Pseudo-Dynamic Test Analysis: Differences in Shape

Figure 20(a) shows a typical MVC from the acquired data and the corresponding values generated from ANSYS. The time scale for the graphs was converted to a percent of beam length for statistical comparison within joist types. The absolute value of the difference between the two curves was

computed on a point-by-point basis and a running average was calculated. Figure 20(b) depicts the average cumulative error between the two curves.

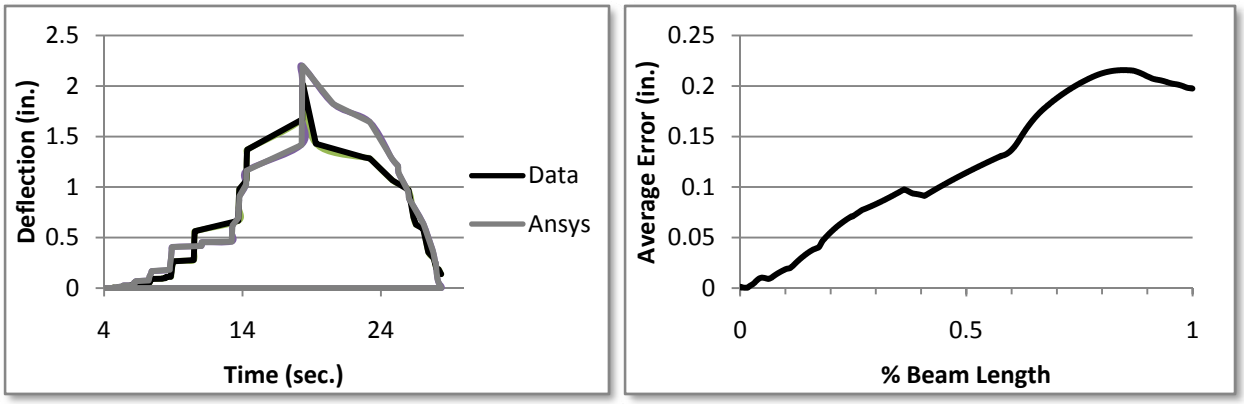

Figure 20. (a) MVC for Acquired Data and ANSYS Model (b) Average Error in Model

A pair of curves was generated for each recorded deflection and calculated rotation, each test subject, and each experimental replication. The allowable amount of error was arbitrarily set to 10 percent of the maximum recorded deflection for each pair of curves. Once the amount of error exceeded 10 percent, the percent of beam length reached was recorded. During some comparisons, the maximum amount of error was exceed and dropped back below the threshold of 10 percent. This was not factored into any of the analysis; once the limit was reached, the comparison was concluded.

In almost all instances, the model diverged at some point from the experimental data. During the acquisition of data, the vibration of the joist created additional deformations and lateral loads. This influence was concentrated on the latter half of the beam; therefore, a percent length value of 50 percent would be considered a good model. Moreover, on several recorded data sets, there were deflections at the time the test was concluded indicating that the beam was still in motion when the test subject stepped off. From visual observations after the test subject removed their weight, the joist had entered a state of free vibration.

Although the top and bottom flange deflections generated by ANSYS for a particular analysis may fit the acquired test data very well, the corresponding rotation of the beam may not be a very good

fit. The rotations were calculated on a point-by-point basis from the ANSYS data and the maximum rotation may not occur during periods of maximum lateral displacement.

Table 8 summarizes the results of the comparison between the acquired test data and the ANSYS model. According to the results of the comparison, the finite element model was able to predict the average deflections and rotations of the GP12 and GP14 joist with the stated 10% average error until 54.5% and 51.2% of the beam length, respectively. However, the model was only able to predict the average TJI12 movements until 31.2% of the beam length. The model predicted the lateral displacement of the top flange of the beam, regardless of location, the best, followed by the rotation and bottom flange displacement. An ANOVA was conducted to detect the differences due to the location of measurement on the percent of beam that passed. The results of the test stated that there was no statistical significance difference.

Table 8. Percent of Beam at which Model No Longer Corresponds to Test Data

	Midpoint			Quarter Point			
Joist Type	Top Flange	Bottom Flange	Rotation	Top Flange	Bottom Flange	Rotation	Average
GP14	59.7%	47.9%	61.1%	46.8%	46.9%	44.5%	51.2%
GP12	60.0%	49.6%	68.0%	38.8%	60.2%	50.2%	54.5%
TJI12	39.5%	23.8%	40.2%	18.7%	35.0%	29.9%	31.2%
Average	53.1%	40.4%	56.4%	34.8%	47.4%	41.5%	

4.1.1.2 Pseudo-Dynamic Test Analysis: Differences in Peak Value

In addition to determining the time at which the model no long fit the acquired data, the peak values of each curve and the corresponding time in the peak values were compared. This statistical analysis would determine how well the model predicted the peak value with respect to time. These two variables are defined in Figure 21. For the statistical analysis, these two variables are referred to as Time and Value and were calculated for each lateral displacement and rotation recorded.

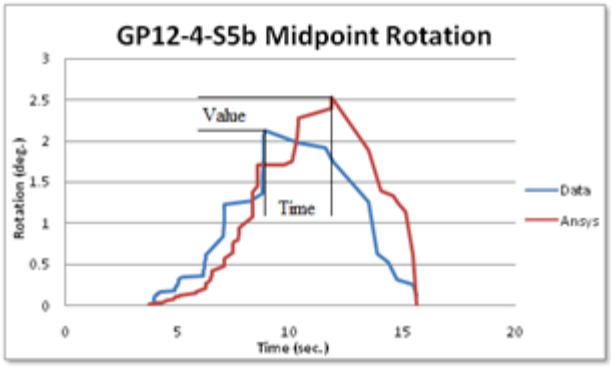

Figure 21. Definition of Time and Value for Pseudo-Dynamic Analysis

The analysis was accomplished by determining the peak values of both the acquired data and the ANSYS model and then normalizing based on the maximum acquired data value or the total elapsed time of test. A multifactor ANOVA was conducted to analyze the differences due to joist, test subject, location, and the type of deflection measured on both Time and Value. The results from this statistical analysis are summarized in Table 9 and Table 10.

Table 9. p-Values for Effects of Time versus Joist, Subject, Location and Deflection on 'Time'

Joist Type	Joist	Subject	Location	Deflection
GP14	<0.001	0.301	0.876	0.243
GP12	0.001	0.283	0.977	0.081
TJI12	0.023	0.470	0.542	0.950

Table 10. p-Values for Effects of Value versus Joist, Subject, Location and Deflection on 'Value'

Joist Type	Joist	Subject	Location	Deflection
GP14	<0.001	0.058	0.652	0.049
GP12	<0.001	0.071	0.205	0.464
TJI12	<0.001	0.038	0.031	0.156

When comparing the different peak values with respect to time, the only factor with a significant influence is the joist used. This fact makes it difficult to generalize the results of the ANSYS model. However, it is important to recognize that only three joists were dynamically loaded and virtually simulated. Because the sample population is not representative does not mean the models are incorrect. An ANOVA conducted with a larger sample size could provide more accurate results for each joist type.

The same conclusions can be made for the differences in peak value, although there does seem to be a trend between the test subjects. This trend suggests that there is some variability associated with the test subject.

4.4.2 Simplified Pseudo-Dynamic Analysis

The results from the simplified pseudo-dynamic analysis did not conform to any specific statistical test. The recorded deflections were graphed and grouped according to test subject, joist, location, and the type of deflection recorded. Each graph contained data from all joist testing replicates for each joist type, for a total of six different curves. The ANSYS model was also plotted and visually graded for goodness of fit. Ideally, the ANSYS model would fully encase the acquired data with only one or two peak values exceeding the curve created by the ANSYS model. Data from the first half of the joist was given more emphasis due to the dynamic effects in the second half of the joist not captured by the computer model. The graphs were visually rated one to five depending on how conservative or un-conservative the ANSYS model represented the acquired test data. Graphs where the peak values were approximately 50% or more apart were deemed either 1 for overly conservative or 5 for overly un-conservative. A value of 3 was assigned to those graphs that resembled the acquired data very well. The graphs were graded twice in a random order, to prevent any bias from a particular joist type. Figure 22 shows a graphical representation of grades 1, 3, and 5.

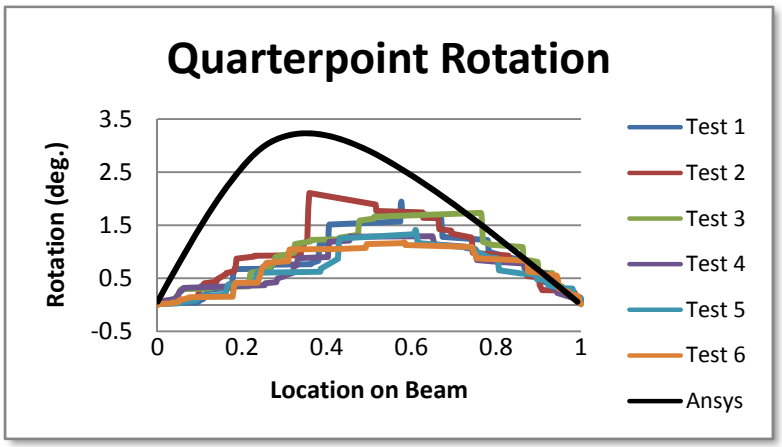

(a) Rating 1

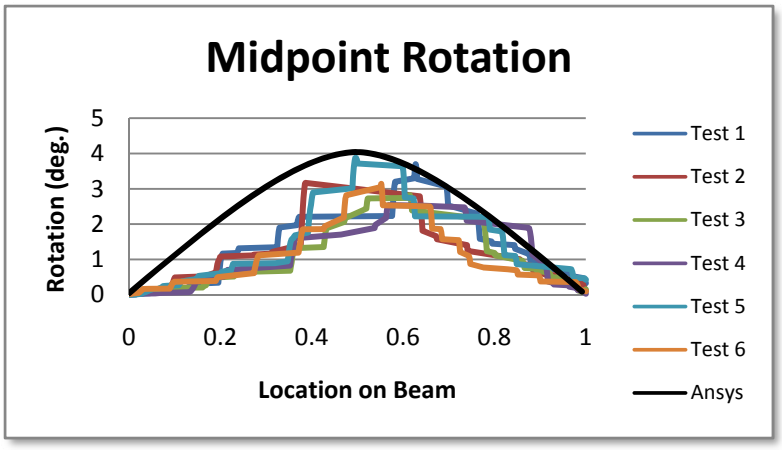

(b) Rating 3

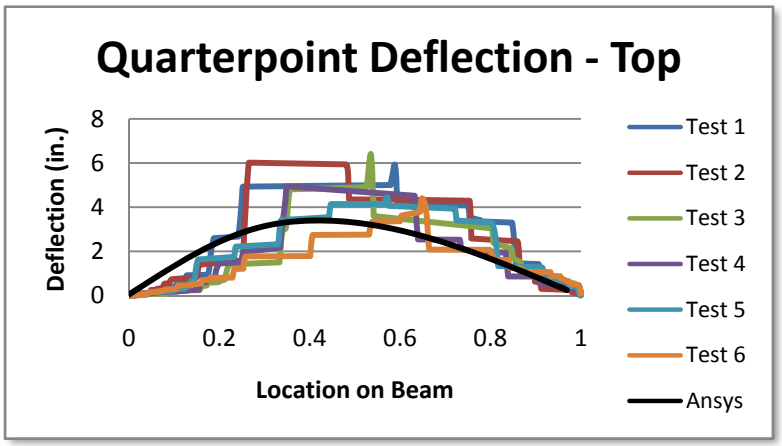

(c) Rating 5

Figure 22. Representations of Ratings used to Categorize Simplified Pseudo-Dynamic Graphs

Table 11 shows the number of average rating for each deflection measurement classified by joist type. Average values lower than 3.0, as in the GP14 and GP12, indicate that the model is slightly conservative, while the TJI12 joists had average values above 3.0, indicating that the model is not conservative. The load values used in the ANSYS model were generated by using a constant percentage of the test subjects body weight for all three simplified models. From observing the results of the simplified analysis, it may be more appropriate to relate the induced load to the length of the beam and the polar moment of inertia. There does not appear to be any effect on the location of the measurement and the applicability of the ANSYS model; however, the type of measurement does show a trend. The model predicted the bottom flange lateral deflection the best, followed by the rotation and then the top

flange lateral displacement. This contrasts the results from the full pseudo-dynamic tests in which the order of the measurement type was reversed.

Table 11. Results from Simplified ANSYS Model

Joist Type	Midpoint			Quarter Point			Average
	Top Flange	Bottom Flange	Rotation	Top Flange	Bottom Flange	Rotation	
GP14	2.40	3.05	2.20	2.25	2.90	2.10	2.48
GP12	2.65	2.80	2.65	2.55	2.60	2.75	2.67
TJI12	3.20	3.30	3.40	3.25	3.10	4.10	3.39

Overall the finite element model was judged to be applicable to describe the lateral torsional buckling behavior of the GP14 and GP12 wood composite I-joists. The ANSYS model predicted the deflections of these beams to the midpoint of the beam within the 10 percent deviation limit. However, the variability in the numerous analytical comparisons indicates that the model does not represent the behavior of the TJI12 I-joists. The full pseudo-dynamic analysis indicated that the model deviated from the acquired test data almost immediately and the simplified analysis indicated that the model was un-conservative for all measurements.

Chapter 5: Summary and Conclusions

5.1 Summary

The focus of this research was to characterize the behavior of dynamic loads on wood composite I-joist through the use of finite element models. Wood I-joists were tested statically and dynamically. Dynamic loads were induced by human test subjects traversing the beam. In both testing configurations, the lateral displacement of the top and bottom flanges at both the midpoint and quarter-point were recorded. In the static tests, the rotation of the beam at the two locations was measured through the use of clinometers. In the dynamic test, the rotation was calculated from the difference of the top and bottom flange lateral deflection measurements. Three different types of wood composite I-joists were tested ranging in depth from 11 7/8 to 14 inches and in length from 20 to 24 feet. The measured loads were then used as inputs for a finite element model generated using ANSYS. The results of the dynamic test were then compared to the results of the finite element model.

5.2 Conclusions

The following trends have been observed from the acquired test data, the finite element model, and their corresponding relationship:

5.2.1 Static Test

- Variability within replicate tests was not significant. Only a few replicate tests are needed in order to characterize the behavior of a particular joist.
- Variability within joists increased as lateral and rotational stiffness decreased. This is related to the effects of outside influences; as stiffness decrease, these influences become more present in the recorded deflections and rotations. These outside effects may be a slight misalignment of the joist underneath the load cell or friction forces generated in the bearing support beneath the load cell

5.2.2 Dynamic Test

- As the weight of a person traversing the I-joist increases, the amount of lateral deflection and rotation increase. This trend increased as the length of the joist increased or the polar moment of inertia decreased.
- As the weight of a person traversing the I-joist increased, the amount of load transferred to the top and bottom flanges also increased. This trend increased with length, although the results show no significant difference within the polar moment of inertia.

5.2.3 Validity of Finite Element Model

- The full pseudo-dynamic finite element model was able to predict the GP12 and GP14 joist types beyond the halfway point of the beam; however the TJI12 joist types failed to reach this goal, being accurate to only 31.2 percent.
- The difference in both the peak values and the corresponding time from the acquired test data and the ANSYS models were dependent on the particular joist. Further testing and modeling are required to generalize the lateral torsional buckling behavior of an entire joist type.
- The simplified finite element model, based on the constant percentage of the test subject's weight proved a decent model for deflections and rotations of the GP14 and GP12 joist types over the first half of the beam. The model generated un-conservative results for the TJI12 joists.

5.3 Limitation

Some limitations of this research were subject to the availability of resources or the time frame of the project. Due to the resources at hand, 5 GP12, 5 GP14, and 4 TJI joists of each type were available for the static testing. The time frame of this project further reduced the dynamic testing of the joists to 3 joists of each type as well as limiting the number of test subjects.

Ideally a full dynamic finite element model would have been created. However due to time limitations associated with creating and solving the model effects due to vibration, dampening or any other harmonic effects were negated. As a result the model was deemed sufficient if it could accurately predict the deflections and rotations up to the midpoint of the beam.

The simulated model relied on a constant relationship between the test subject and the induced loads. The scope of this research prohibited the development of any factor that would modify the induced loads to account for balancing abilities of the test subject.

5.4 Future Work

Due to the difficult nature of testing long slender beams it is recommended that future work conducted on unbraced wood composite I-joists be limited to lengths no longer than 20 feet.

A correlation between the polar moment of inertia of the I-joist and the induced loads and or deflections could be determined. Using many joists of the same type as well as numerous test subjects of varying weights, could provide a valuable correlation between these variables. A similar study could be conducted by varying the joist length within a set joist type. This could yield a correlation between joist length and the induced loads and or deflections. These relationships could be used to refine the inputs used in the simplified dynamic analysis to generate more consistent results.

Further studies could concentrate on developing a fully dynamic finite element response. This could result in a model capable of accounting for the vibration effects seen in the latter half of the beam. Combined with the possible results of the aforementioned relationship studies, this research could yield a finite element model capable of accurately modeling a test subject's movement across the entire I-joist.

Future research could focus on different loading conditions of the beam. In addition to traversing the beam longitudinally, construction workers in the field would often side step across the beams. This loading condition could induce larger deflections and loads than those recorded in this research. Finite element modeling of this loading condition could be conducted. Combined with the modeling results of this and other future research, guidelines to I-joist design and bracing could be imposed.

Literature Cited

AF&PA (2003). Technical Report 14: Designing for Lateral-Torsional Stability in Wood Members. Washington, DC, American Forest & Paper Association, Inc.

AF&PA (2005). National Desgin Specifications for Wood Construction. Washington, DC, AF&PA American Wood Council.

Bodig, J. and B. A. Jayne (1982). Mechanics of Wood and Wood Composites. New York, Van Nostrand Reinhold Compnay Inc.

Bolotin, V. V. (1964). The Dynamic Stability of Elastic Systems. San Francisco, Holden-Day, Inc.

Bowyer, J. L., R. Shmulsky and J. G. Haygreen (2002). Forest Products and Wood Science. Ames, Iowa, Iowa State Press.

Burow, J. R., H. B. Manbeck and J. J. Janowiak (2006). "Lateral Stability of Composite Wood I-joist Under Concentrated-Load Bending." Transactions of the ASABE **49**(6): 1867-1880.

Chen, W. F. and W. M. Lui (1987). Structural Stability: Theory and Implementation. New York, Elsevier Science Publishing Co., Inc.

Cook, Robert D., D. S. Malkus, M. E. Plesha, R. J. Witt (2002). Concepts and Applications of Finite Element Analysis. John Wiley & Sons, Inc.

Croll, J. G. A. and A. C. Walker (1972). Elements of Structural Stability. London and Basingstoke, The Macmillan Press Ltd.

Figueiredo, F. P., J. G. S. d. Silva, L. R. O. d. Lima, P. C. G. d. S. Vellasco and S. A. L. d. Andrade (2007). "A Parametric Study of Composite Footbridges Under Pedestrian Walking Loads." Engineering Structures **30**(3): 605-615.

Guan, Z. E. and E. C. Zhu (2004). "Nonlinear Finite Element Modeling of Cracked Behavior in Oriented Strand Board Webbed Wood I-Beams with Openings." Journal of Structural Engineering **130**(10): 1562-1569.

Literature Cited

Hindman, D. P., H. B. Manbeck and J. J. Janowiak (2005a). "Measurement and Prediction of Lateral Torsional Buckling Loads of Composite Wood Materials: I-joists Sections." Forest Products Journal **55**(10): 43-48.

Hindman, D. P., H. B. Manbeck and J. J. Janowiak (2005b). "Torsional Rigidity of Rectangular Wood Composite Materials." Wood and Fiber Science **37**(2): 283-291.

Hindman, D. P., H. B. Manbeck and J. J. Janowiak (2005c). "Torsional Rigidity of Wood Composite I-joists." Wood and Fiber Science **37**(2).

Hooley, R. F. and R. H. Devall (1972). Lateral Buckling of Simply Supported Glued Laminated Beams. Report to Laminated Timber Institute of Canada. Dept. of Civil Engineering, University of British Columbia.

Hooley, R. F. and B. Madsen (1964). "Lateral Stability of Glued Laminated Beams." ASCE -- Proceedings -- Journal of the Structural Division.

Huang, M.-H., D. P. Thambiratnam and N. J. Perera (2006). "Dynamic Performance of Slender Suspension Footbridges Under Eccentric Walking Dynamic Loads." Journal of Sound and Vibration **303**(1): 239-254.

Huang, X. and J. Hinze (2003). "Analysis of Construction Worker Fall Accidents." Journal of Construction Engineering and Management **129**(3): 262-271.

Janowiak, J. J., D. P. Hindman and H. B. Manbeck (2001). "Orthotropic Behavior of Lumber Composite Materials." Wood and fiber science **33**(4).

Jones, R. M. (1999). Mechanics of Composite Materials. Philadelphia, PA, Taylor & Francis, Inc.

Lipscomb, H. J., L. Li and J. M. Dement (2003). "Falls Among Union Carpenters." American Journal of Industrial Medicine **44**(2): 148-156.

Nethercot, D. A. and K. C. Rockey (1971). "Finite Element Sotions for the Buckling of Columns and Beams." International Journal of Mechanical Science **13**(11): 945-949.

Simitses, G. J. (1986). An Introduction to the Elastic Stability of Structure. Malabar, FL, Rober E. Krieger Publishing Company, Inc.

Literature Cited

Tabiei, A. and J. Wu (2000). "Three-dimensional Nonlinear Orthotropic Finite Element Model for Wood." Composite Structures **50**(2): 143-149.

Timoshenko, S. P. and J. M. Gere (1961). Theory of Elastic Stability, McGraw Hill.

USDA (1999). Wood Handbook - Wood as and Engineering Material. Madison, Wisconsin, Forest Products Laboratory.

Wang, Y. C., M. A. El-Khenfas and D. A. Nethercot (1987). "Lateral-Torsional Buckling of End-Restrained Beams." Journal of Constructional Steel Research **7**(5): 335-362.

Weyerhaeuser (2004). "Design Values for Structurwood® Panels." techbulletin: Technical Updates G1401. Weyerhaeuser Company.

Zhu, E. C., Z. W. Guan, P. D. Rodd and D. J. Pope (2005). "Buckling of Oriented Strand Board Webbed Wood I-Joists." Journal of Structural Engineering **131**(10): 1629-1637.

Ziemian, R. D., J. E. Schwarz, M. R. Emerson and D. R. Potts (2004). Stability of Unbraced Steel Joists Subject to Mid-span Loading. Annual Stability Conference, Structural Stability Research Council.

Appendix A: MATLAB Programs

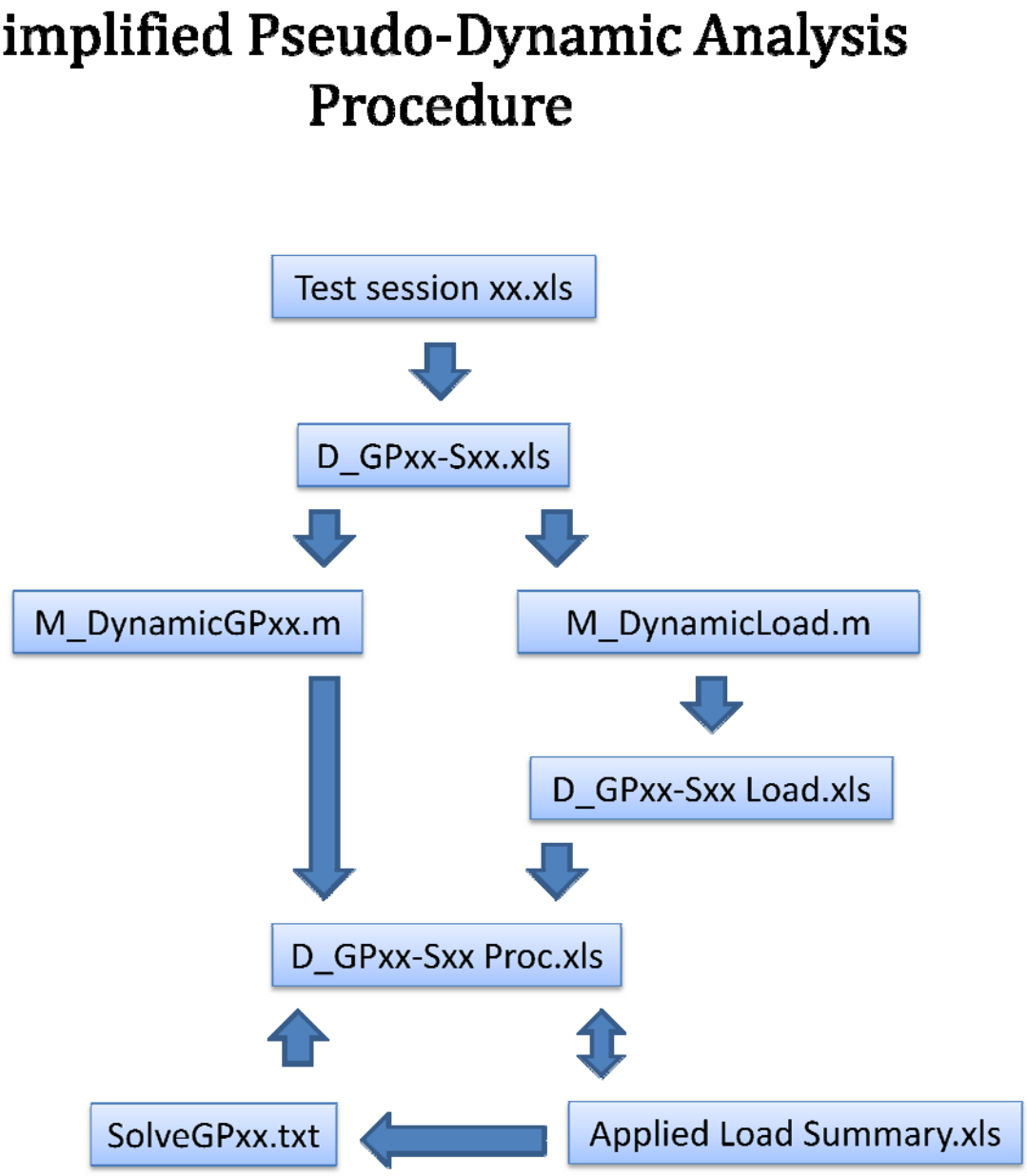

Full Pseudo-Dynamic Analysis Procedure

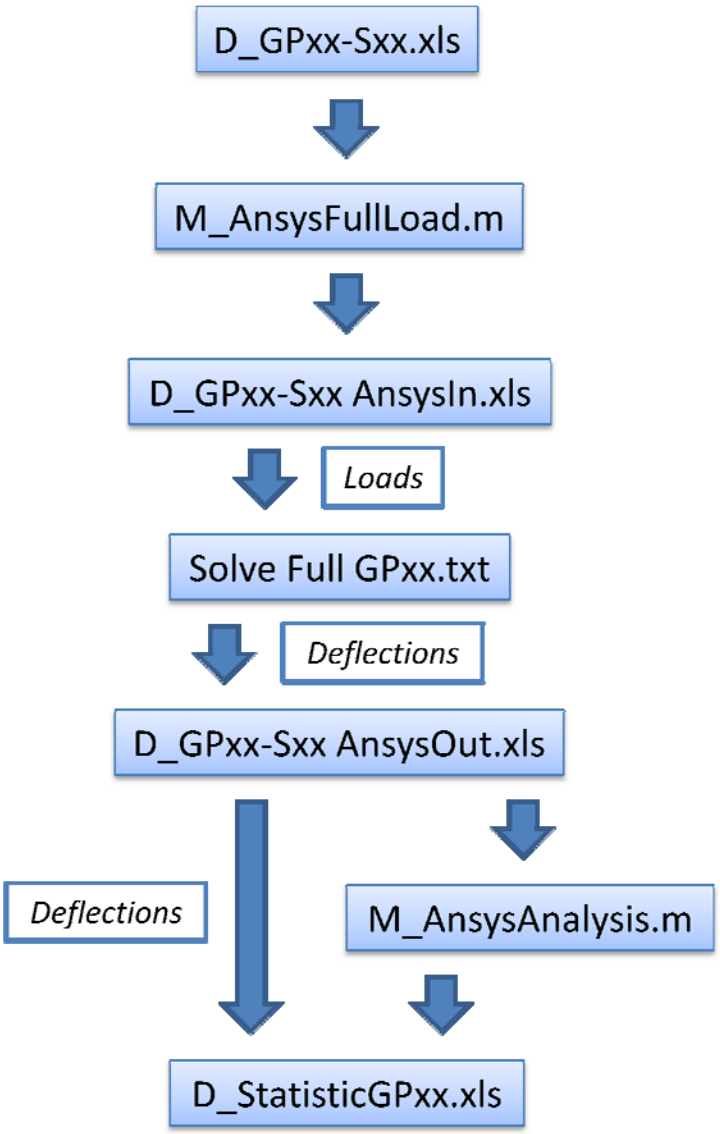

M_DynamicLoad.m

```
%  This file reduces the data from the individual test set files D_GPxx-Sxx
%  or D_GPxx-Sxx.  The load cell values are adjusted to zero but no
%  adjustment is made to the sign of the values.  This file outputs
%  'D_GPxx-Sxx Load.xls'

clear all;
%% Inputs
filename='D_GP14-S5';
var=[filename,' Load'];

for sheet=1:6
    data=xlsread(filename,sheet);

%% Determine Start & Stop Point of Data Based on Non-Zero Load
x=1;
while x<length(data)
    x=x+1;
    if data(x,3)>75
        start=x;
        x=length(data);
    end
end
x=length(data)+1;
while x<length(data)+2
    x=x-1;
    if data(x,4)>75
        stop=x;
        x=length(data)+3;
    end
end

%% Condense Data Based on Starting Point and Zero Data
data1(stop-start,10)=0;
for x=1:stop-start+1
    data1(x,1)=data(x+start,1);
    for y=2:10
        data1(x,y)=data(x+start,y)-data(1,y);
    end
end

%% Create Absolute Value Curve (AVC)
for x=1:length(data1)
    for y=3:6
        if data1(x,y)<0
            data1(x,y)=-data1(x,y);
        end
    end
end

%% Reset ID to %Completed
for x=1:length(data1)
    data1(x,1)=(data1(x,1)-start)/(stop-start+1);
```

```
end

%% Determine Maximum Value Curve (MVC) Points
dataset=data1;
data2(1,1)=0;
counter=2;
for Row=3:6
    output=MF_MVCData(dataset,Row);
    for x=1:length(output)
        data2(x,Row-counter)=output(x,1);
        data2(x,Row-counter+1)=output(x,2);
    end
    counter=counter-1;
end

%% Adjust Ch23 and Ch24 to Zero Starting Load

ch23=data2(1,6);
ch24=data2(1,8);
for x=1:length(data2)
    data2(x,6)=data2(x,6)-ch23;
    data2(x,8)=data2(x,8)-ch24;
end

%% Write Excel File
xlswrite(var,data2,sheet);
clear data;
clear data1;
clear data2;
clear dataset;
clear start;
clear stop;
clear row;
clear counter;
clear output;

end
```

MF_MVCData.m

```
%  This MatLAB function reduces the absolute value curve created from the
%  actual test data into the maximum value curve.

function [output]=MF_MVCData(dataset,Row)

%% Separate Increasing from Decreasing Data Points
z(length(dataset),1)=0;
for x=2:length(dataset)
    if dataset(x,Row)>dataset(x-1,Row)
        z(x,1)=x;
    end
end
```

```
%% Determine Maximum Points
Max(1,1)=1;
a=2;
for x=1:length(z)-1
    if z(x,1)>1
        Max(a,1)=x;
        a=a+1;
    end
end
Max(length(Max)+1,1)=length(z);

%% Determine Only Increasing Slopes
Max2(1,1)=1;
a=2;
Maxval=0;
for x=2:length(Max)
    if dataset(Max(x),Row)>Maxval
        Max2(a,1)=Max(x);
        Maxval=dataset(Max(x),Row);
        a=a+1;
    end
end

%% Determine Only Decreasing Slopes
Max3(1,1)=Max(length(Max));
a=2;
Maxval=0;
for x=2:length(Max)
    if dataset(Max(length(Max))-x,Row)>Maxval
        Max3(a,1)=Max(length(Max))-x;
        Maxval=dataset(Max(length(Max))-x,Row);
        a=a+1;
    end
end

%% Combine Max2 and Max3
Max4=Max2;
a=length(Max2)+1;
for x=1:length(Max3)-1
    Max4(a,1)=Max3(length(Max3)-x);
    a=a+1;
end

%% Create Maximum Value Curve
output(length(Max4),2)=0;
for x=1:length(Max4)
    output(x,1)=dataset(Max4(x),1);
    output(x,2)=dataset(Max4(x),Row);
end

end
```

M_DynamicGPxx.m

```
%  This file reduces the data from the individual test set files D_GPxx-Sxx
%  The rotations are calculated and the Absolute Value Curve for the
%  deflections and rotations are created.  The center to center distance
%  between flanges (jheight) is required.  This file outputs
%  'D_GPxx-Sxx Proc.xls'

clear all;
%% Inputs
filename='D_GP12-S10';
jheight=10.447;
var=[filename,' Proc'];

for sheet=1:6
    data=xlsread(filename,sheet);

%% Determine Start & Stop Point of Data Based on Non-Zero Load
x=1;
while x<length(data)
    x=x+1;
    if data(x,3)>75
        start=x;
        x=length(data);
    end
end
x=length(data)+1;
while x<length(data)+2
    x=x-1;
    if data(x,4)>75
        stop=x;
        x=length(data)+3;
    end
end

%% Condense Data Based on Starting Point and Zero Data
data1(stop-start,10)=0;
for x=1:stop-start+1
    data1(x,1)=data(x+start,1);
    for y=2:10
        data1(x,y)=data(x+start,y)-data(1,y);
    end
end

%% Determine Angle of Rotation at MP and QP
data2=data1;
for x=1:length(data2)
    data2(x,11)=asind((data2(x,7)-data2(x,8))/jheight);
    data2(x,12)=asind((data2(x,9)-data2(x,10))/jheight);
end

%% Create Absolute Value Curve (AVC)
data3=data2;
for x=1:length(data3)
```

```
    for y=7:12
        if data3(x,y)<0
            data3(x,y)=-data3(x,y);
        end
    end
end

%% Reset ID to %Completed
for x=1:length(data3)
    data3(x,1)=(data3(x,1)-start)/(stop-start+1);
end

%% Determine Maximum Value Curve (MVC) Points
dataset=data3;
data4(1,1)=0;
counter=6;
for Row=7:12
    output=MF_MVCData(dataset,Row);
    for x=1:length(output)
        data4(x,Row-counter)=output(x,1);
        data4(x,Row-counter+1)=output(x,2);
    end
    counter=counter-1;
end

xlswrite(var,data4,sheet);
clear data;
clear data1;
clear data2;
clear data3;
clear data4;
clear dataset;
clear start;
clear stop;
clear row;
clear counter;
clear output;

end
```

M_AnsysFullLoad.m

```
% This M-File produces the loads and deflections/rotations from a test
% session.  The values are adjusted to zero.  The ID number of the input
% file is reset to the %of beam completed which is used to determine the
% point at which the load is applied and the magnification factor. This
% function requires the input excel spreadsheet formated in accordance
% with D_GP12-S1.  The center to center flange distance (jheight) and beam
% length (Length) must also be changed according to the joist size being
% analyzed.  The output of this code is 'D_GPxx-Sxx AnsysIn'.

clear all;
%% Inputs
filename='D_TJI12-S5';
```

```
jheight=10.456;
Length=288;
var=[filename,' AnsysIn'];

for sheet=1:6
    data=xlsread(filename,sheet);

%% Determine Start & Stop Point of Data Based on Non-Zero Load
x=1;
while x<length(data)
    x=x+1;
    if data(x,3)>75
        start=x;
        x=length(data);
    end
end
x=length(data)+1;
while x<length(data)+2
    x=x-1;
    if data(x,4)>185
        stop=x;
        x=length(data)+3;
    end
end

%% Condense Data Based on Starting Point and Zero Data
data1(stop-start,10)=0;
for x=1:stop-start+1
    data1(x,1)=data(x+start,1);
    for y=2:10
        data1(x,y)=data(x+start,y)-data(1,y);
    end
end

%% Determine Angle of Rotation at MP and QP
data2=data1;
for x=1:length(data2)
    data2(x,11)=asind((data2(x,7)-data2(x,8))/jheight);
    data2(x,12)=asind((data2(x,9)-data2(x,10))/jheight);
end

%% Reset ID to %Completed
for x=1:length(data2)
    data2(x,1)=(data2(x,1)-start)/(stop-start+1);
end

%% Row 13 Load Point
for x=1:length(data2)
    data2(x,13)=round(data2(x,1)*Length);
end

%% Row 14 Magnification Factor
for x=1:length(data2)
    data2(x,14)=1/(1-data2(x,13)/Length);
end
```

```
%% Write Excel File
xlswrite(var,data2,sheet);
clear data;
clear data1;
clear data2;
clear start;
clear stop;

end
```

M_AnsysAnalysis.m

```
% This M-File formates the recorded data and the data generated by ANSYS
% into Maximum Value Curves.  This code only uses certain parts of the
% input spreadsheets. This file requires the input variables to be
% formated in accordance with 'D_GP12-S1 AnsysIn.xls' and 'D_GP12-S1
% AnsysOut.xls'.  The output of this code is D_StatisticGP12.xls'.

clear all;

for sheet=1:6
    if sheet<7
     Sheet2='3b';
    end
    if sheet<6
     Sheet2='3a';
    end
    if sheet<5
     Sheet2='2b';
    end
    if sheet<4
     Sheet2='2a';
    end
    if sheet<3
     Sheet2='1b';
    end
    if sheet<2
     Sheet2='1a';
    end

%% Read Excel Input File
Data=xlsread('D_TJI12-S5 AnsysIn.xls',['sheet',num2str(sheet)],'G1:L2000');
Ansys=xlsread('D_TJI12-S5 AnsysOut.xls',Sheet2,'G3:L2000'); %K3:P2000 for 14
Time=xlsread('D_TJI12-S5 AnsysOut.xls',Sheet2,'A3:A2000');  %G3:L2000 for 12


%% Insert Time Values Into Data1 and Ansys1
Data1=Time;
for y=1:6
for x=1:length(Data1)
    Data1(x,y+1)=Data(x,y);
end
end
```

```
Ansys1=Time;
for y=1:6
for x=1:length(Ansys1)
    Ansys1(x,y+1)=Ansys(x,y);
end
end

%% Create Absolute Value Curves (AVC)
for x=1:length(Ansys1)
    for y=2:7
        if Ansys1(x,y)<0
            Ansys1(x,y)=-Ansys1(x,y);
        end
    end
end

for x=1:length(Data1)
    for y=2:7
        if Data1(x,y)<0
            Data1(x,y)=-Data1(x,y);
        end
    end
end

%% Determine Maximum Value Curve (MVC) Points
counter=24;
for Row=2:7
    Out_Data=MF_MVCAnsys(Data1,Row);
    Out_Ansys=MF_MVCAnsys(Ansys1,Row);
    for x=1:length(Out_Data)
        Output(x,25-counter)=Out_Data(x,1);
        Output(x,25-counter+1)=Out_Data(x,2);
    end
    for x=1:length(Out_Ansys)
        Output(x,25-counter+2)=Out_Ansys(x,1);
        Output(x,25-counter+3)=Out_Ansys(x,2);
    end
    counter=counter-4;
end

%% Write Excel File

xlswrite('D_StatisticTJI12-S5.xls',Output,Sheet2);
clear Data
clear Data1
clear Out_Data
clear Ansys
clear Ansys1
clear Out_Ansys
clear Time
clear counter
clear Output

end
```

MF_MVCAnsys.m

```
%  This MatLAB function reduces the absolute value curve created from the
%  ANSYS computer model into the maximum value curve.

function [output]=MF_MVCAnsys(dataset,Row)
%% Determine Increasing Data Points
Max1(1,1)=1;
a=2;
for x=2:length(dataset)
    if dataset(x,Row)>dataset(x-1,Row)
        Max1(a,1)=x;
        a=a+1;
    end
end
%% Determine Only Increasing Slopes
Max2(1,1)=1;
a=2;
Maxval=0;
for x=2:length(Max1)
    if dataset(Max1(x),Row)>Maxval
        Max2(a,1)=Max1(x);
        Maxval=dataset(Max1(x),Row);
        a=a+1;
    end
end

%% Determine Only Decreasing Slopes
Max3(1,1)=length(dataset);
aa=2;
Maxval=dataset(length(dataset),Row);
for x=0:length(Max1)-1
    if dataset(Max1(length(Max1)-x),Row)>Maxval
        Max3(aa,1)=Max1(length(Max1)-x);
        Maxval=dataset(Max1(length(Max1)-x),Row);
        aa=aa+1;
    end
end

%% Combine Max2 and Max3
Max4=Max2;
a=length(Max2)+1;
for x=1:length(Max3)-1
    Max4(a,1)=Max3(length(Max3)-x);
    a=a+1;
end

%% Create Maximum Value Curve
output(length(Max4),2)=0;
for x=1:length(Max4)
    output(x,1)=dataset(Max4(x),1);
    output(x,2)=dataset(Max4(x),Row);
end
end
```

M_PostProc1.m

```
% This file creates D_ModSXGPXX.xls for processing the relationship
% between the Ansys model and the data collected.

clear all
fileout='D_ModS5TJI12.xls';
sheetname='D_StatisticTJI12-S5.xls';

for i=1:6
%% Identify Range of Inputs for the 6 Test Summary Sheets
    if i<7
        cell='U1:X2000';
    end
    if i<6
        cell='Q1:T2000';
    end
    if i<5
        cell='M1:P2000';
    end
    if i<4
        cell='I1:L2000';
    end
    if i<3
        cell='E1:H2000';
    end
    if i<2
        cell='A1:D2000';
    end

%% Import Test Summary
data1=xlsread(sheetname,'1a',cell);
data2=xlsread(sheetname,'1b',cell);
data3=xlsread(sheetname,'2a',cell);
data4=xlsread(sheetname,'2b',cell);
data5=xlsread(sheetname,'3a',cell);
data6=xlsread(sheetname,'3b',cell);

ts=0.01;

%% Separate Ansys model form Data

set1=MF_Difference(data1,ts);
set2=MF_Difference(data2,ts);
set3=MF_Difference(data3,ts);
set4=MF_Difference(data4,ts);
set5=MF_Difference(data5,ts);
set6=MF_Difference(data6,ts);

Maxl(1,1)=length(set1);
Maxl(2,1)=length(set2);
Maxl(3,1)=length(set3);
Maxl(4,1)=length(set4);
Maxl(5,1)=length(set5);
```

```
Maxl(6,1)=length(set6);

ML=max(Maxl)+1;

set1(ML,3)=0;
set2(ML,3)=0;
set3(ML,3)=0;
set4(ML,3)=0;
set5(ML,3)=0;
set6(ML,3)=0;

output=[set1,set2,set3,set4,set5,set6];

xlswrite(fileout,output,i);

end
```

M_PostProc2.m

```
% This file creates D_PeakSXGPXX.xls for processing the peak load values
% and corresponding peak time values to determine the relationship
% between the Ansys model and the data collected.

clear all
% fileout='D_PeakS1GP12.xls';
sheetname='D_StatisticGP12-S5.xls';

for i=1:2
%% Identify Range of Inputs for the 6 Test Summary Sheets
    if i<7
        cell='U1:X2000';
    end
    if i<6
        cell='Q1:T2000';
    end
    if i<5
        cell='M1:P2000';
    end
    if i<4
        cell='I1:L2000';
    end
    if i<3
        cell='E1:H2000';
    end
    if i<2
        cell='A1:D2000';
    end

%% Import Test Summary
data1=xlsread(sheetname,'1a',cell);
data2=xlsread(sheetname,'1b',cell);
data3=xlsread(sheetname,'2a',cell);
data4=xlsread(sheetname,'2b',cell);
```

```
data5=xlsread(sheetname,'3a',cell);
data6=xlsread(sheetname,'3b',cell);

ts=0.01;

%% Separate Ansys model form Data
set1=MF_PeakDiff(data1);
set2=MF_PeakDiff(data2);
set3=MF_PeakDiff(data3);
set4=MF_PeakDiff(data4);
set5=MF_PeakDiff(data5);
set6=MF_PeakDiff(data6);
ifout=vertcat(set1,set2,set3,set4,set5,set6);

if i<2
    output=ifout;
end
if i>1
    output=vertcat(output,ifout);
end
end
```

MF_Difference.m

```
function [output]=MF_Difference(data1,ts)

for x=1:length(data1)
    data1_Ansys(x,1)=data1(x,1);
    data1_Ansys(x,2)=data1(x,2);
end

for x=1:length(data1)
    data1_Data(x,1)=data1(x,3);
    data1_Data(x,2)=data1(x,4);
end

DataN=MF_Norm(data1_Data,ts);
AnsysN=MF_Norm(data1_Ansys,ts);

average=0;

for x=1:length(DataN)
    output(x,1)=DataN(x,1);
    output(x,2)=abs(DataN(x,2)-AnsysN(x,2))*ts*100;
    average=average*(x-1)/x+abs(DataN(x,2)-AnsysN(x,2))*ts*(1/x)*100;
    output(x,3)=average;
end
end
```

MF_Difftime.m

```
function [difftime]=MF_Difftime(matrix)

for x=1:length(matrix)
    if matrix(x,1)>0
        difftime=matrix(x,1)-matrix(1,1);
    end
end
end
```

MF_Interp.m

```
function [output]=MF_Interp(x1,x2,t1,t2,tval)
if tval<t1
    Interpolation_Error_tvall<t1
end
if tval>t2
    Interpolation_Error_tval>t2
end
output=(tval-t1)/(t2-t1)*(x2-x1)+x1;
```

MF_Norm.m

```
function [output]=MF_Norm(data,ts)

% Determine Start/End Times
tstart=data(1,1);
tend=0;

for x=0:length(data)
    tend=data(length(data)-x,1);
    if tend>0
        break;
    end
    x=x+1;
end

counter=1;
counter1=1;
for tcur=tstart:ts:tend-ts
    if tcur>data(counter+1,1)
        counter=counter+1;
    end

xcur=MF_Interp(data(counter,2),data(counter+1,2),data(counter,1),data(counter
+1,1),tcur);
    output(counter1,1)=tcur;
    output(counter1,2)=xcur;
    counter1=counter1+1;
end
```

```
% Reset ID to %Completed
for x=1:length(output)
    output(x,1)=(output(x,1)-tstart)/(tend-tstart);
end

end
```

MF_PeakDiff.m

```
function [output]=MF_PeakDiff(Data)

difftime=MF_Difftime(Data);

for x=1:length(Data)
    data1_Ansys(x,1)=Data(x,1);
    data1_Ansys(x,2)=Data(x,2);
end

for x=1:length(Data)
    data1_Data(x,1)=Data(x,3);
    data1_Data(x,2)=Data(x,4);
end

DataN=data1_Data;
AnsysN=data1_Ansys;
cdval=0;
tdval=0;
caval=0;
taval=0;

for x=1:length(DataN)
    if DataN(x,2)>cdval
        cdval=DataN(x,2);
        tdval=DataN(x,1);
        test=x;
    end
    if AnsysN(x,2)>caval
        caval=AnsysN(x,2);
        taval=AnsysN(x,1);
    end
end

output(1,1)=(tdval-taval)/difftime;
output(1,2)=(cdval-caval)/cdval;
end
```

Appendix B: Sample Graphical Data

Sample Static Test Results: Average Replicate Load-Deflection for GP12 Joists

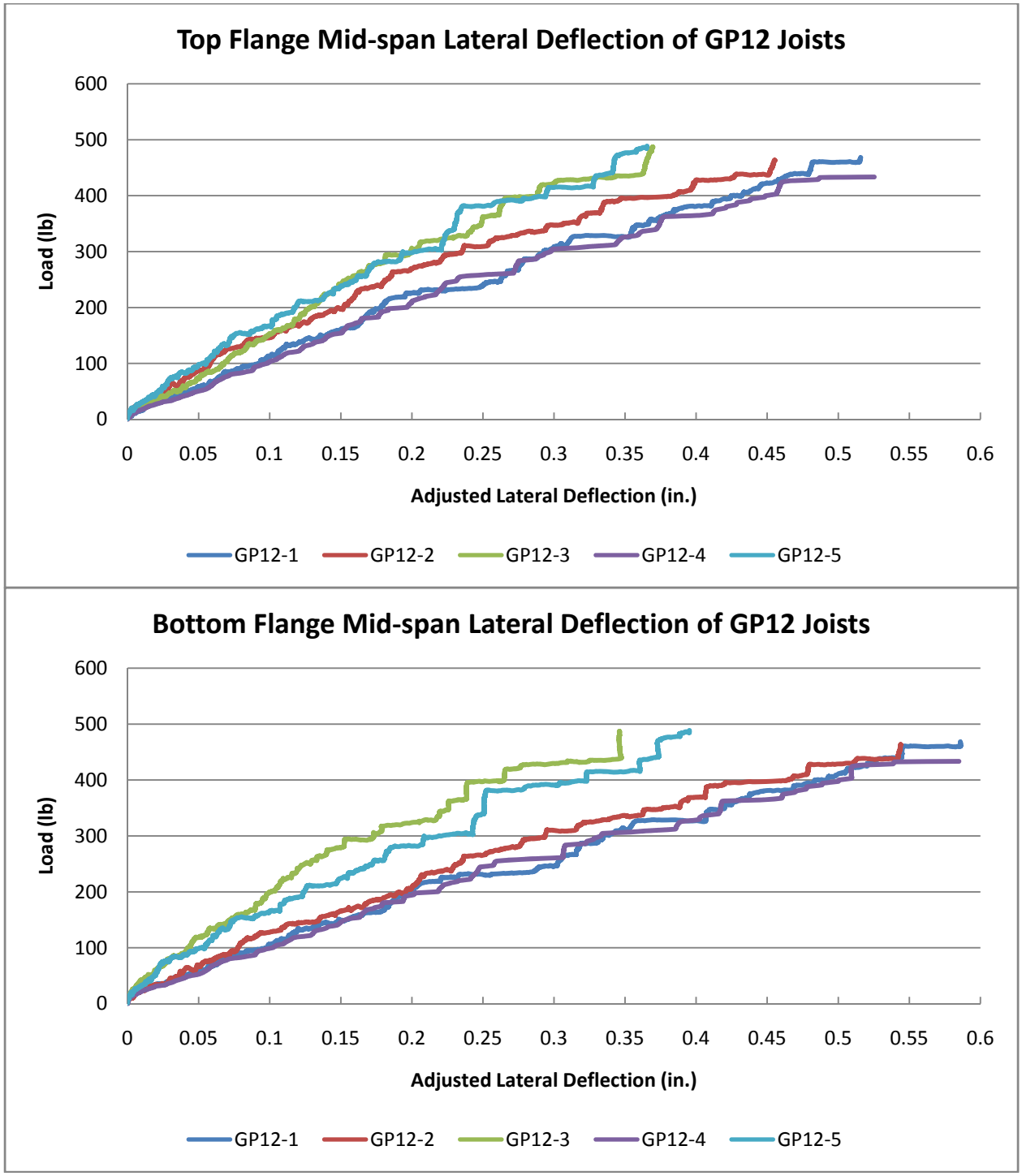

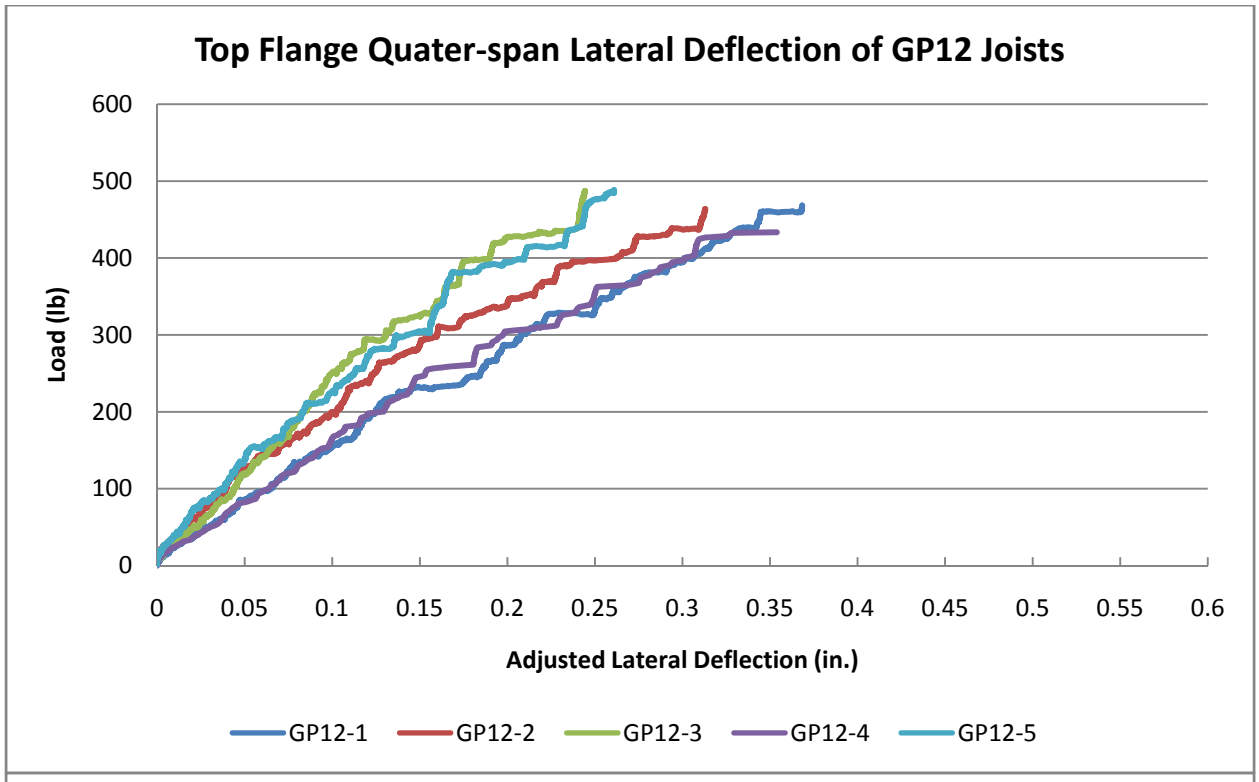
Top Flange Quater-span Lateral Deflection of GP12 Joists
Load (lb)
600
500
400
300
200
100
0
0
0.05
0.1
0.15
0.2
0.25
0.3
0.35
0.4
0.45
0.5
0.55
0.6
Adjusted Lateral Deflection (in.)
GP12-1
GP12-2
GP12-3
GP12-4
GP12-5

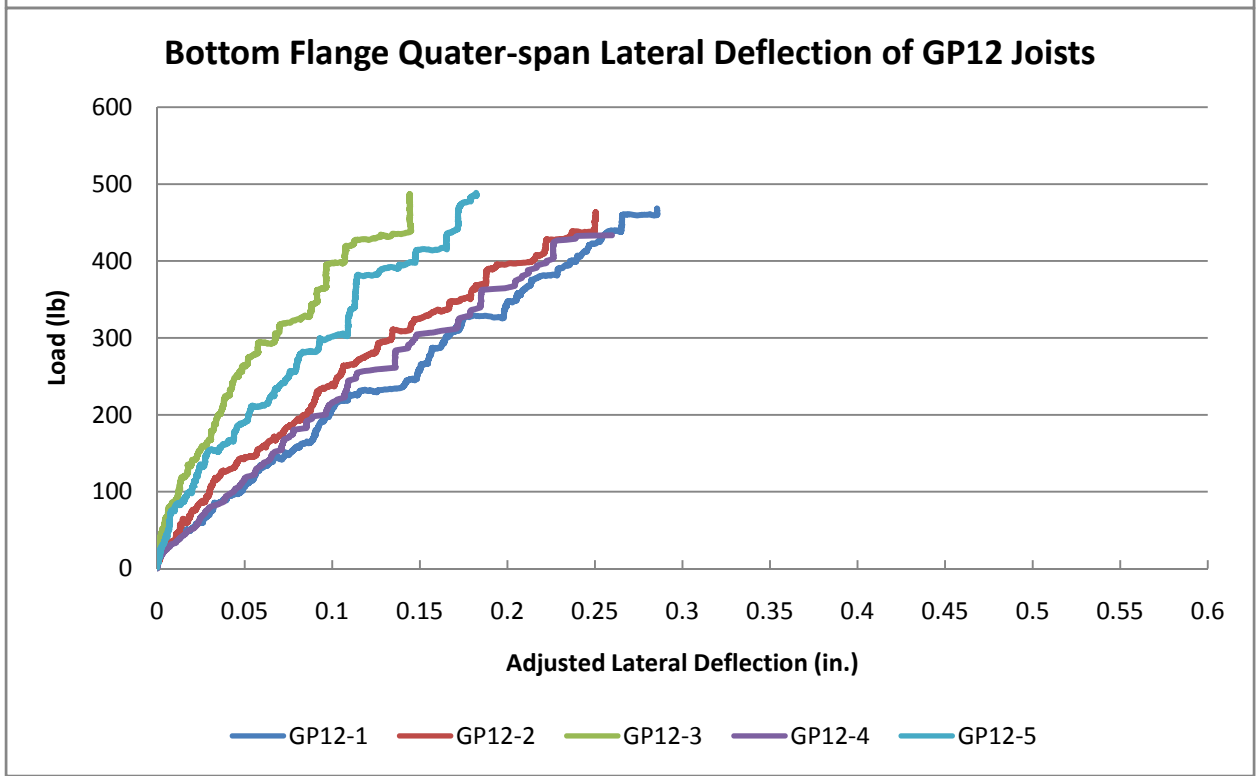
Bottom Flange Quater-span Lateral Deflection of GP12 Joists
Load (lb)
600
500
400
300
200
100
0
0
0.05
0.1
0.15
0.2
0.25
0.3
0.35
0.4
0.45
0.5
0.55
0.6
Adjusted Lateral Deflection (in.)
GP12-1
GP12-2
GP12-3
GP12-4
GP12-5

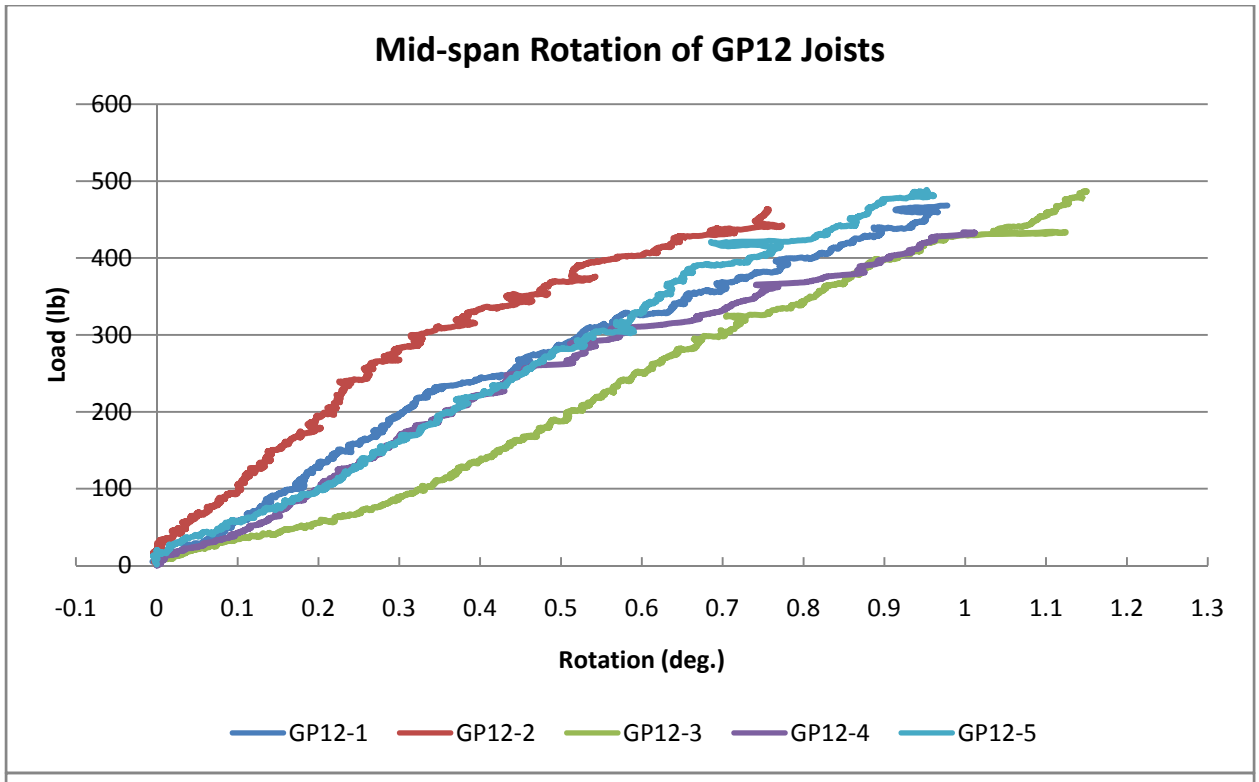
Mid-span Rotation of GP12 Joists
Load (lb)
600
500
400
300
200
100
0
-0.1
0
0.1
0.2
0.3
0.4
0.5
0.6
0.7
0.8
0.9
1
1.1
1.2
1.3
Rotation (deg.)
GP12-1
GP12-2
GP12-3
GP12-4
GP12-5

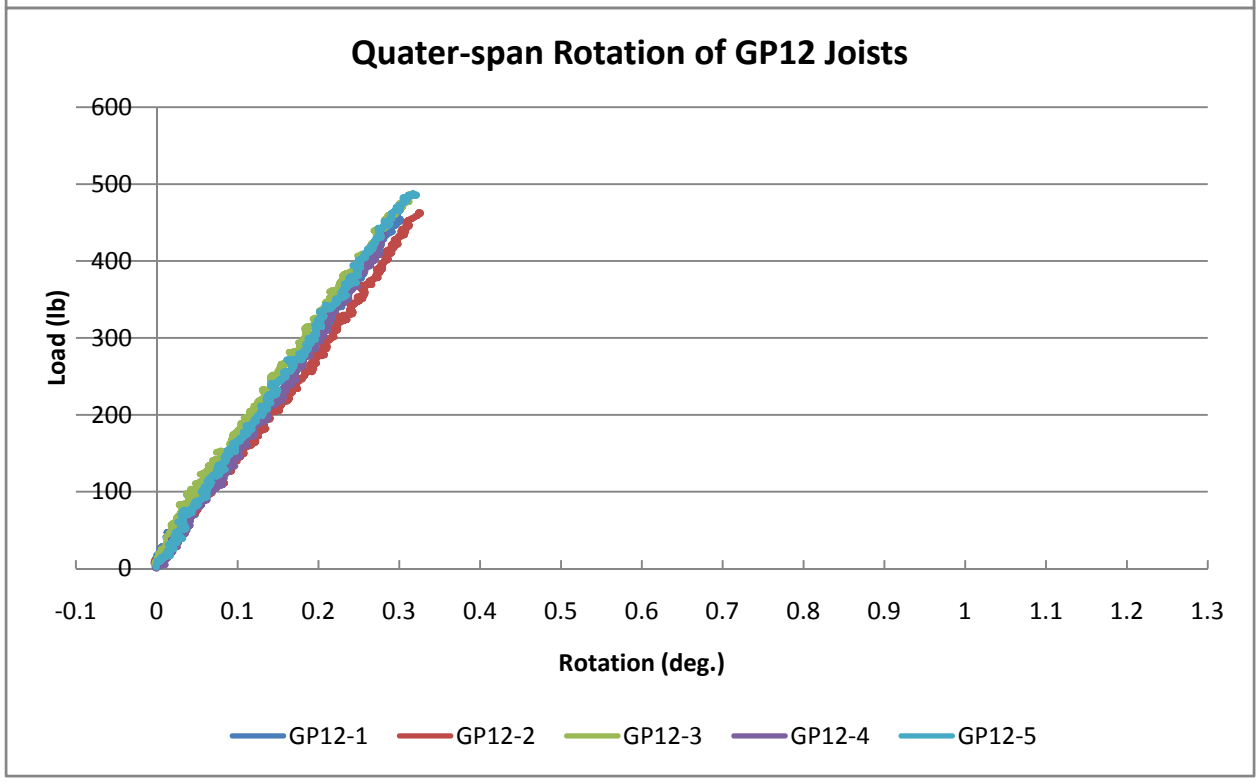
Quater-span Rotation of GP12 Joists
Load (lb)
600
500
400
300
200
100
0
-0.1
0
0.1
0.2
0.3
0.4
0.5
0.6
0.7
0.8
0.9
1
1.1
1.2
1.3
Rotation (deg.)
GP12-1
GP12-2
GP12-3
GP12-4
GP12-5

Sample Simplified Pseudo- Dynamic Test Results: Maximum value curves generated from GP12-S3 loads for input into analysis

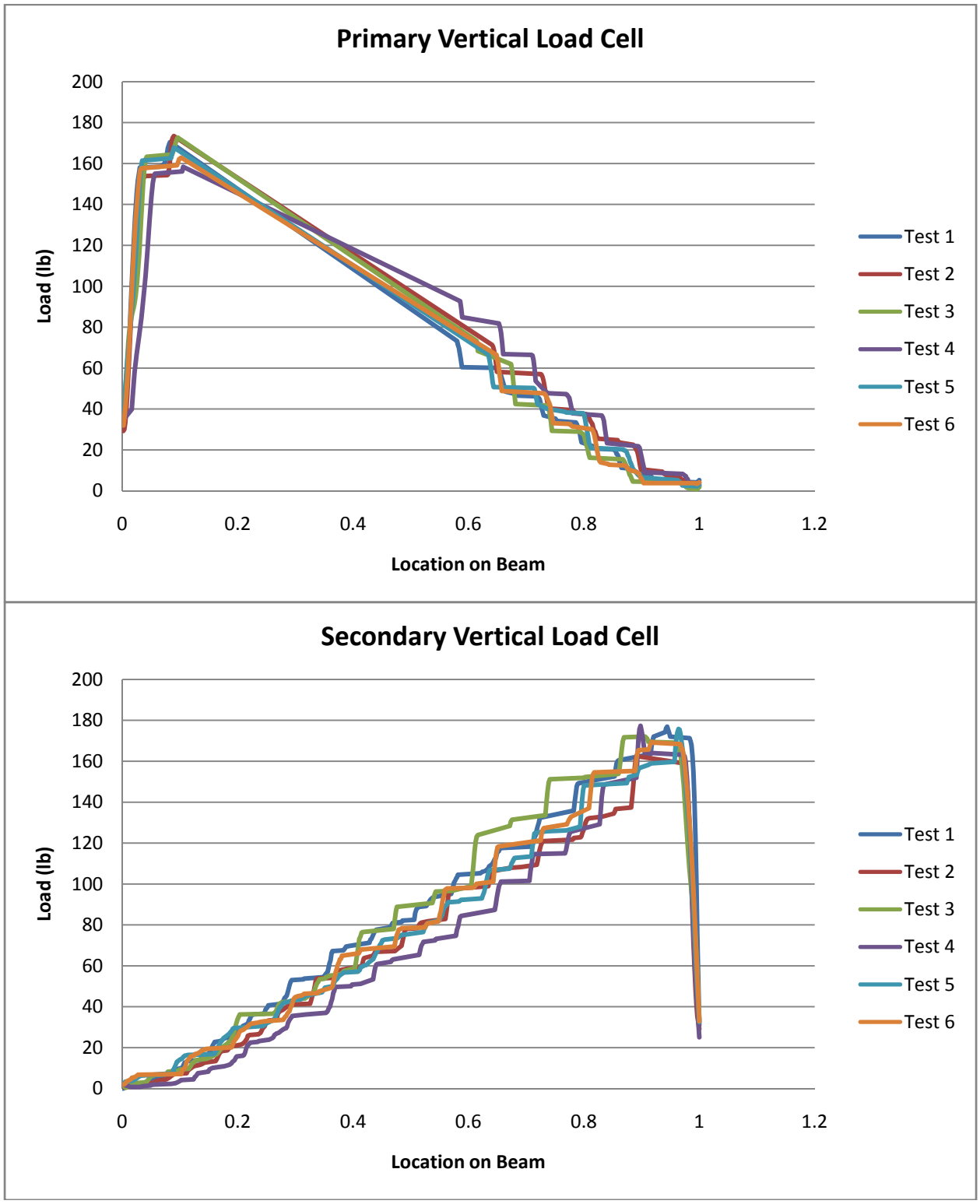

Appendix B: Sample Graphical Data

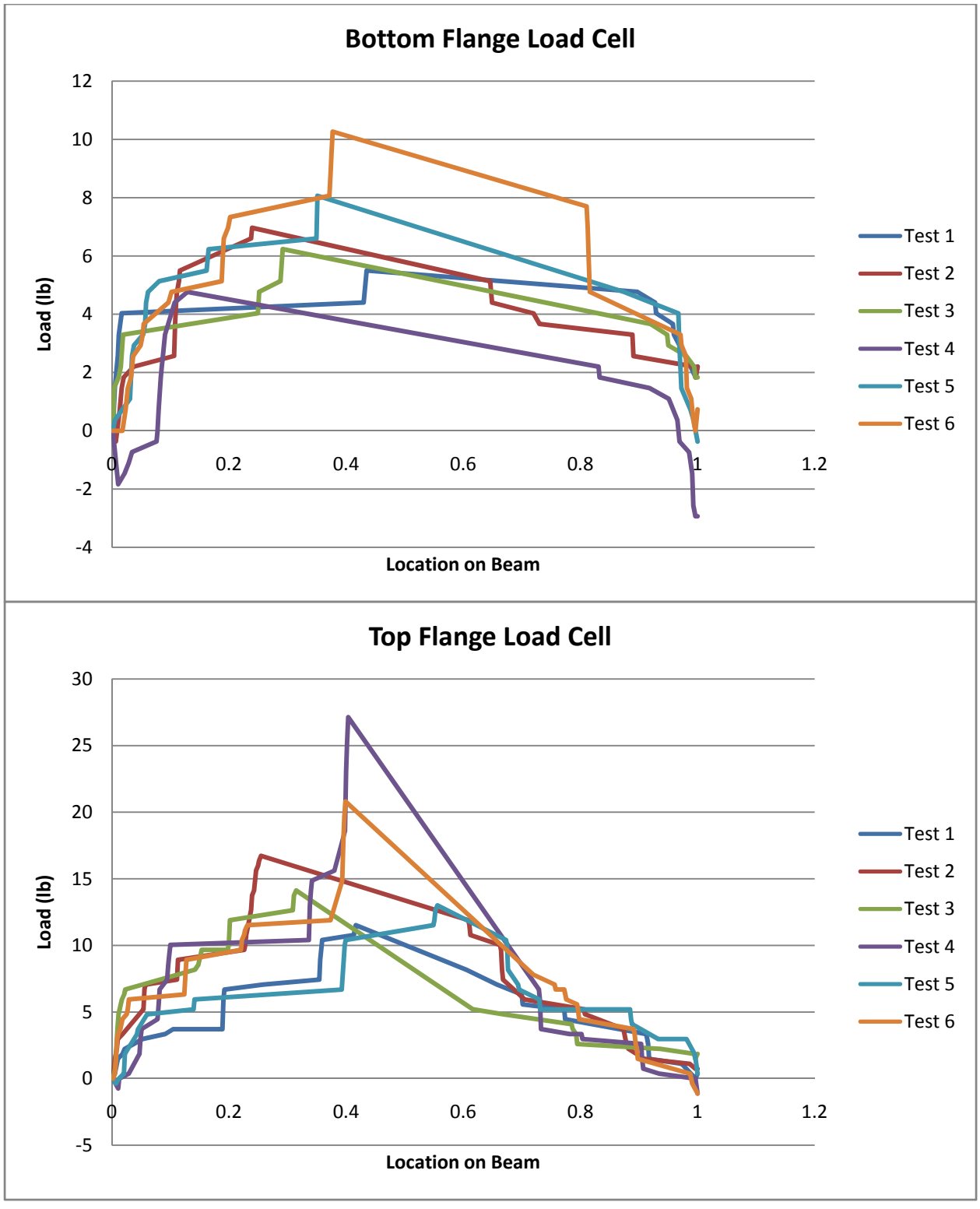

Sample Simplified Pseudo-Dynamic Test Results: Maximum value curves generated from deflections of GP12-S1 with ANSYS results

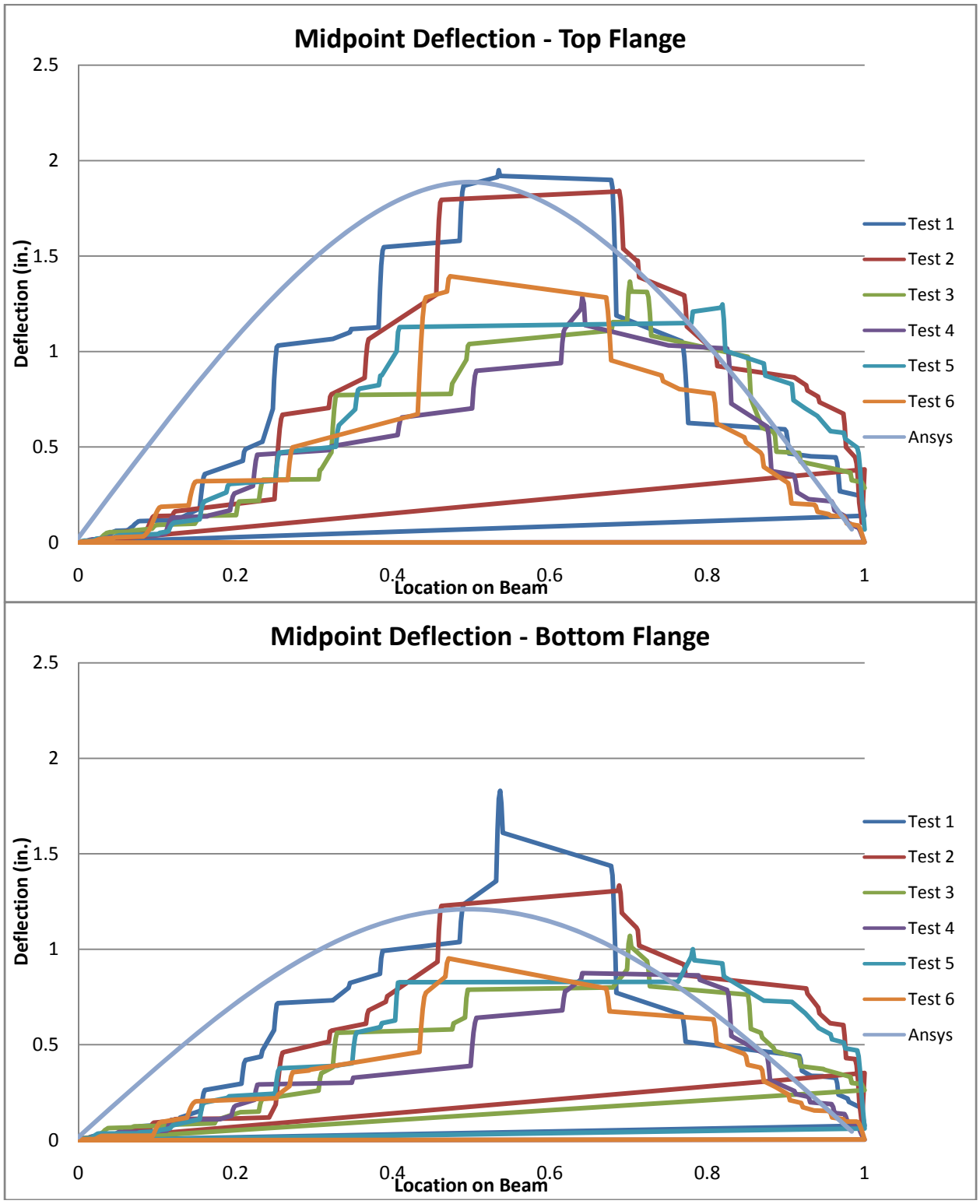

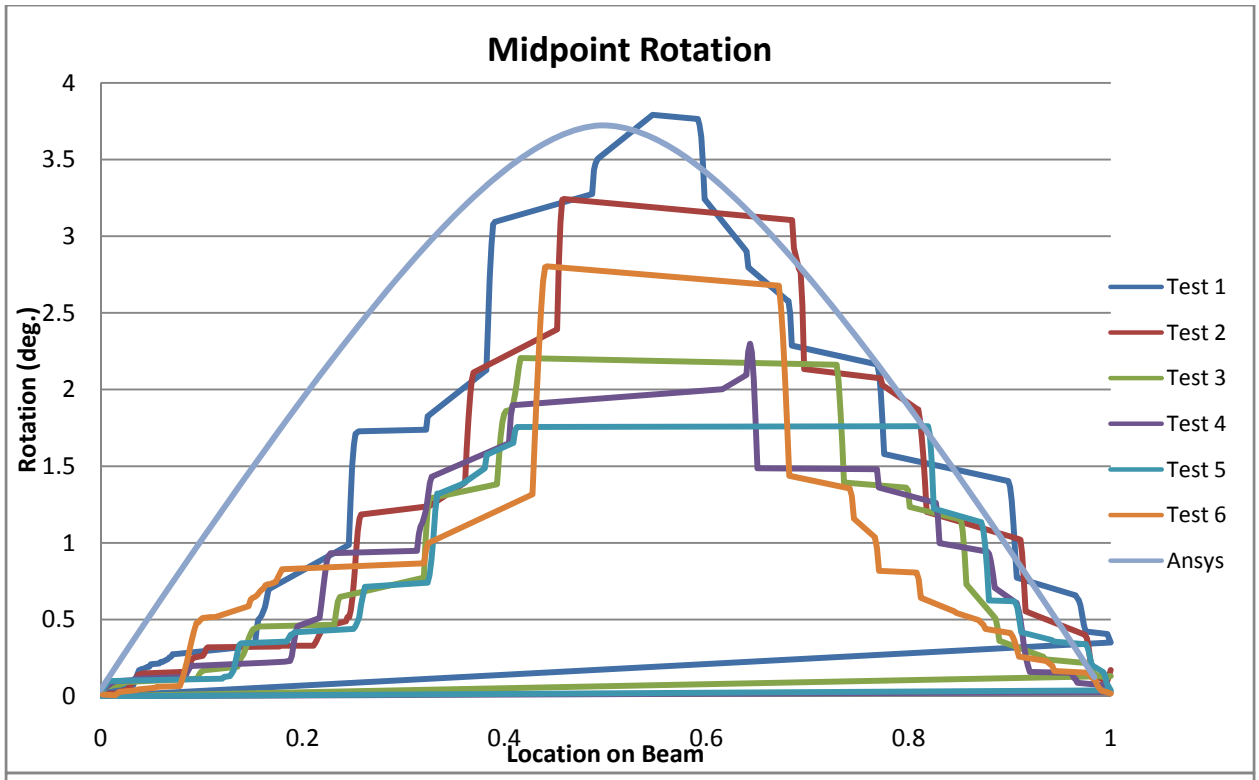
Midpoint Rotation
Rotation (deg.)
4
3.5
3
2.5
2
1.5
1
0.5
0
0
0.2
0.4
0.6
0.8
1
Location on Beam
Test 1
Test 2
Test 3
Test 4
Test 5
Test 6
Ansys

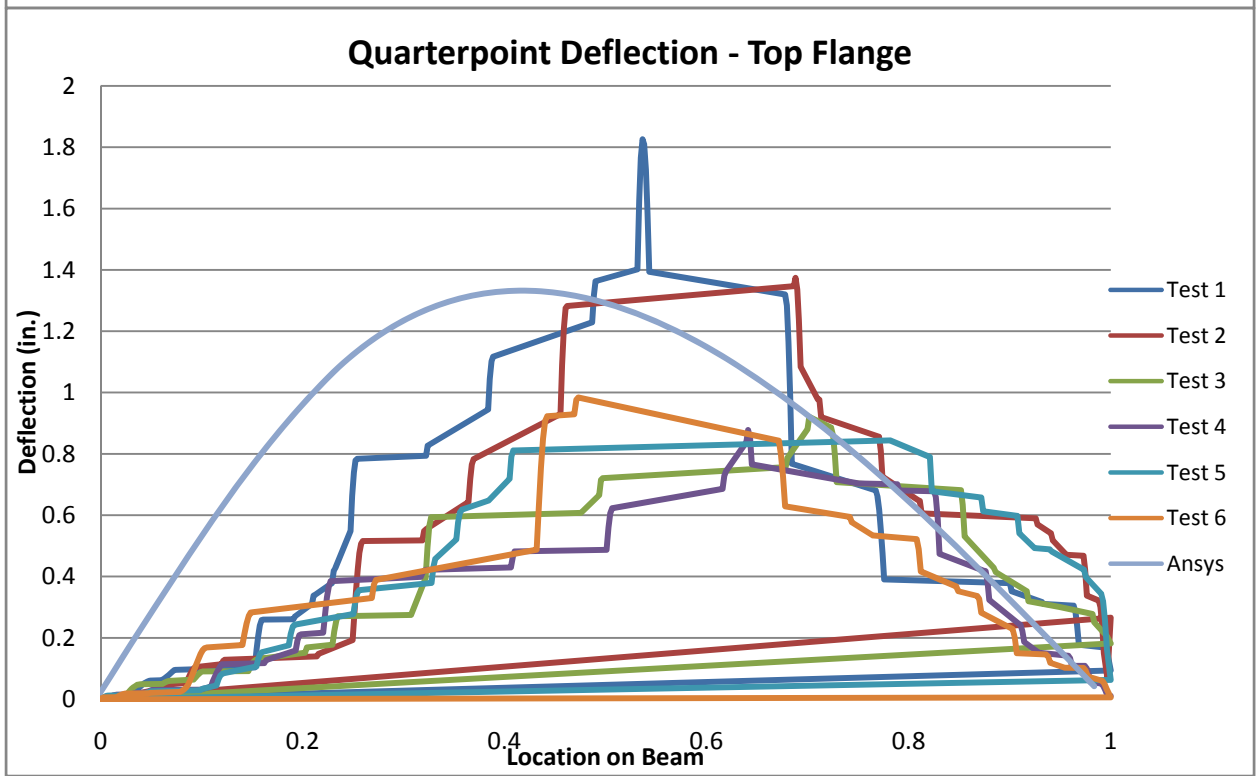
Quarterpoint Deflection - Top Flange
Deflection (in.)
2
1.8
1.6
1.4
1.2
1
0.8
0.6
0.4
0.2
0
0
0.2
0.4
0.6
0.8
1
Location on Beam
Test 1
Test 2
Test 3
Test 4
Test 5
Test 6
Ansys

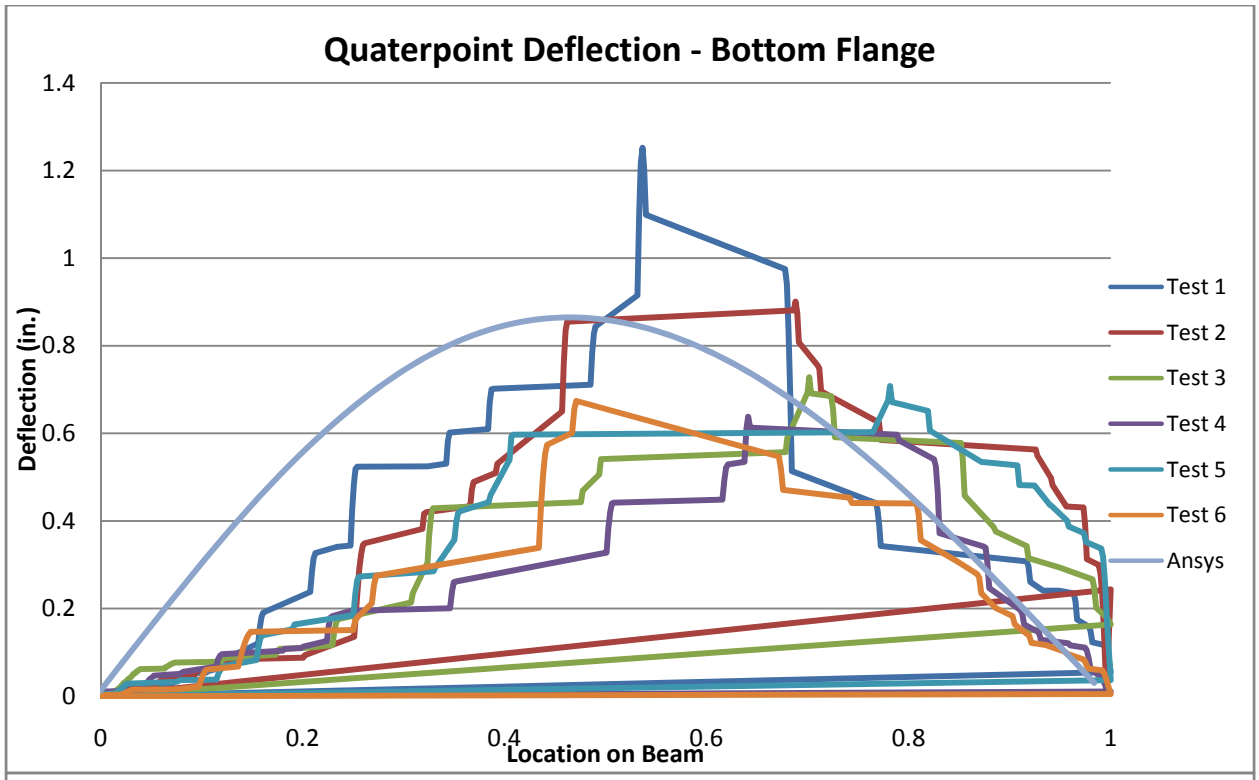
Quaterpoint Deflection - Bottom Flange
Deflection (in.)
1.4
1.2
1
0.8
0.6
0.4
0.2
0
0
0.2
0.4
0.6
0.8
1
Location on Beam
Test 1
Test 2
Test 3
Test 4
Test 5
Test 6
Ansys

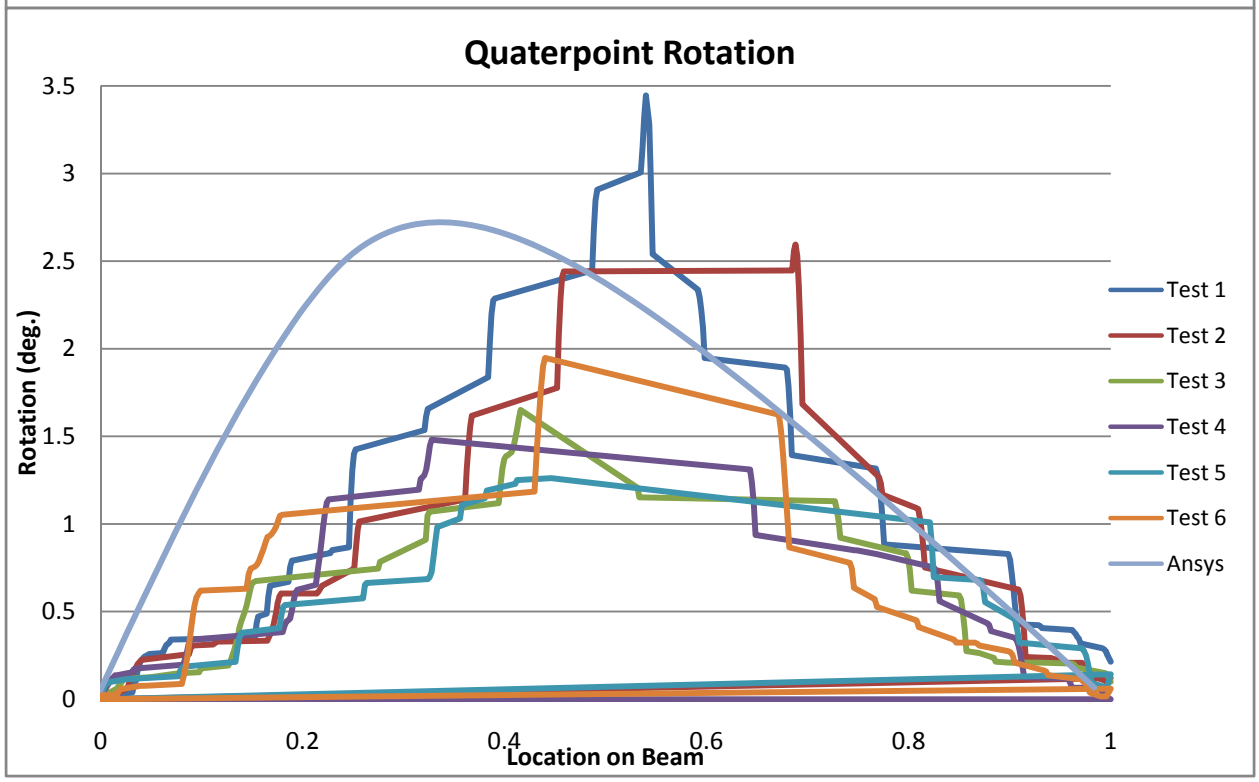
Quaterpoint Rotation
Rotation (deg.)
3.5
3
2.5
2
1.5
1
0.5
0
0
0.2
0.4
0.6
0.8
1
Location on Beam
Test 1
Test 2
Test 3
Test 4
Test 5
Test 6
Ansys

Sample Full Pseudo- Dynamic Test Results: Raw Ansys deflections from GP12-S5-3b with corresponding test data

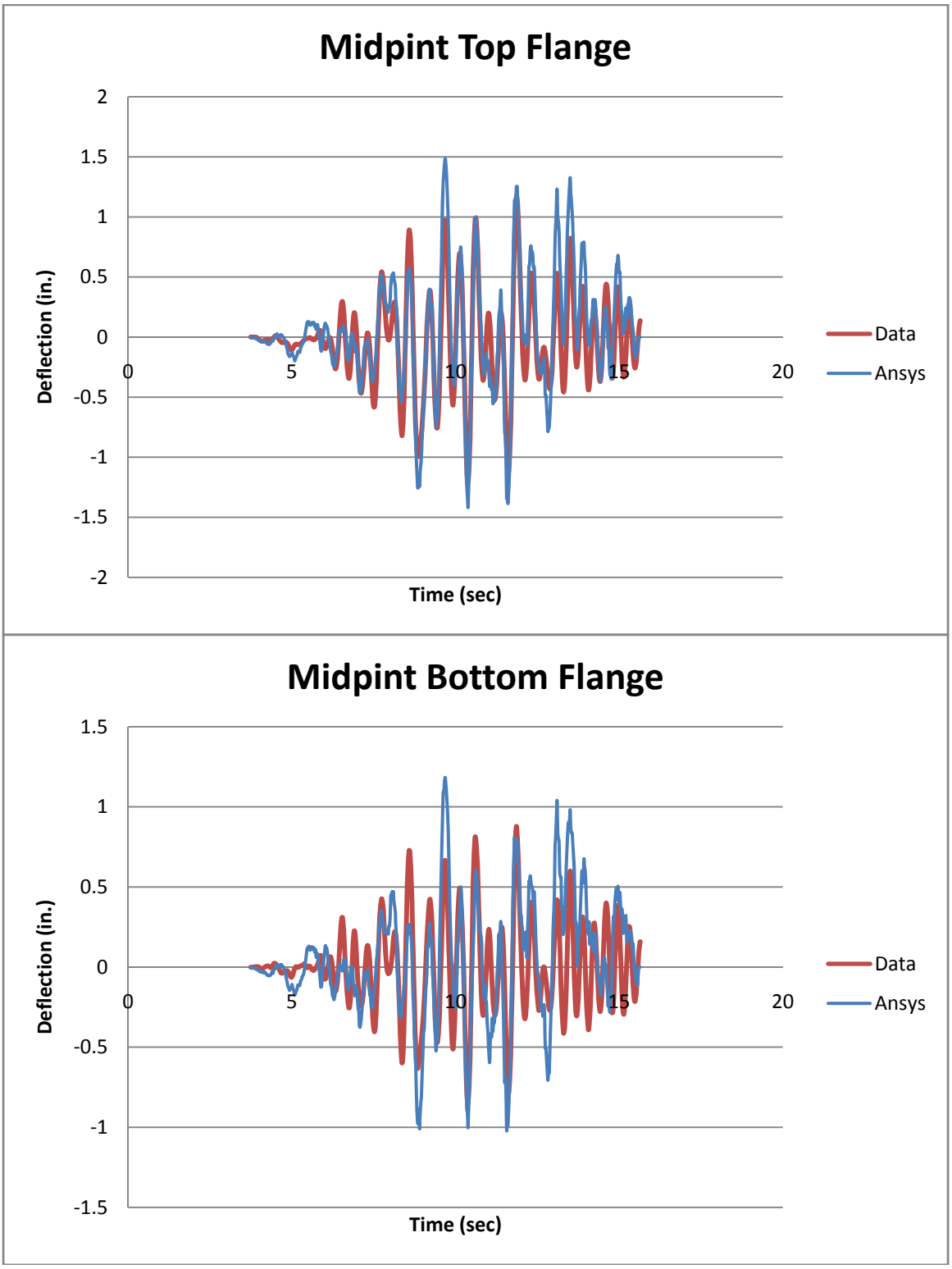

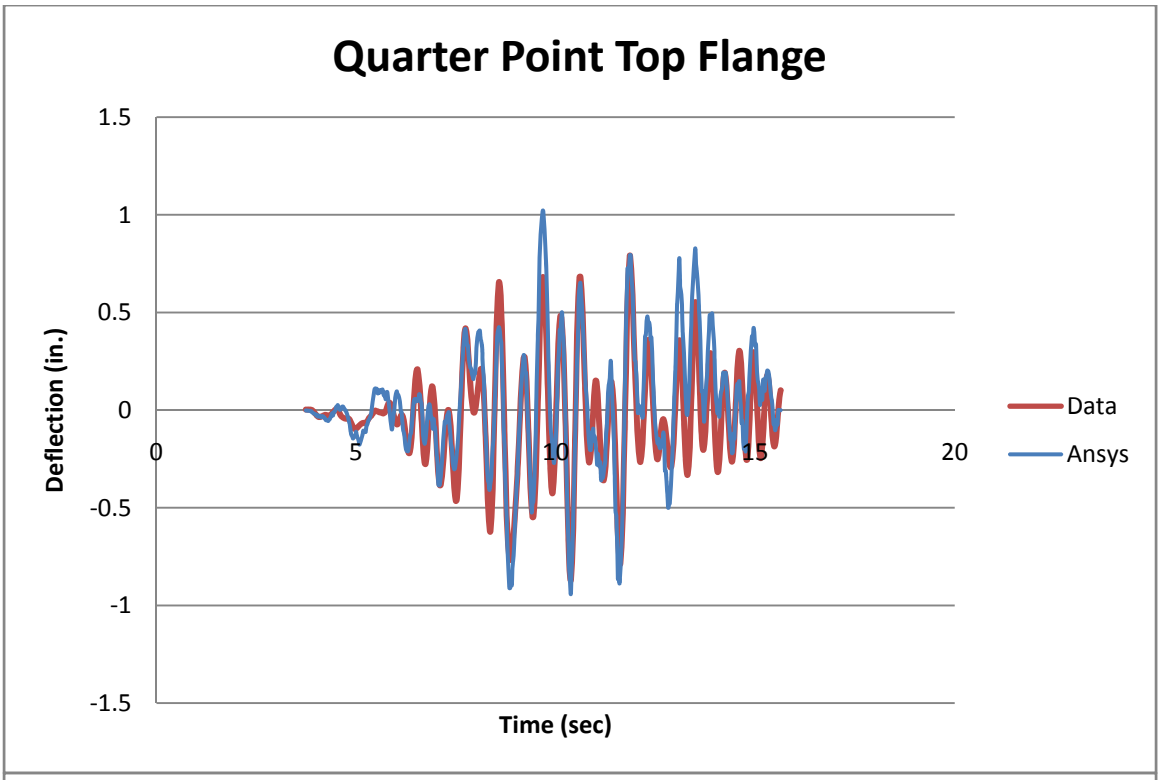
Quarter Point Top Flange
1.5
1
0.5
0
-0.5
-1
-1.5
Deflection (in.)
0
5
10
15
20
Time (sec)
Data
Ansys

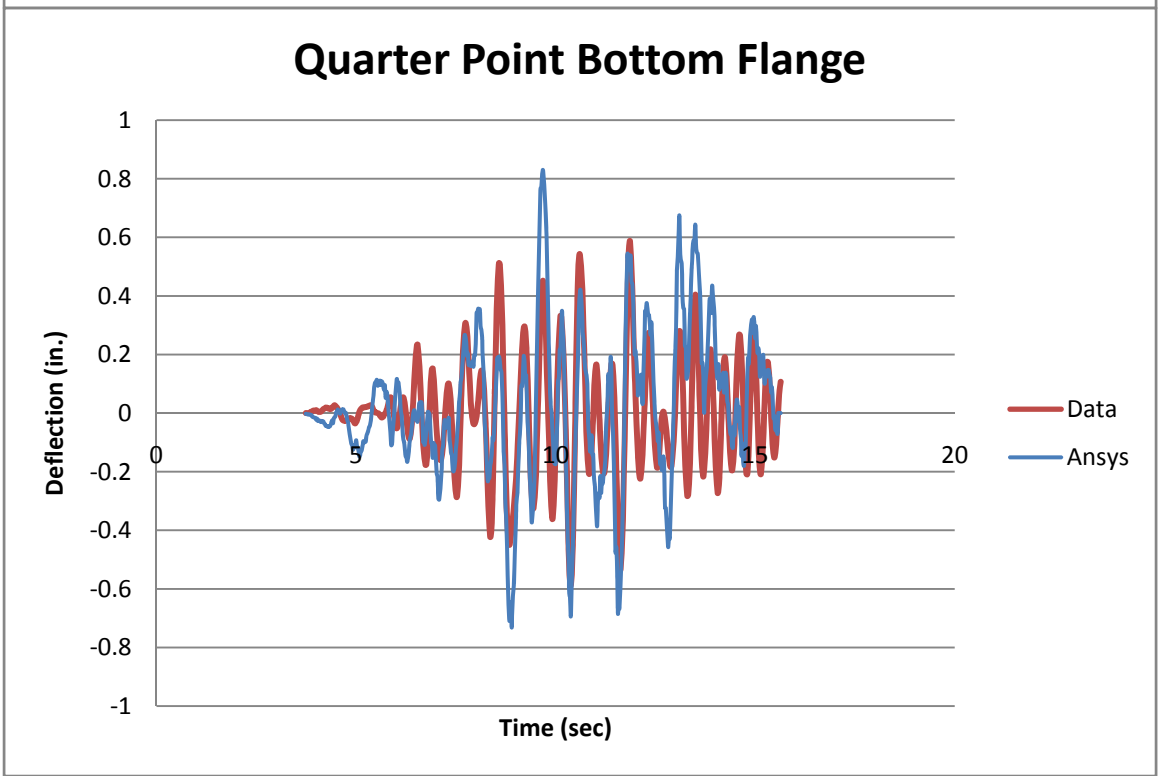
Quarter Point Bottom Flange
1
0.8
0.6
0.4
0.2
0
-0.2
-0.4
-0.6
-0.8
-1
Deflection (in.)
0
5
10
15
20
Time (sec)
Data
Ansys

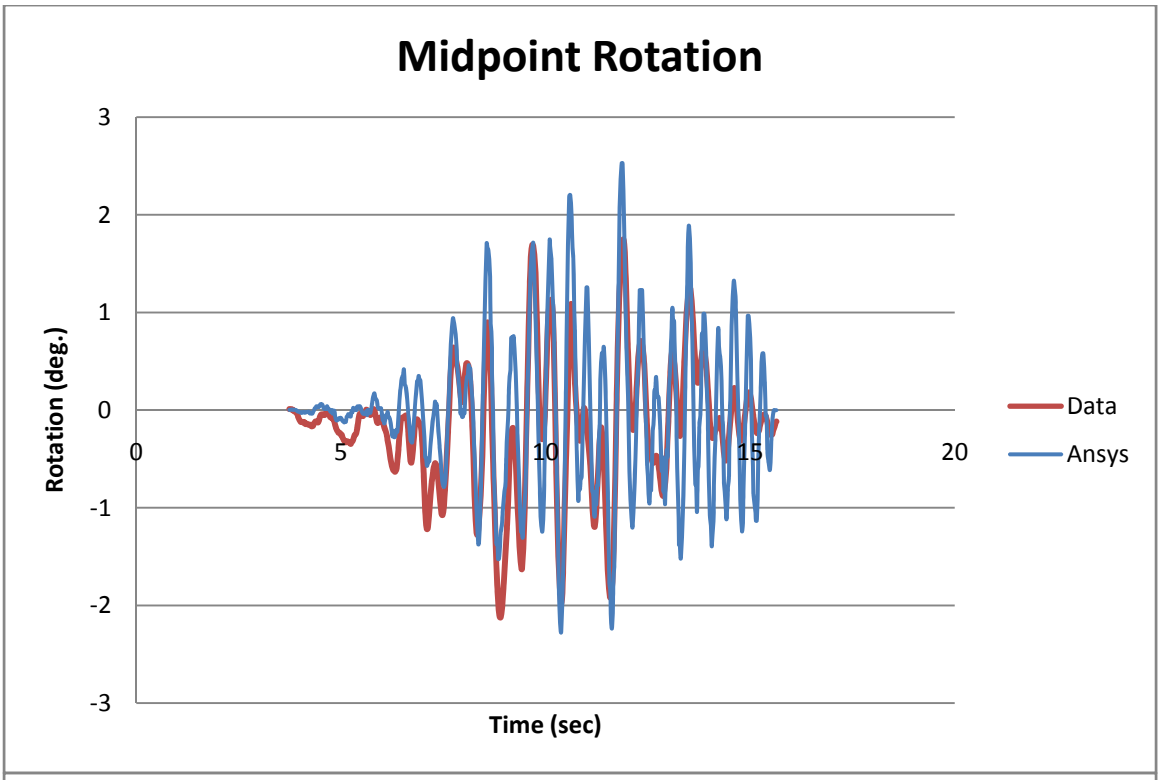
Midpoint Rotation
Rotation (deg.)
3
2
1
0
-1
-2
-3
0
5
10
15
20
Time (sec)
Data
Ansys

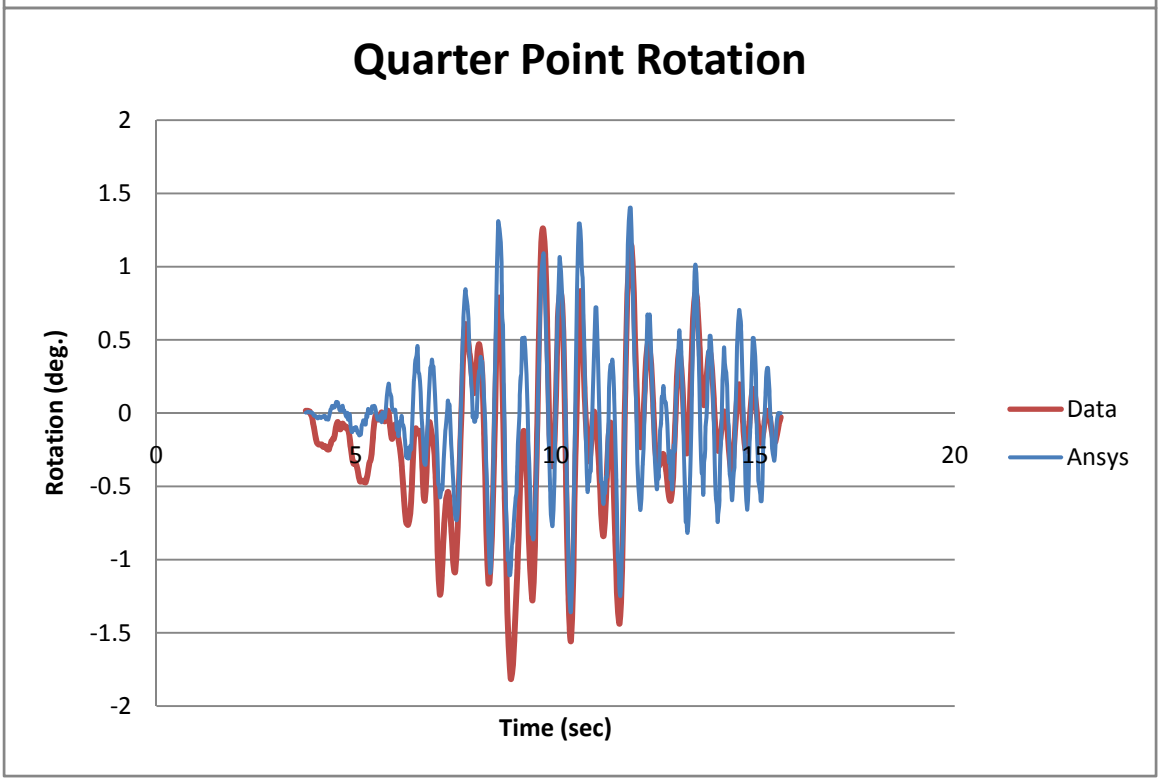
Quarter Point Rotation
Rotation (deg.)
2
1.5
1
0.5
0
-0.5
-1
-1.5
-2
0
5
10
15
20
Time (sec)
Data
Ansys

Sample Full Pseudo- Dynamic Test Results: MVC generated from GP14-S7-1a overlaid with MVC generated from Ansys test results

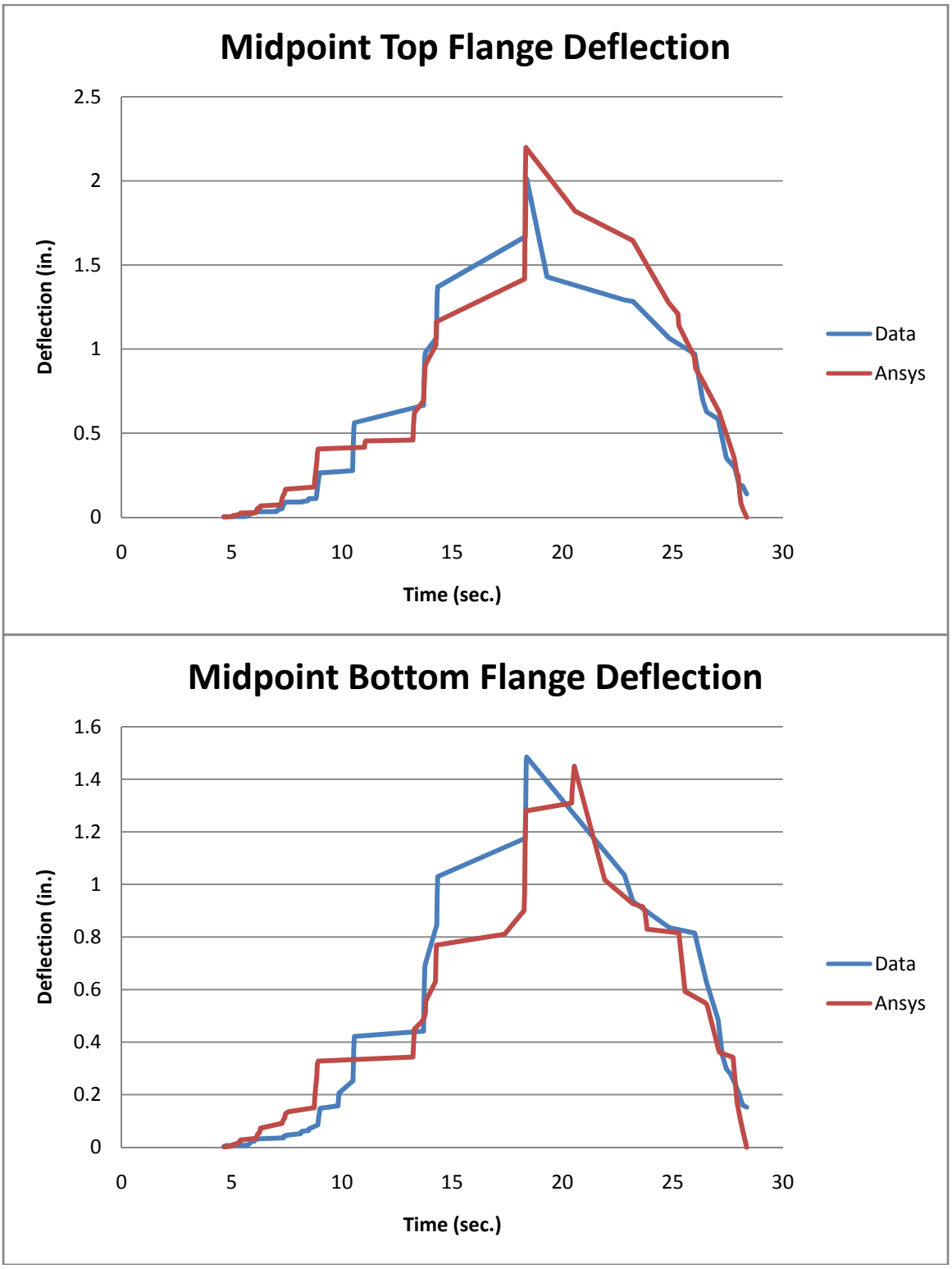

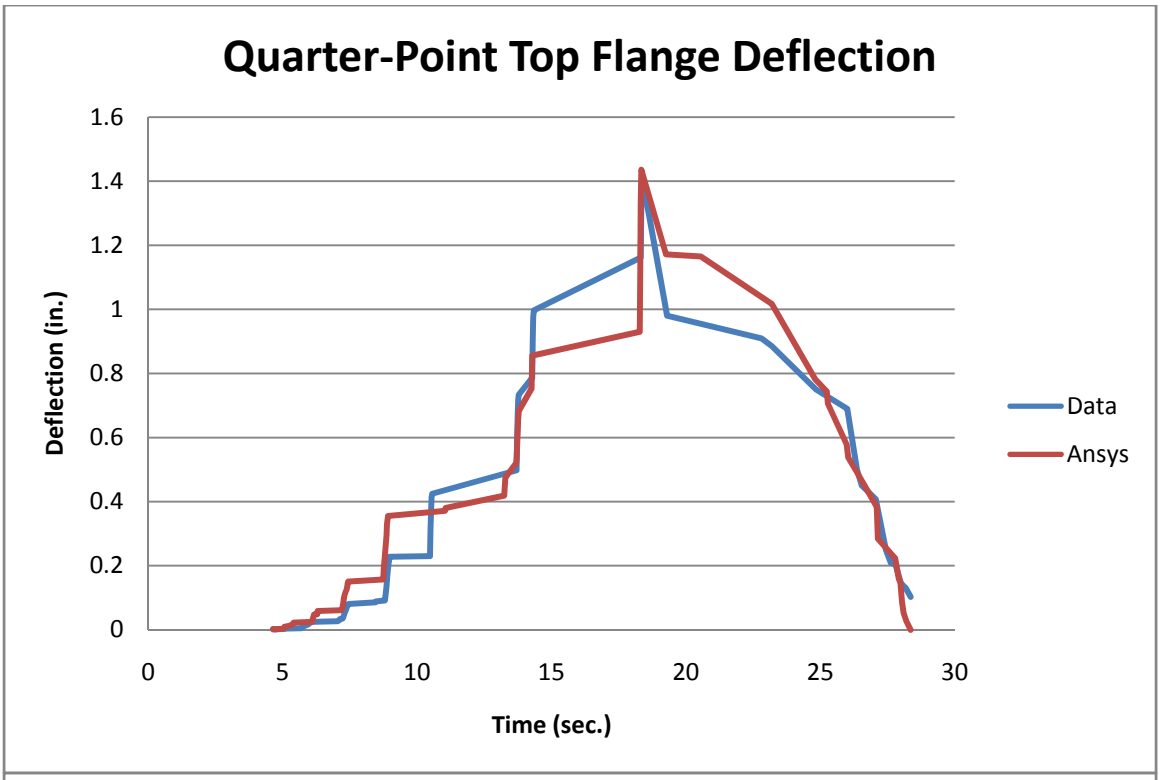
Quarter-Point Top Flange Deflection
Deflection (in.)
1.6
1.4
1.2
1
0.8
0.6
0.4
0.2
0
0
5
10
15
20
25
30
Time (sec.)
Data
Ansys

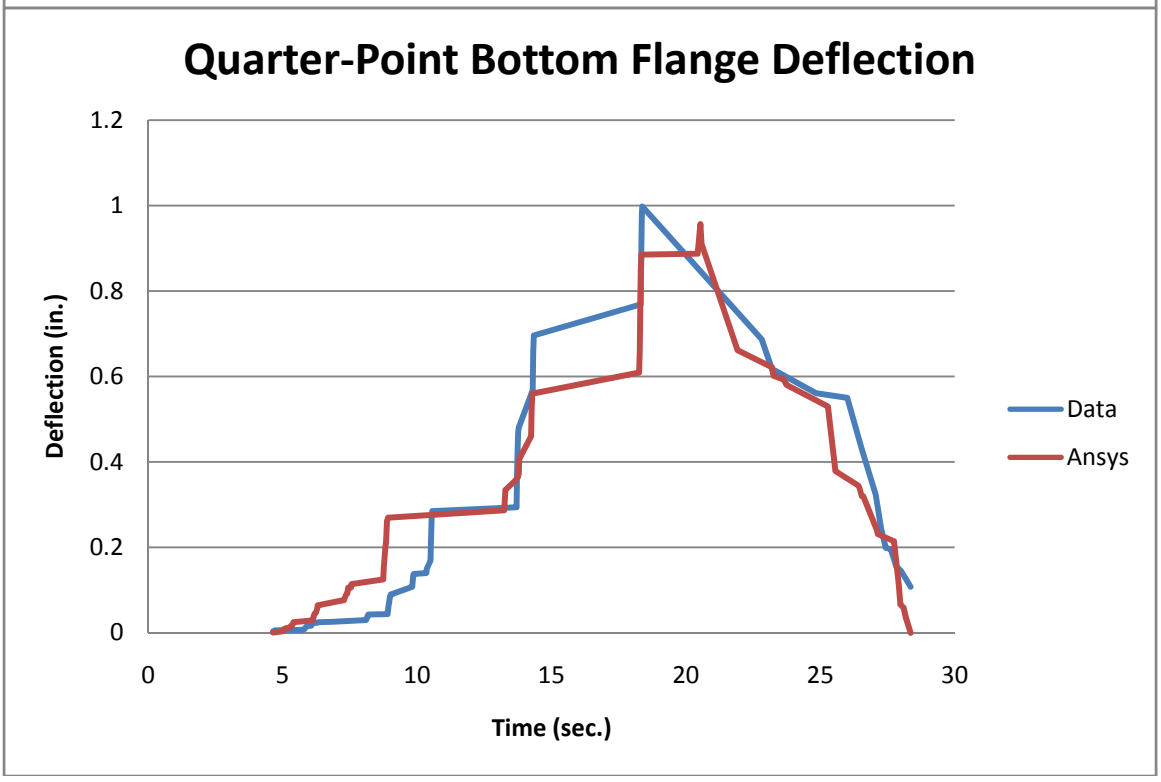
Quarter-Point Bottom Flange Deflection
Deflection (in.)
1.2
1
0.8
0.6
0.4
0.2
0
0
5
10
15
20
25
30
Time (sec.)
Data
Ansys

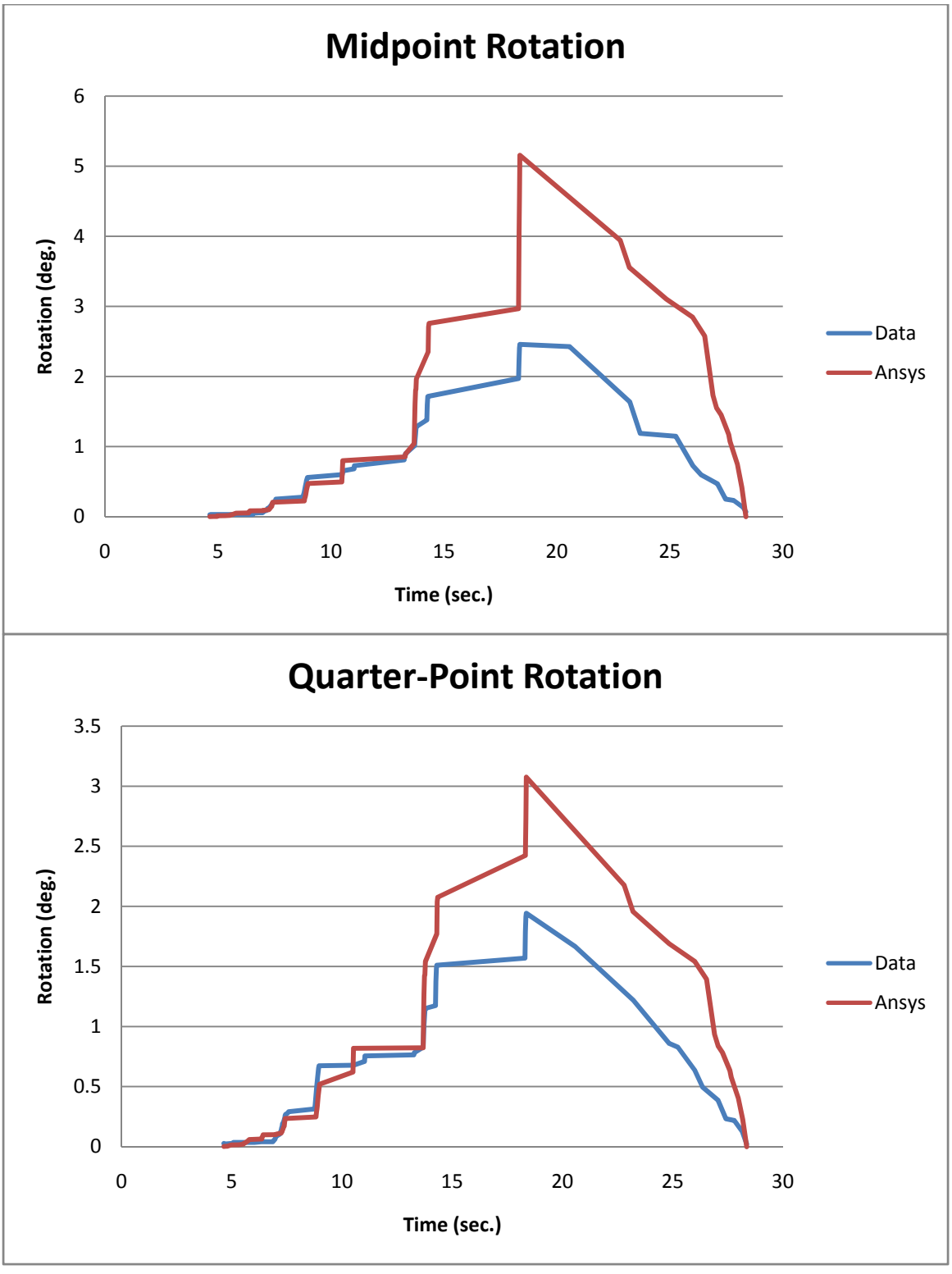
Midpoint Rotation
Rotation (deg.)
0
1
2
3
4
5
6
0
5
10
15
20
25
30
Time (sec.)
Data
Ansys
Quarter-Point Rotation
Rotation (deg.)
0
0.5
1
1.5
2
2.5
3
3.5
0
5
10
15
20
25
30
Time (sec.)
Data
Ansys

Sample Full Pseudo- Dynamic Test Results: Deviation of Ansys model from acquired test data for GP14-S8

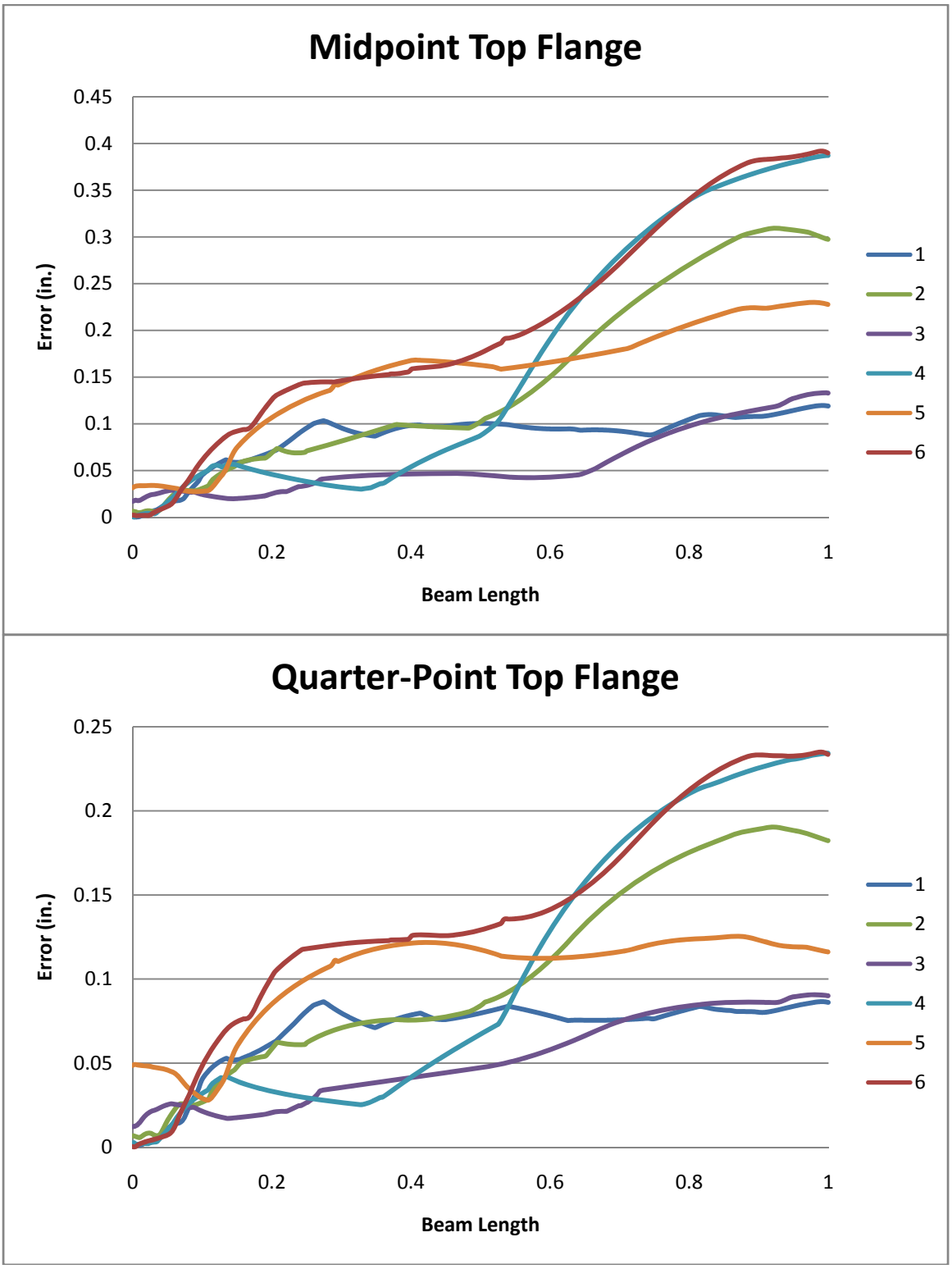

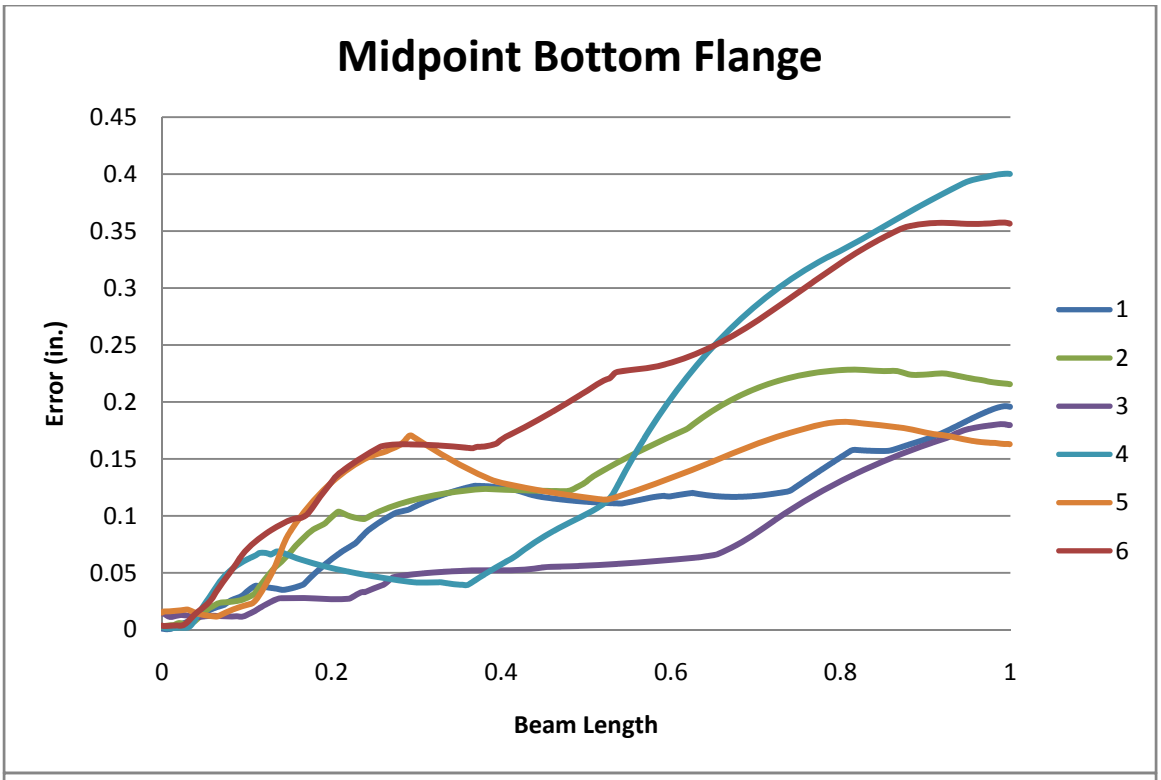
Midpoint Bottom Flange
Error (in.)
0.45
0.4
0.35
0.3
0.25
0.2
0.15
0.1
0.05
0
0
0.2
0.4
0.6
0.8
1
Beam Length
1
2
3
4
5
6

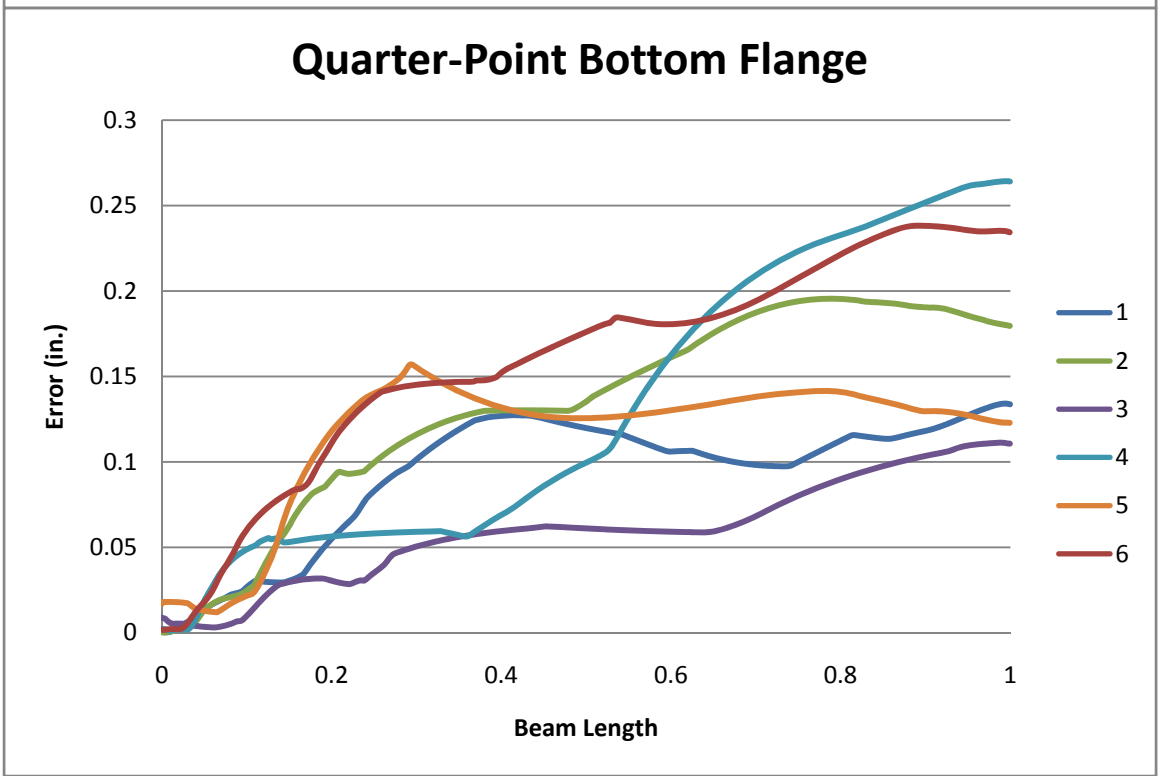
Quarter-Point Bottom Flange
Error (in.)
0.3
0.25
0.2
0.15
0.1
0.05
0
0
0.2
0.4
0.6
0.8
1
Beam Length
1
2
3
4
5
6

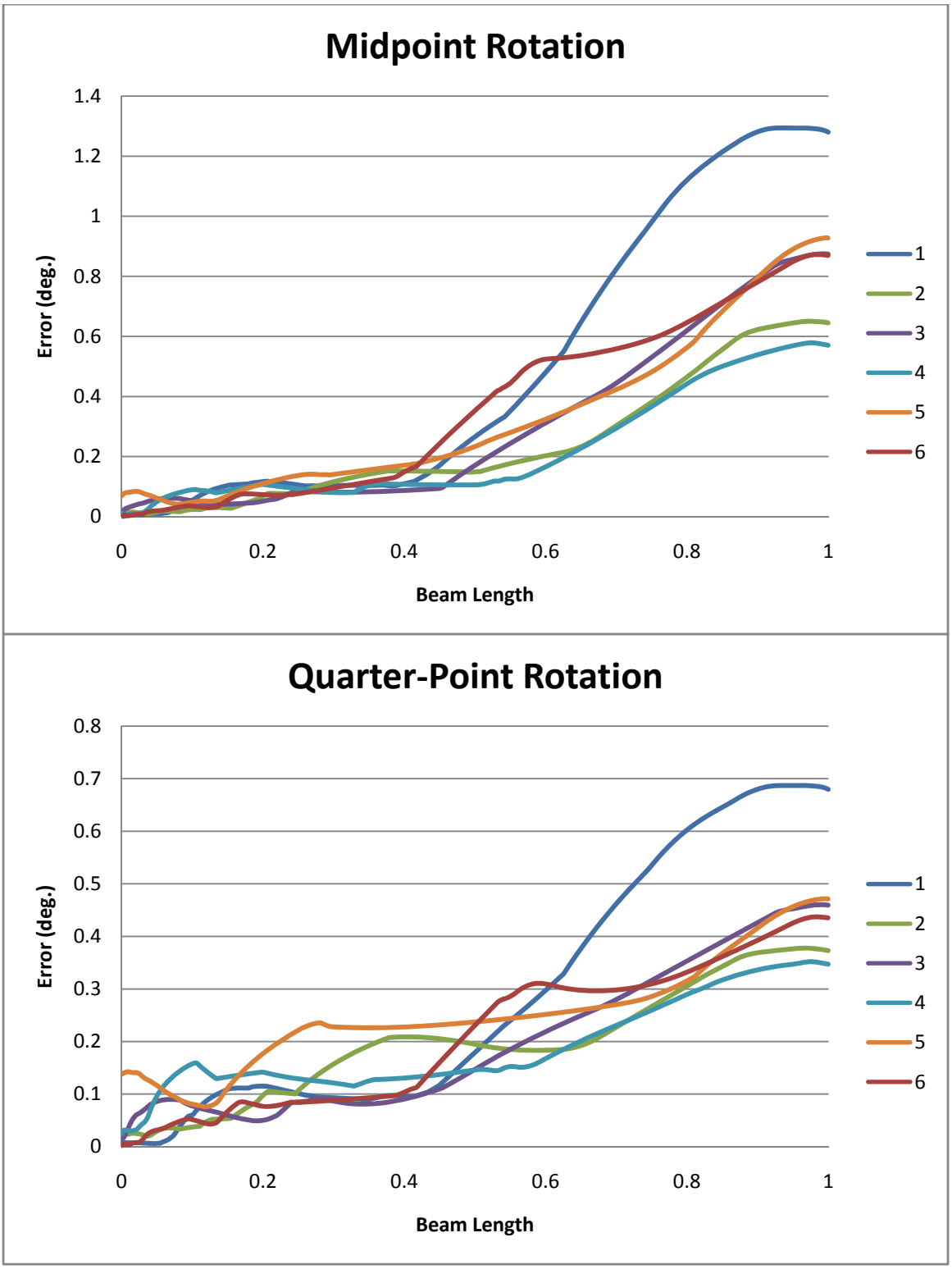
Midpoint Rotation
Error (deg.)
1.4
1.2
1
0.8
0.6
0.4
0.2
0
0
0.2
0.4
0.6
0.8
1
Beam Length
1
2
3
4
5
6
Quarter-Point Rotation
Error (deg.)
0.8
0.7
0.6
0.5
0.4
0.3
0.2
0.1
0
0
0.2
0.4
0.6
0.8
1
Beam Length
1
2
3
4
5
6